Nuclear physics School for Young Scientists
(NUSYS-2024)

Core course:

Single-particle and collective motions in atomic nuclei

鈴木大介
理化学研究所
仁科加速器科学研究センター
Daisuke Suzuki
RIKEN Nishina Center

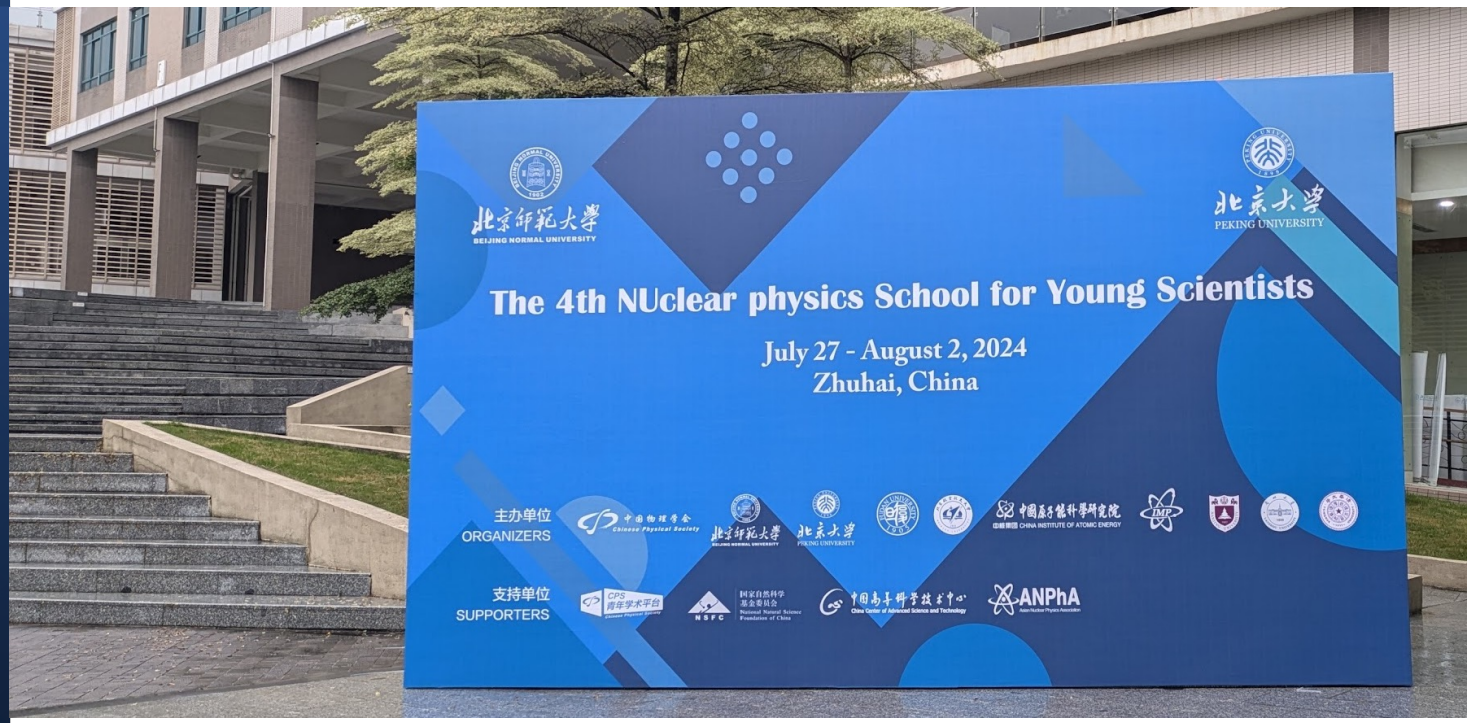

Beijing Normal University (Zhuhai, Guangdong)
July 27 to August 2, 2024

RIKEN
RIKEN NiSHiNA CENTER

RIKEN

RIKEN is **Japan's largest and most comprehensive research organization for basic and applied science** and a world leader in a diverse array of scientific disciplines.

Petascale supercomputer
FUGAKU

Synchrotron radiation facility
SPring-8

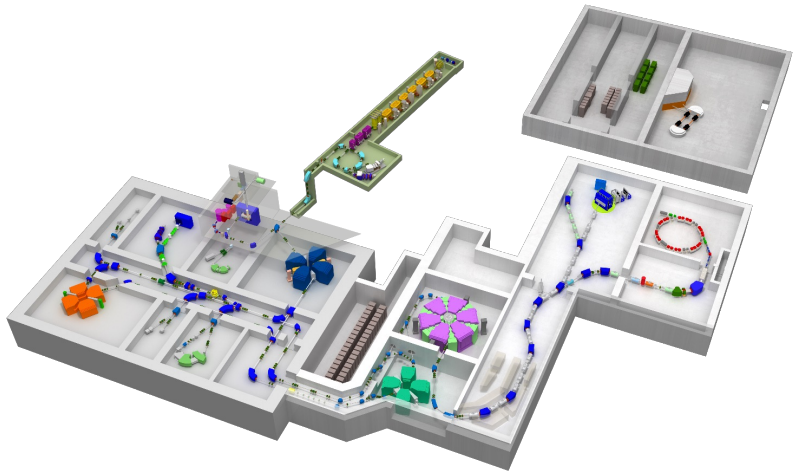

RI Beam Factory (RIBF)

RIKEN Wako campus

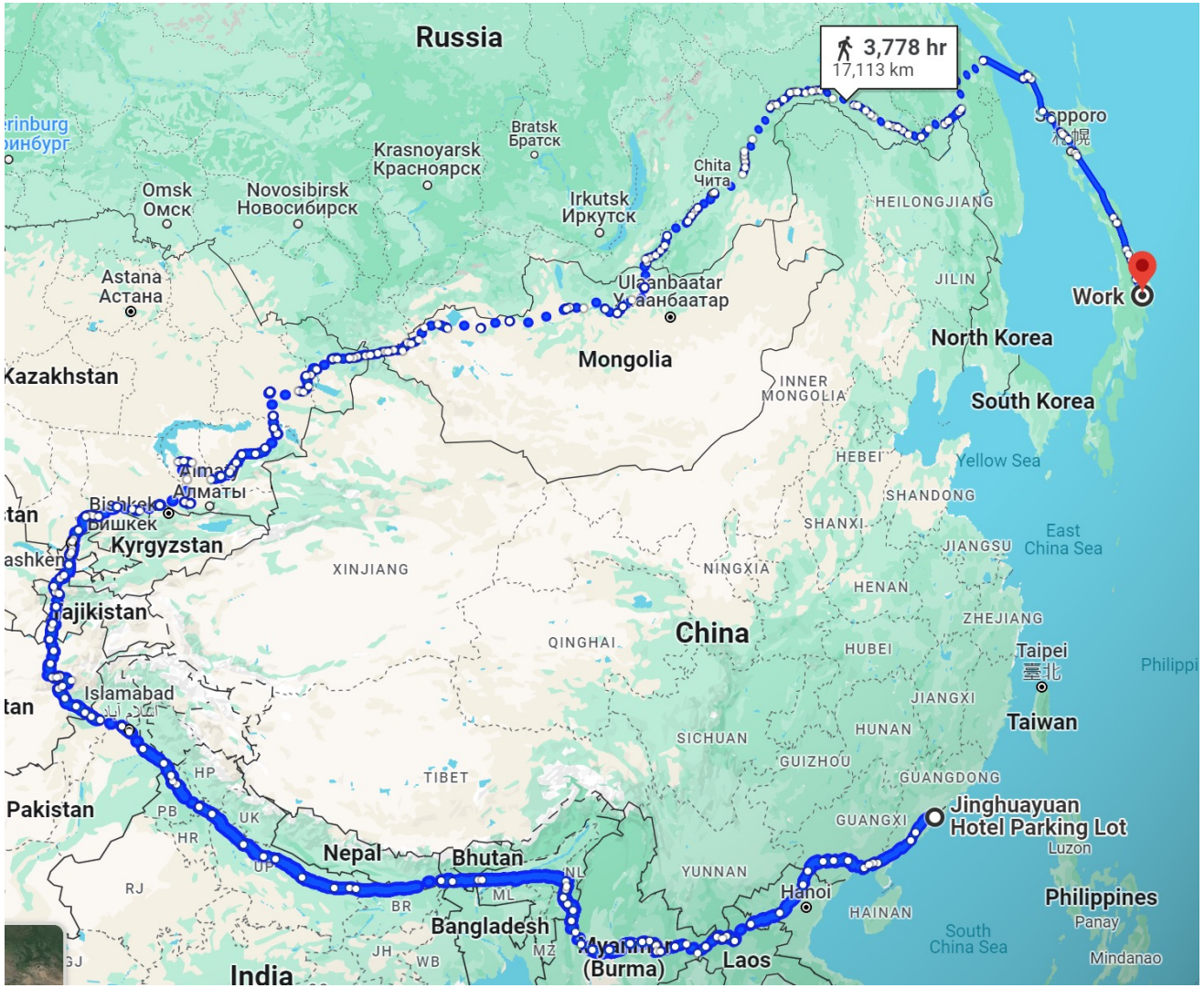

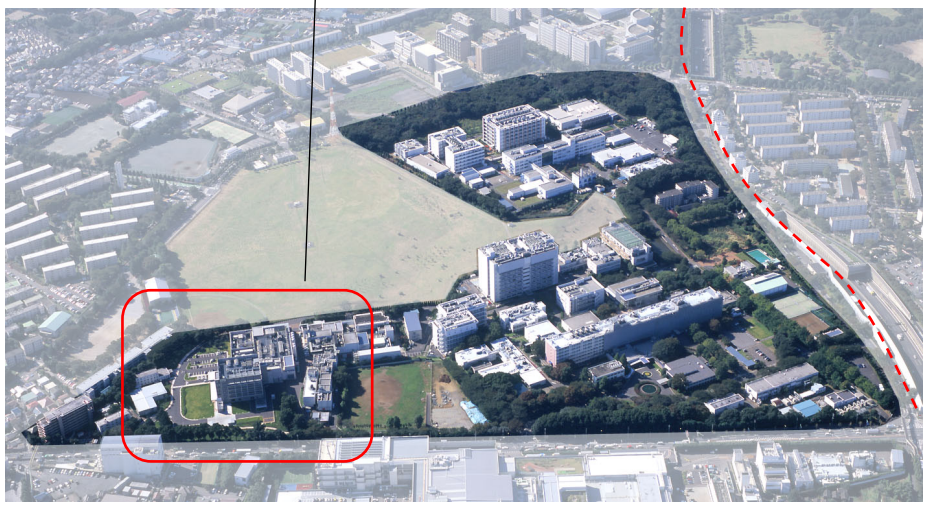

東京外環

Tokyo ← 川越街道 → Kawagoe, Takasaki

RIKEN Nishina Center for Accelerator-Based Science

RIKEN Nishina Center is a **research center of nuclear science.**

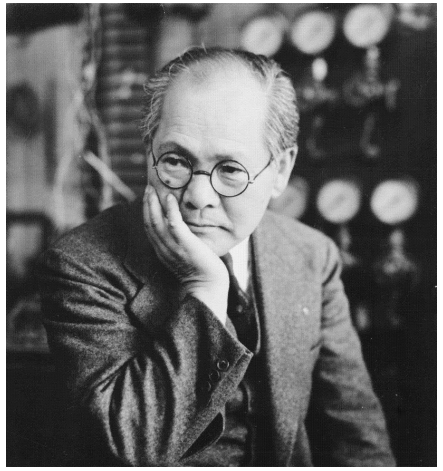

Yoshio Nishina
(1890-1951)

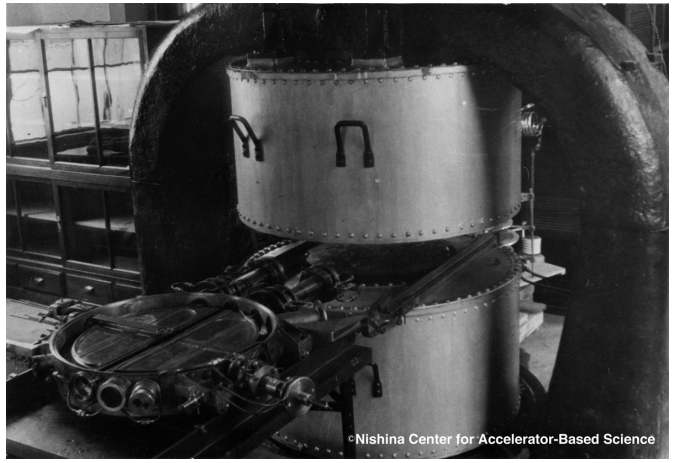

First particle accelerator (1937)

RI Beam Factory (RIBF)

Since 2007

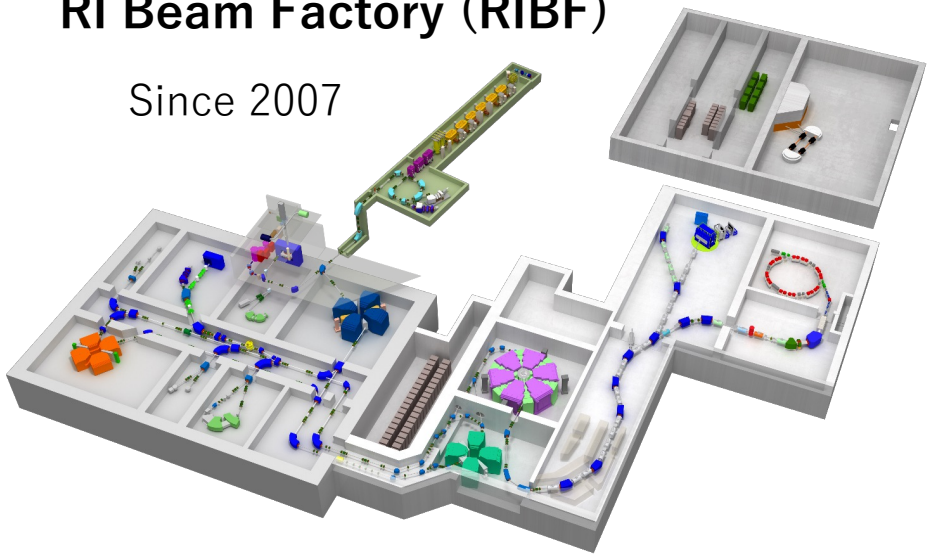

Nuclear science

Particle accelerator is central instrument of science today. Nishina Center encompasses **RIBF as world-leading facility of radioactive isotope beam for nuclear science**.

Fundamental nuclear physics

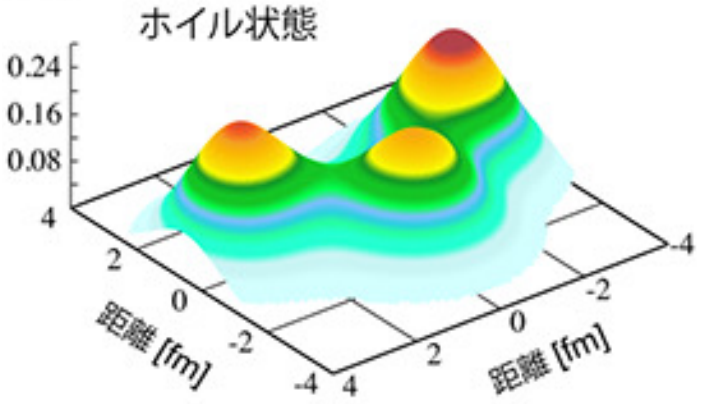

Nuclear application

CV

- Experimental nuclear physics
- Radioactive isotope beams
- Spectroscopy = radiation counting

2000 – 2004	University of Tokyo	
2004 – 2009	Graduate School of Science, University of Tokyo	Master degree (2006) PhD degree (2009)
2009 – 2011	NSCL, Michigan State University	Visiting research associate
2012 – 2015	IPN Orsay (France)	Research scientist (CR2)
2015 to present	RIKEN Nishina Center	Research scientist

CV

2000 – 2004 University of Tokyo

2004 – 2009 Graduate School of Science, University of Tokyo Master degree (2006)
PhD degree (2009)

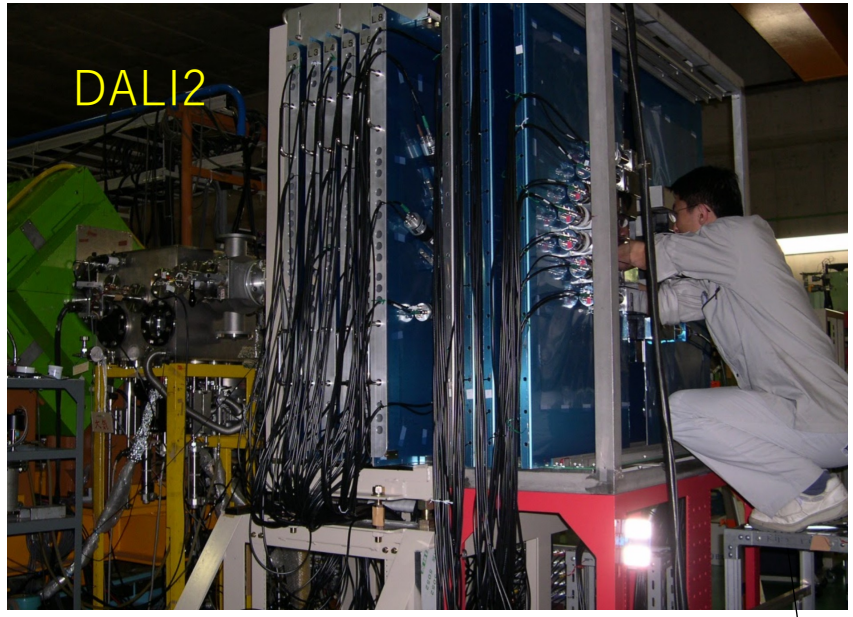

RIKEN RIPS 2004

GANIL 2007

Deformation and halo **Mirror symmetry**

Ong Hooi Jin (王恵仁)

CV

2009 – 2011	NSCL, Michigan State University	Visiting research associate
2012 – 2015	IPN Orsay (France)	Research scientist (CR2)

Prototype AT-TPC (2011)

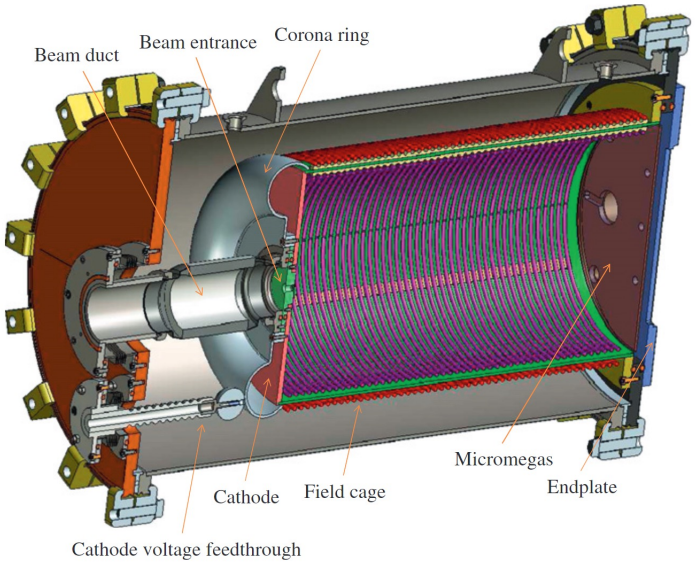

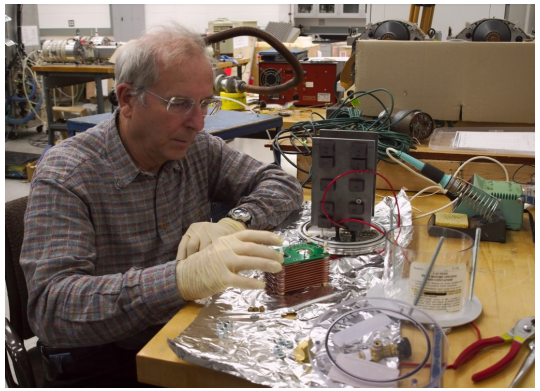

Molecular cluster

^{10}Be via ^{6}He(α,α)

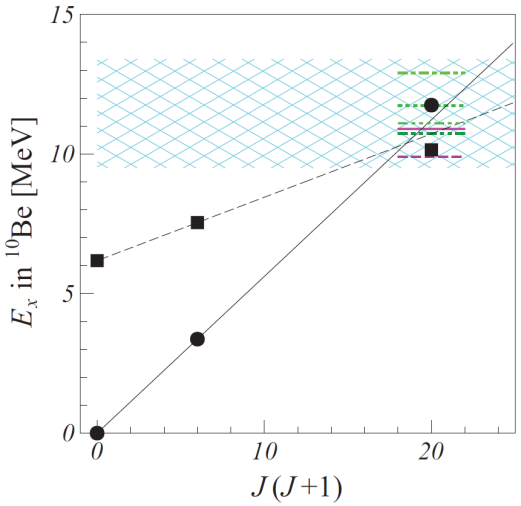

D. Suzuki+ PRC 2013

Linear chain

^{14}C via ^{10}Be(α,α)

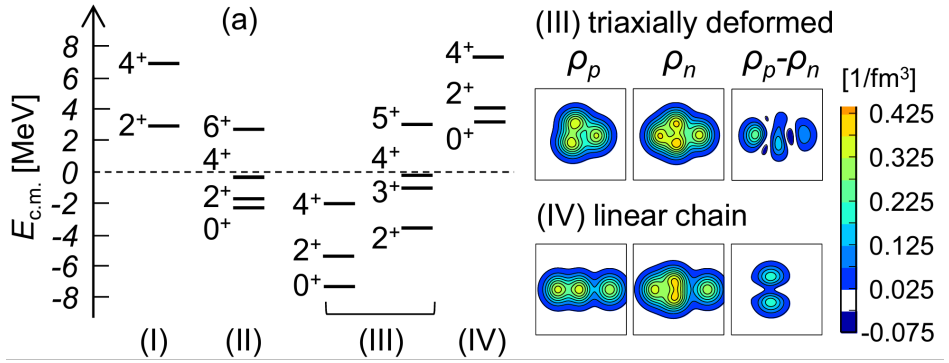

A. Fritsch+ PRC 2016

HiCARI project at RIBF

First in-beam gamma-ray spectroscopy using tracking Ge detectors array at RIBF.
Various physics including possible magicity loss of N = 50 onset beyond ^{78}Ni.

IMP clover detectors
(not shown in photo)

^{78}Ni

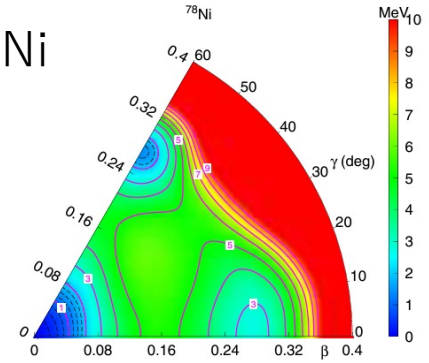

^{76}Fe

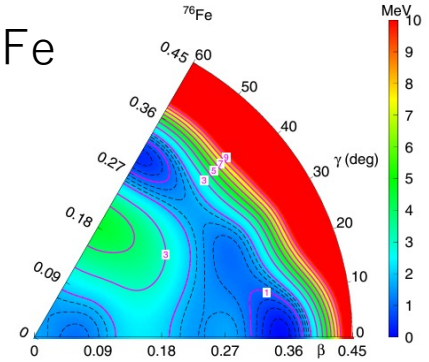

^{74}Cr

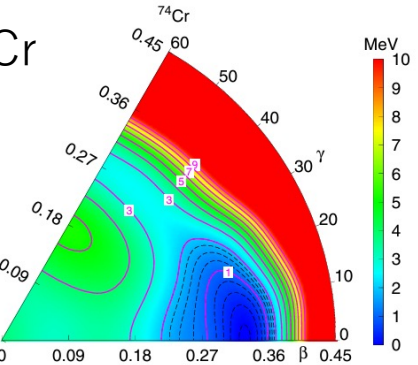

SAKURA project at OEDO

(d,p) surrogate reactions for neutron capture cross sections
for explosive burnings

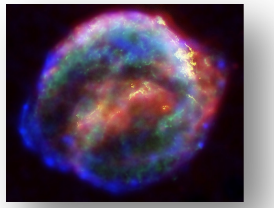

Molybdenum isotope abundance puzzle

5.5%, 1.9% ^{94,96}Ru

14.7%, 9.2% ^{92,94}Mo

^{56}Ni

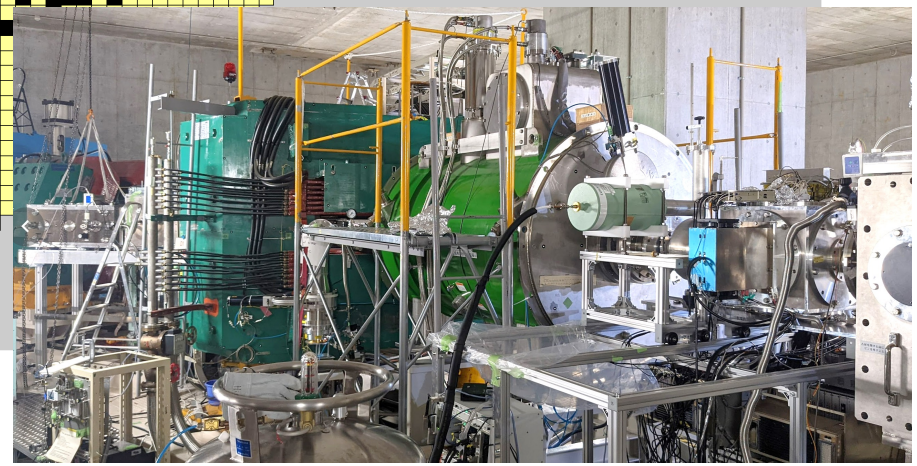

Today, I will talk about nuclear structure studies with RI beams.
But to introduce, please let me ask one question.

We are in 2024.
This is 50 years anniversary of ( ) ?

Do you recall any memorable events in 1974?

50 years anniversary of Rubik's Cube

Simplicity → **Complex puzzle**

- Cube geometry
- 8 corners, 12 edges
- 3 x 3 x 3 faces
- 6 colors

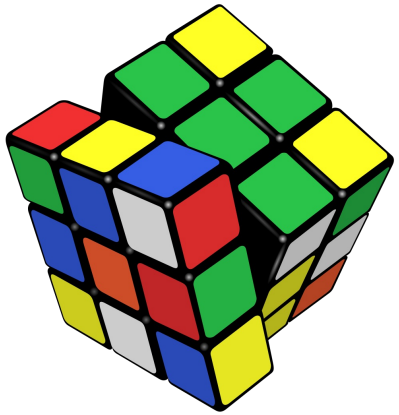

Total number of permutations

$$8! \times 3^7 \times \frac{12!}{2} \times 2^{11} = 43{,}252{,}003{,}274{,}489{,}856{,}000$$

$$4 \times 10^{19}$$

Order

e.g. 'God's number'

The fewest possible moves to solve any scrambled configurations.

God number of Rubik Cube is 20 (proved in 2010).

Nuclear structure

Simplicity

- 2 ~ 300 particles
- 2 colors (proton and neutron)
- Nuclear force / Coulomb force
- Quantum states
- Self-organizing object

Complex puzzle

Infinite possibilities of
nucleon many-body states

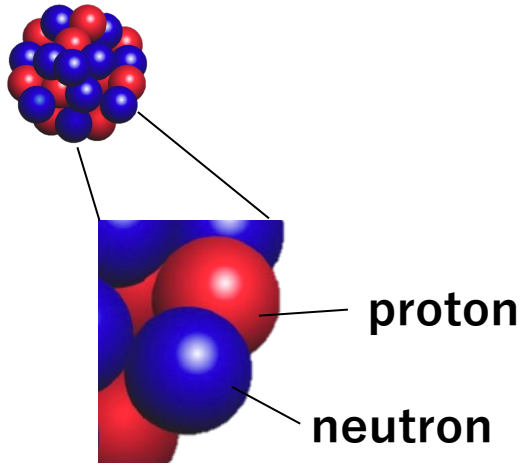

Order

e.g. Magic numbers

Single-particle motion & collective motion

Almost 50 years anniversary

The Nobel Prize in Physics 1975

Photo from the Nobel Foundation archive.
Aage Niels Bohr
Prize share: 1/3

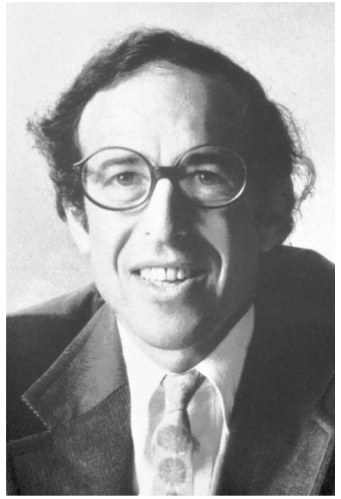

Photo from the Nobel Foundation archive.
Ben Roy Mottelson
Prize share: 1/3

Photo from the Nobel Foundation archive.
Leo James Rainwater
Prize share: 1/3

The Nobel Prize in Physics 1975 was awarded jointly to Aage Niels Bohr, Ben Roy Mottelson and Leo James Rainwater "for the discovery of the connection between collective motion and particle motion in atomic nuclei and the development of the theory of the structure of the atomic nucleus based on this connection"

Particle motion

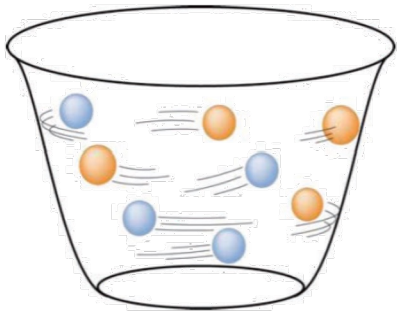

??

Collective motion

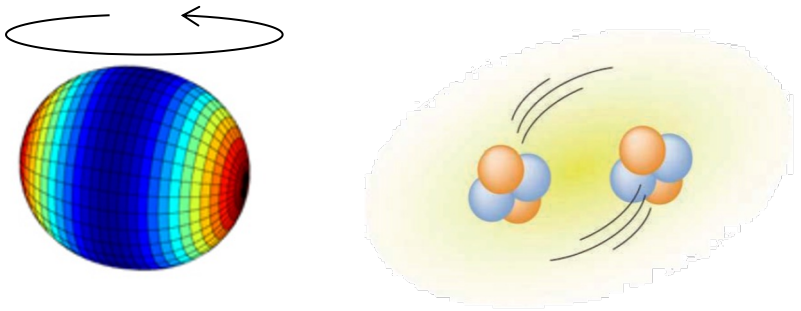

Magic numbers and shell structure

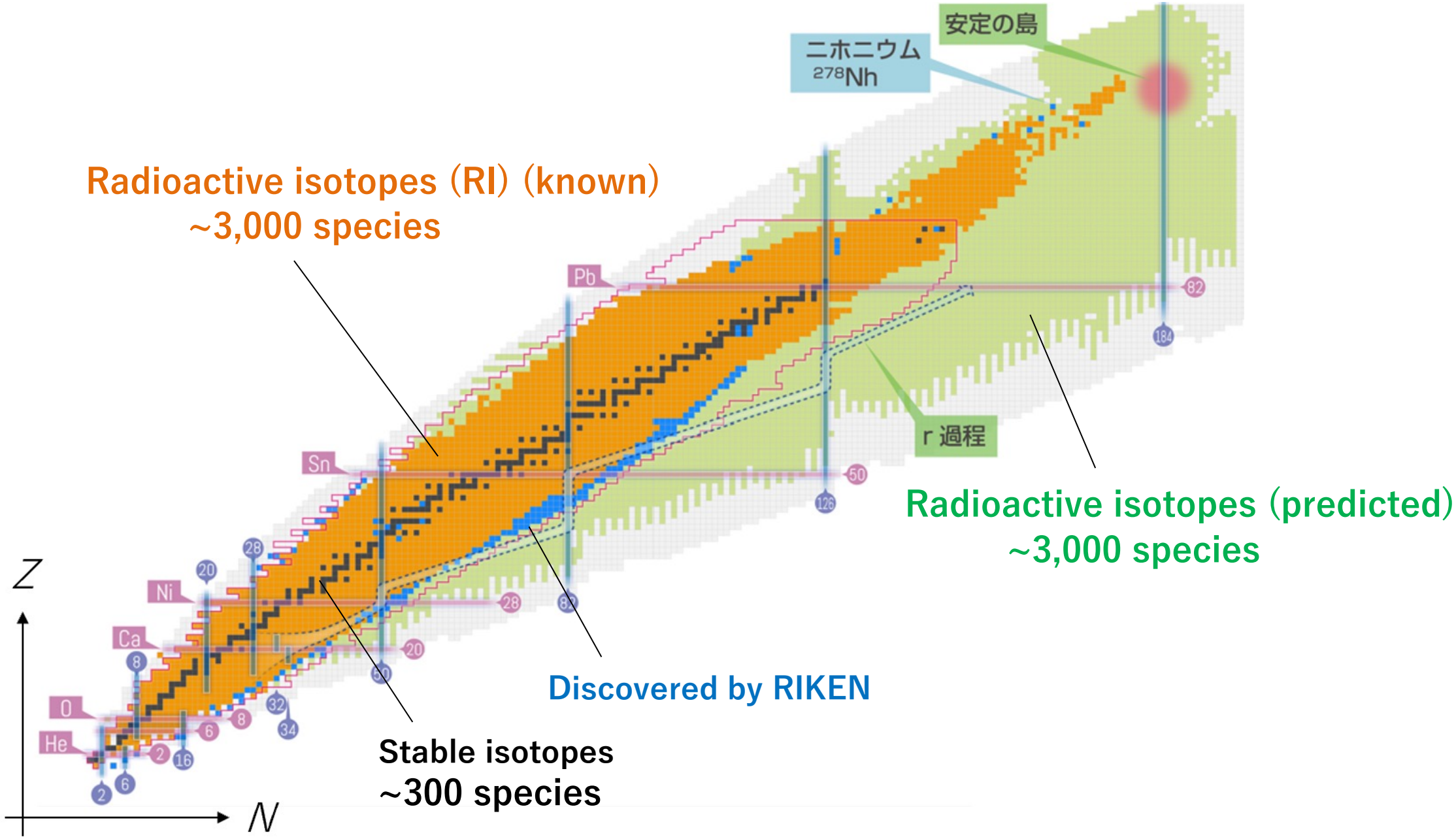

Magic numbers and shell structure

Neutron and proton magic numbers (2, 8, 20, 28, 50, 82, 126) indicate **independent particle motion in a one-body mean field potential**.

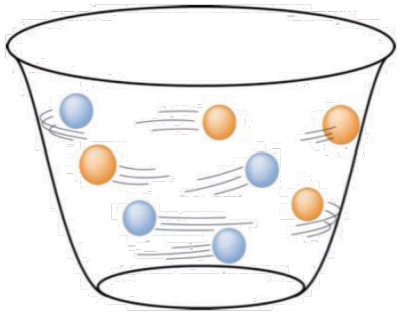

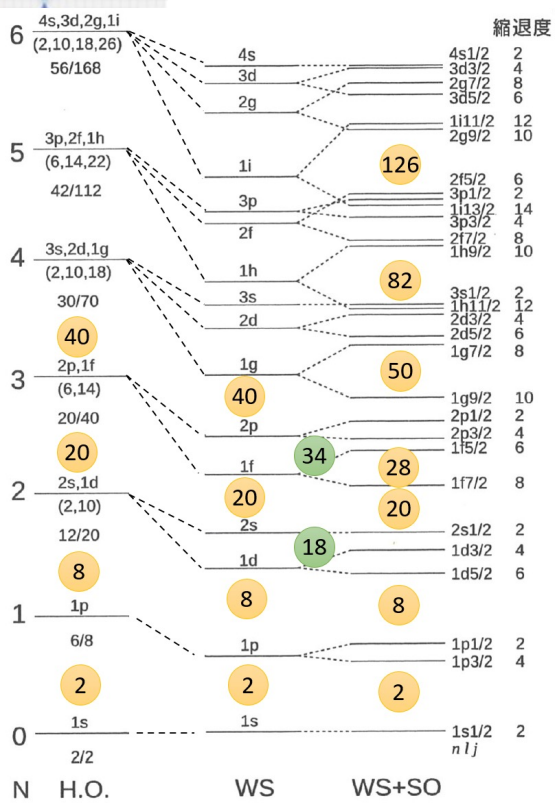

Deformation

Except for magic nuclei, **majority of nuclei are found to be deformed.**

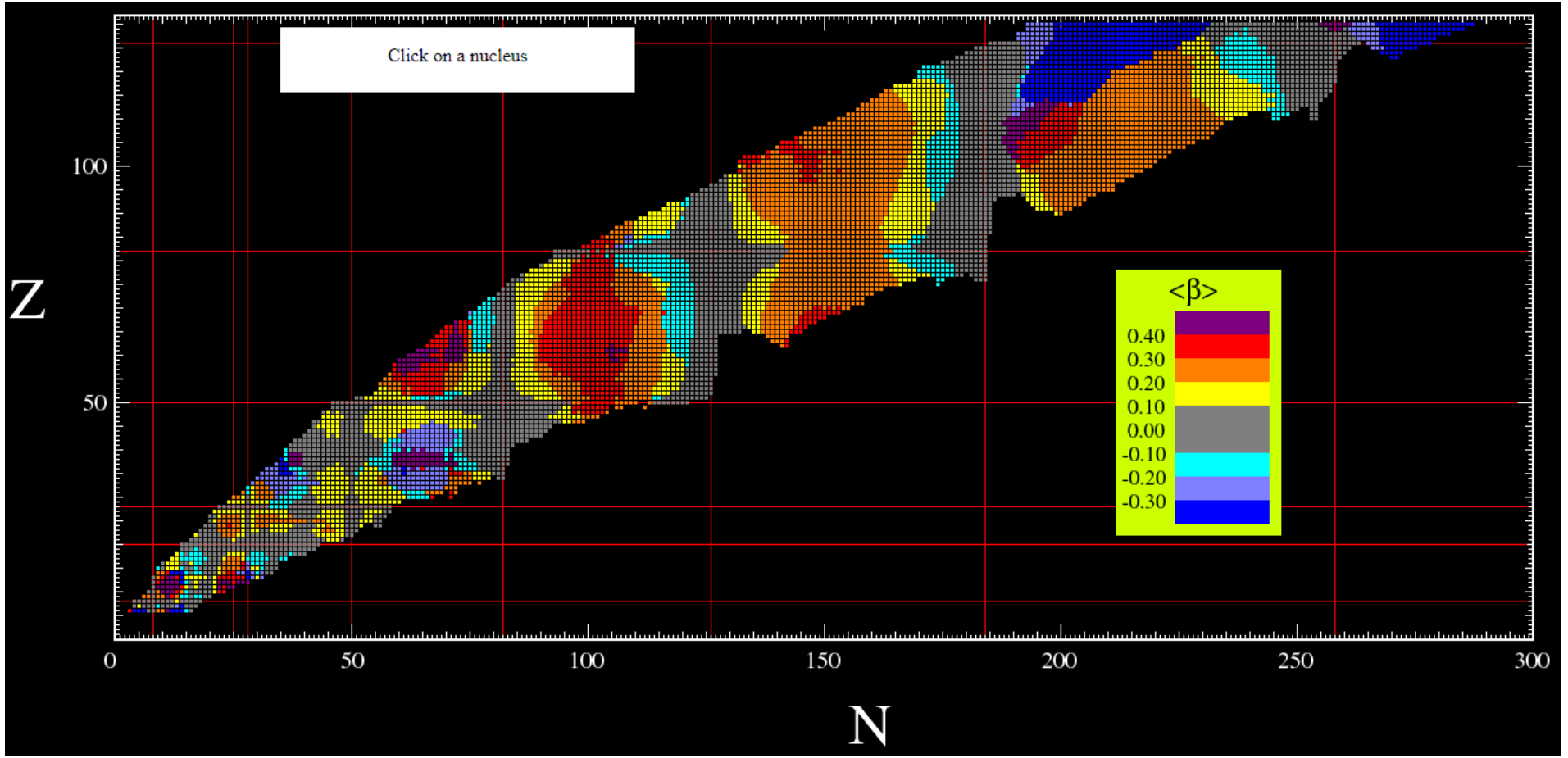

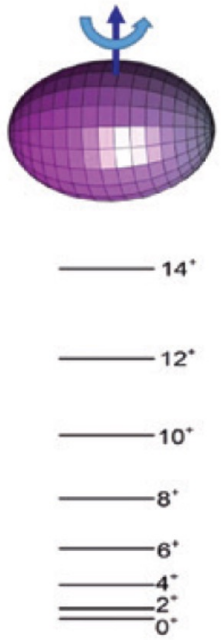

$<\beta>$ for ground states calculated by **Hatree-Fock-Bogoliubov theory** using Gogny force

S.Hilaire, M.Girod http://www-phynu.cea.fr/science_en_ligne/carte_potentiels_microscopiques/carte_potentiel_nucleaire_eng.htm

Outline

How do single-particle and collective motions come into being?

1. Puzzle of single-particle motion
2. Puzzle of magic number N = 20
3. Puzzle of oxygen dripline

- What is the origin of single-particle motion?
- Why are the majority of atomic nuclei deformed?
- Why are the single-particle and collective motions closely linked?
- How do single-particle and collective motions evolve away from stability?

Nuclear physics School for Young Scientists
(NUSYS-2024)

Puzzle of single-particle motion:

One-body nuclear mean-field is not trivial matter

Beijing Normal University (Zhuhai, Guangdong)
July 27 to August 2, 2024

- Historical overview
- Why are studies with RI beams important?

First concept of shell structure in 1930s

Genshikaku Kenkyu (Journal of nuclear physics community in Japan)

原子核研究　第68巻1号

‘Guggenheimer in the year 1934 (I)’

1934 年のグッゲンハイマー　I

T. Uesaka and D. Suzuki

上坂友洋、鈴木大介

理化学研究所・仁科加速器科学研究センター

First concept of shell structure in 1930s

Remarks on the constitution of atomic nuclei. I.

REMARQUES SUR LA CONSTITUTION DES NOYAUX ATOMIQUES. I.

Par K. GUGGENHEIMER.

Sommaire. — Limites de stabilité des diverses catégories d'atomes. Existence probable à l'intérieur des noyaux de couches indépendantes de neutrons et de protons.

概要　－　様々な種類の原子の安定性の境界について。原子核の内部に中性子と陽子の独立した層がおそらく存在すること

Two papers authored by K. Guggenheimer, a Germain exile in Paris in 1934, are today almost forgotten. However, the work provided **several essential concepts** that are imperative in today's nuclear physics.

- **Nulcear chart**
- The word '**isotone**'
- The concept of '**limit of stability**' (which leads to the dripline today)
- **Magicity at 50 and 82**.

First nuclear chart

The constituents of nuclei were thought to be **alpha, proton and electron** 1920s.
Guggenheimer challenged this picture by inventing the nuclear chart, **mapping stable isotopes** (discovered in 1920s) as a function of **proton and neutron** (in 1932).

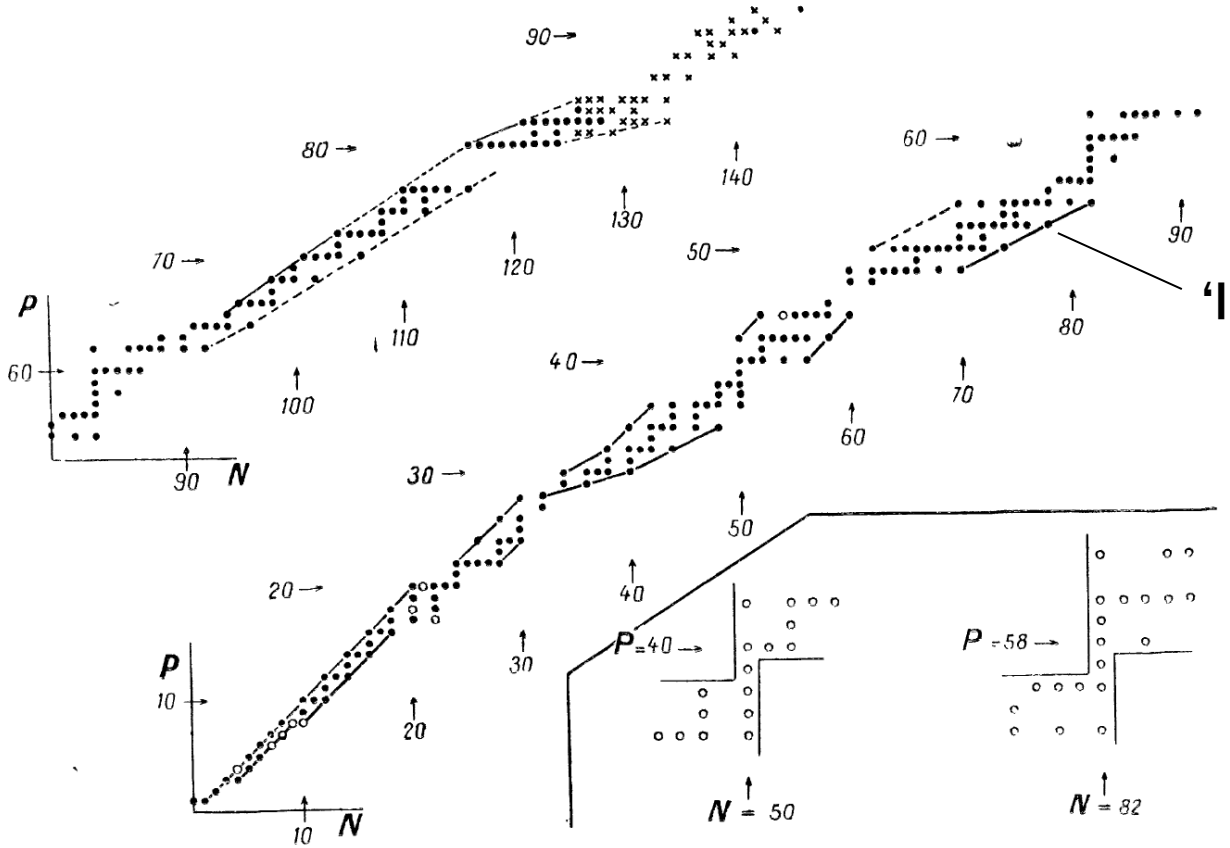

'limit of stability'

Fig 1.

Abscisses : nombre de neutrons } constituant le noyau.
Ordonnées : nombre de protons }

- Noyaux obtenus au spectrographe de masses.
o Noyaux observés spectroscopiquement et extrêmement rares.
× Noyaux naturellement radioactifs.

On n'a pas tenu compte ici des noyaux à radioactivité artificielle.

Magicity at N = 50 and 82

Guggenheimer indicates **extra stability at N = 50 and 82** from the analysis of the length of isotone series and its differential on nuclear chart. He conjectured the energy gaps to shell effects by refering to atomic shell.

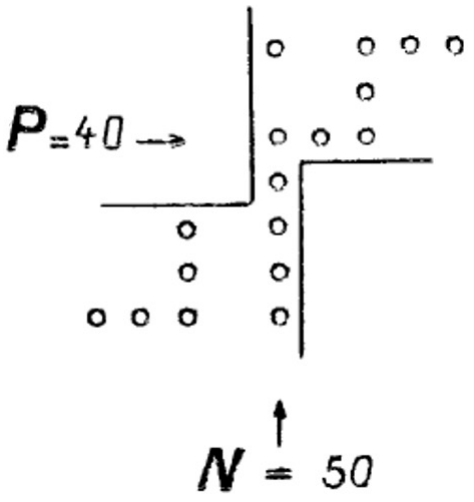

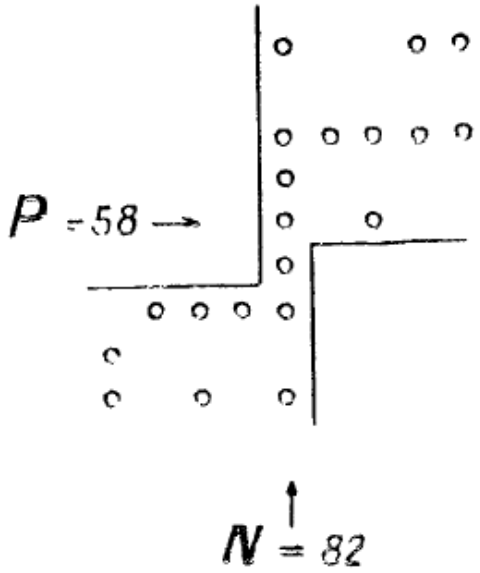

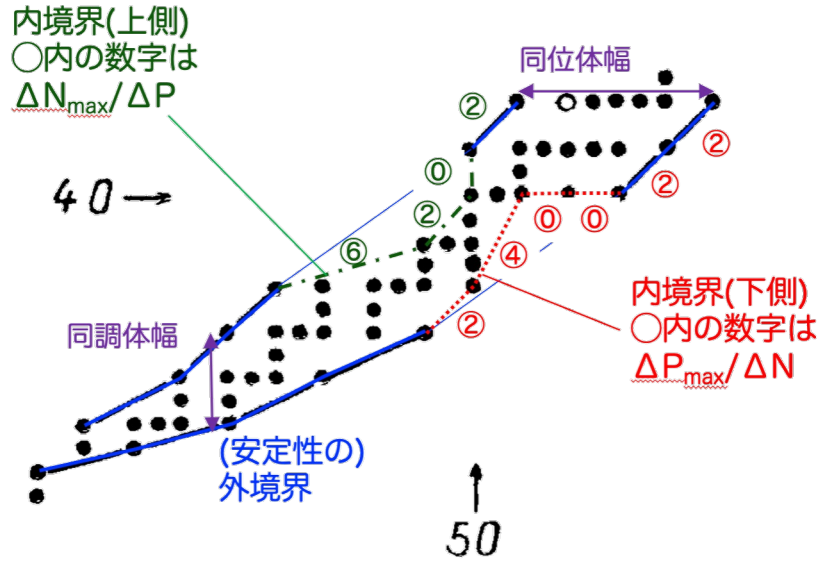

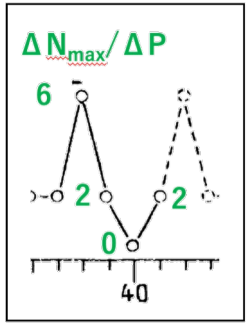

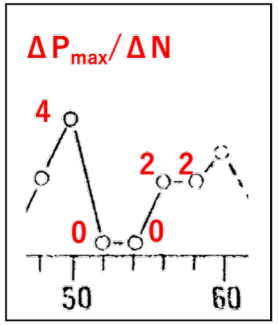

Isotope and isotone

Frederick Soddy
1877-1956

Isotope

‘Isos (**same**) + Topos (**place**)’
in the periodic table

同**位**体

位 = position

Satoyasu Iimori (1885 – 1982)
RIKEN from 1917 to 1952.
Pioneer of radiochemistry in Japan.

↓

Nuclear chemistry group (M. Haba)

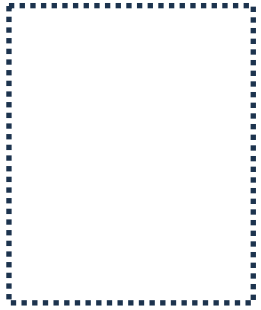

Kurt Guggenheimer

Isotone

Replacing **p**roton with **n**eutron

同**調**体

調 = tone

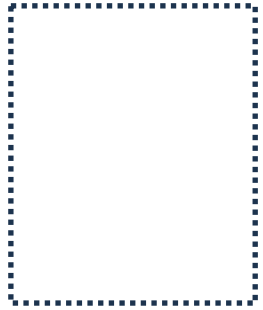

???

Paris in 1934

Walter M. Elsasser was also an exile in University of Paris when Guggenheimer was working at College de France. Elsasser discussed the magicity and the mean field potential.

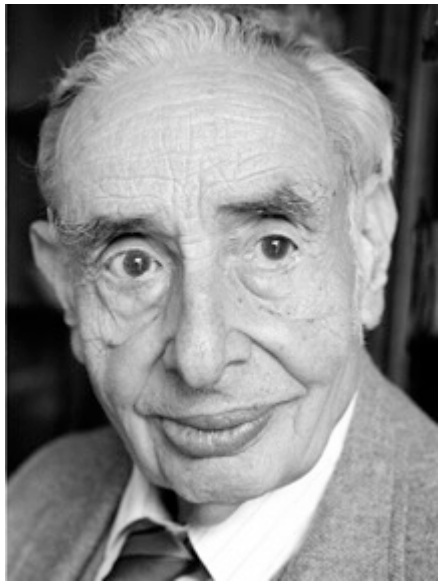

1904-1991

'About the Pauli principle in the nuclei'

SUR LE PRINCIPE DE PAULI DANS LES NOYAUX

Par W. M. ELSASSER.

Sommaire. — En suivant un procédé introduit par Bartlett on établit un système d'enveloppes protoniques et neutroniques et on attribue des nombres quantiques à ces particules, au moins pour les éléments légers. Les enveloppes fermées sont caractérisées par des énergies de liaison spécialement grandes. Ce schéma permet l'explication d'un plus grand nombre de propriétés nucléaires que l'hypothèse du noyau composé de particules α. Dans le cadre de cette structure nucléaire la formation d'une particule α est dûe à une sorte de conversion interne qui précède l'émission. Il est possible d'avoir une indication sur la répartition de l'énergie cinétique et l'énergie potentielle d'une particule nucléaire. On aboutit de cette manière à des énergies potentielles particulièrement grandes.

Elsasser is best known for the dynamo theory as an explanation of the Earth's magnetism and its history.

Mass excess and magicity

Elsasser analysed the **mass of stable isotopes**, and found that extra stability in ^{4}He and ^{16}O, suggesting the **magic numbers 2 and 8**.

$$\Delta = P - N\frac{35.9760}{36}$$

P : 'Poid' = M (mass)
N : 'Nombre' = A (mass number)
Δ : Sort of mass excess

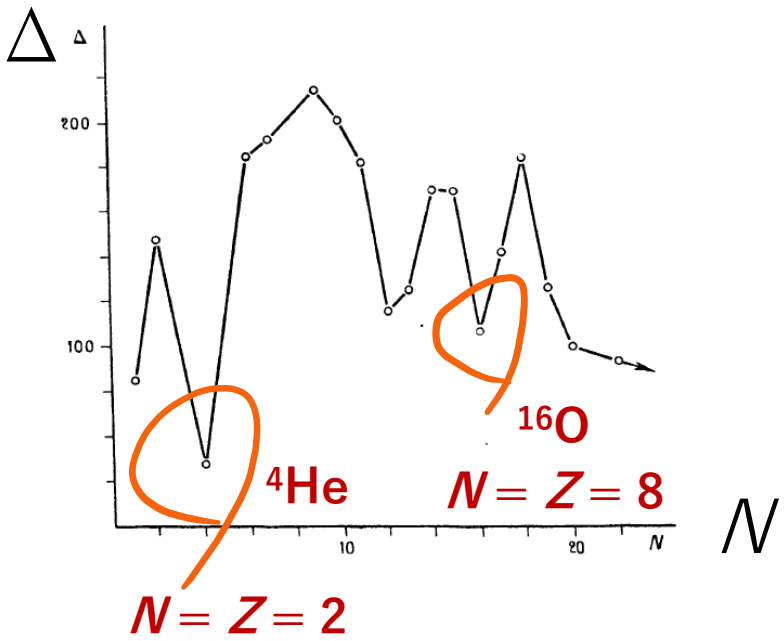

Mean field potential

The **magic number 8 is unexpected** from electronic magic numbers **2 (He), 10 (Ne), 28 (Ar) ....**
→ Potential should be of different shape.

A '**pot' type one-body potential** was introduced to explain the magic number N = 8.

Soit X la valeur d'un certain zéro, on a alors

$$k = \sqrt{\frac{2m}{\hbar}(U - E_l)} = \frac{X}{R_0} \qquad (2)$$

où E désigne la valeur propre de l'énergie. On oblient donc l'ordre suivant pour les énergies appartenant aux divers nombres quantiques

$$1_0,\ 2_1,\ 3_2,\ 2_0,\ 4_3,\ 3_1,\ 5_4,\ 4_2,\ 6_5,\ 3_0 \qquad (3)$$

Une enveloppe avec le nombre quantique azimutal l contient au maximum $2(2l+1)$ particules. De la succession (3), il résulte la possibilité d'arranger les particules dans des enveloppes contenant 2, 6, 10 individus. En identifiant les protons et les neutrons comme ayant les nombres quantiques 1_0, 2_1, 3_2, on peut tirer la conclusion que le potentiel dans lequel une particule nucléaire se meut a une forme relativement plate.

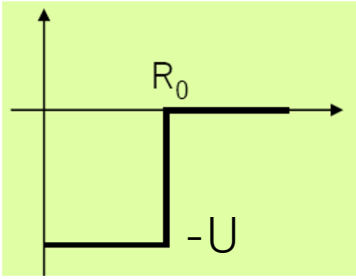

Magic numbers
2, 8, 18

Why flat bottom?

Electronic and nuclear one-body potentials have an essential difference at the origin.
Coulomb potential is divergent, while **nuclear potential has a flat bottom**.
The difference results in the magicity at 8 or 10.

Coulomb potential

$$U(r) = -\frac{e^2}{r}$$

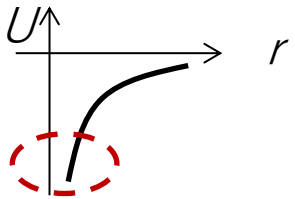

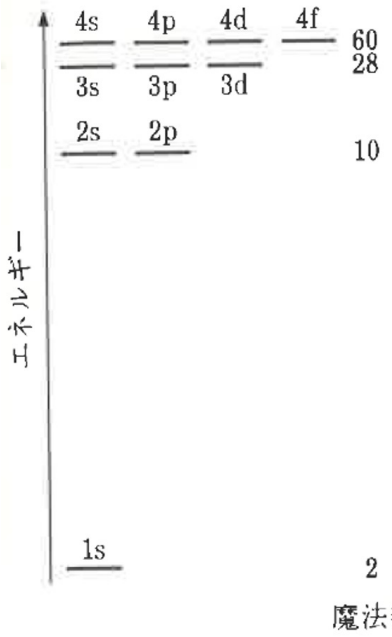

クーロンポテンシャル（原子）

Harmonic oscillator potential

$$U(r) = \frac{1}{2}M_N\omega^2 r^2$$

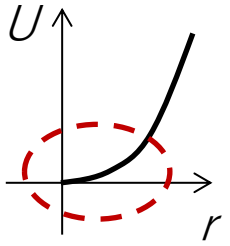

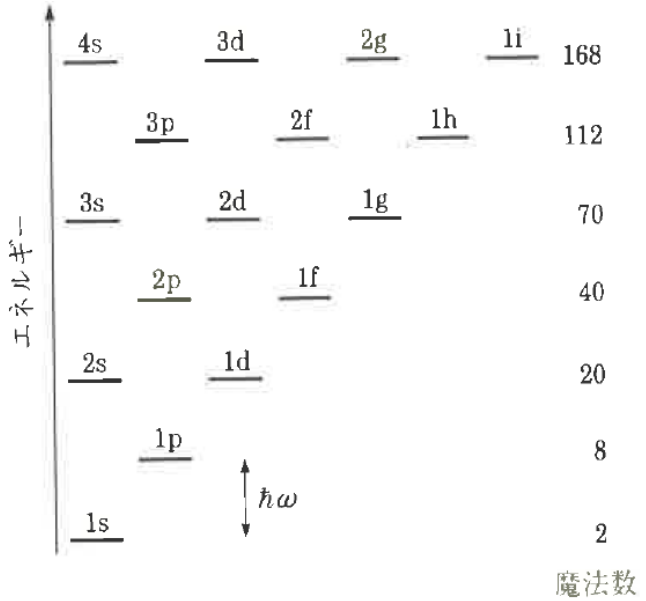

調和振動子ポテンシャル

Saturated and unsaturated matter

Nuclear force in atomic nuclei is saturated.

Unsaturated

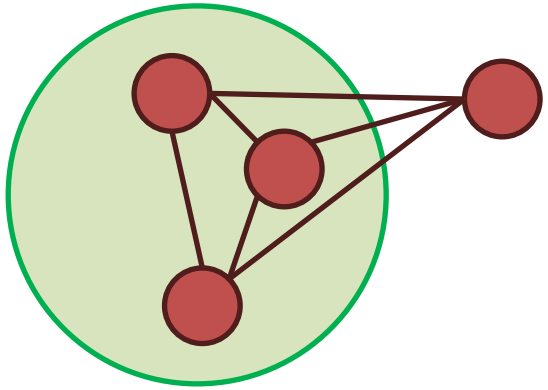

Number of links

A(A-1)/2

Long range

Electromagnetic force
Gravity

Saturated

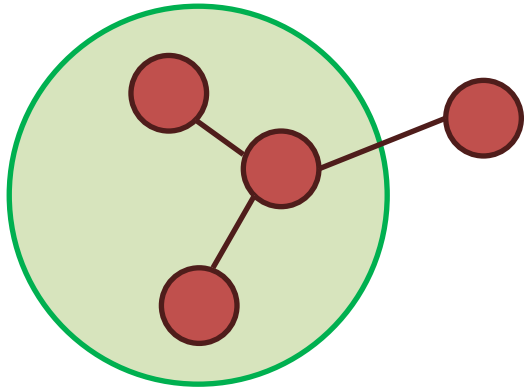

A-1

Short range

Van der waals
Nuclear force

Density saturation

Flat bottom potential reflects the **constant nucleon density** of about 0.16/fm^3 in the interior of nuclei.

Mass number scaling of radii

$r = r_0 A^{1/3}$ r_0 = 1.2 fm (1 fm = 10^{-15} m)

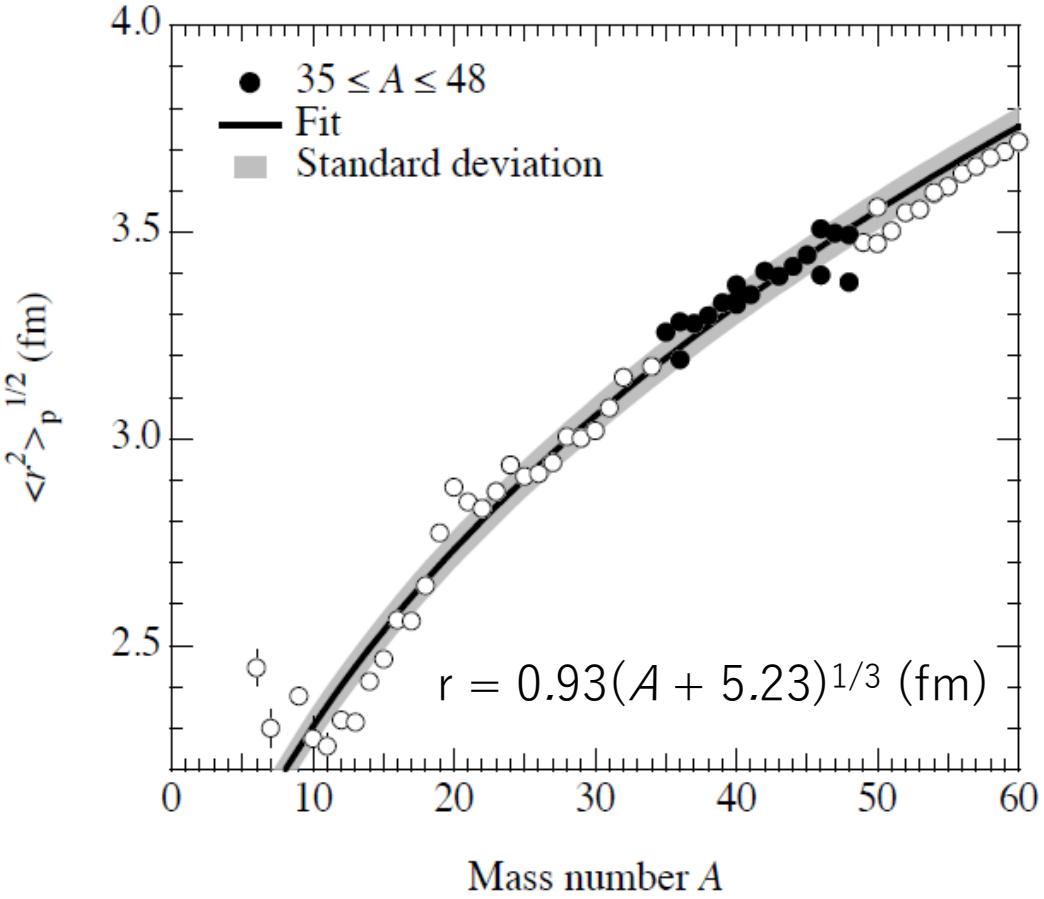

I. Angeli and K.P. Marinova, Atom. Data and Nucl. Data Tabl. 99, 69 ('13).

Almost constant binding energies per nucleon

B.E. /A ~ 8 MeV

Only accouns for 8/940 = 0.7% of nucleon mass

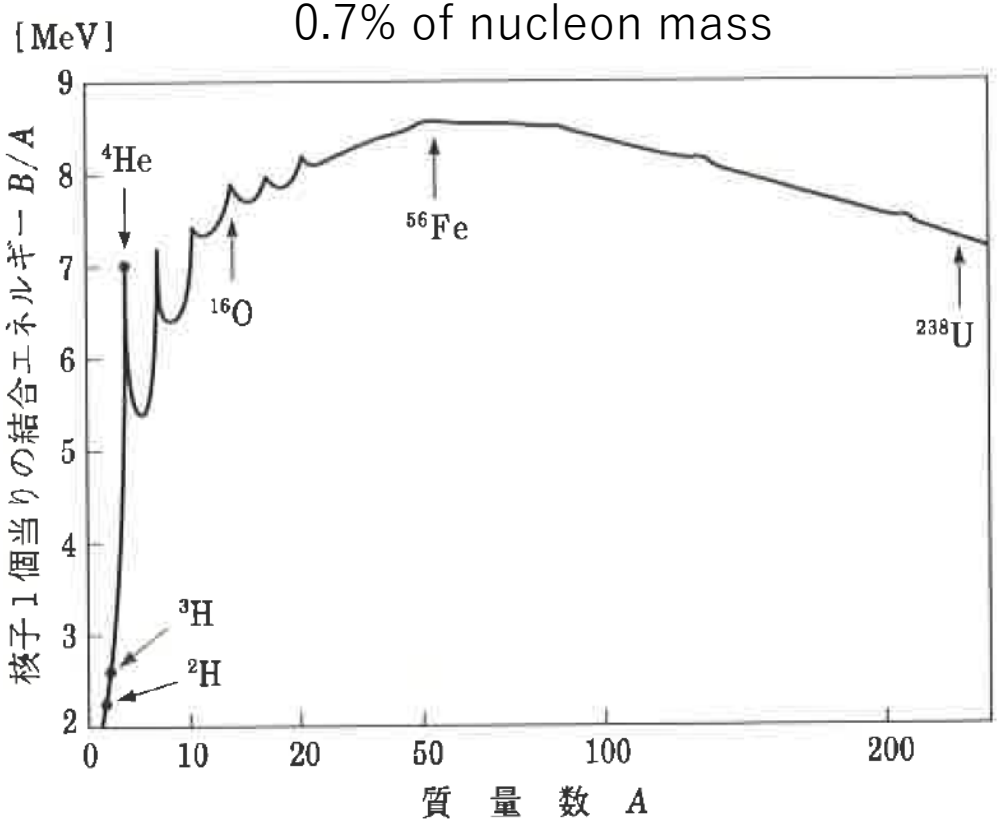

図 2.1 原子核の核子1個当りの結合エネルギー

Density saturation in nuclear mass formula

The saturation nature of atomic nuclei is expressed in the volume term of the mass formula.

Bethe and Weizsacker (1935)

Analogy with classical liquid drop

$$B(A,Z) = b_v A - b_s A^{2/3} - \frac{1}{2} b_{\mathrm{sym}} \frac{(N-Z)^2}{A} - b_C \frac{Z^2}{A^{1/3}} + \delta(A)$$

Symmetry term

Pairing term

r^3 Volume term

r^2 Surface term

$1/r$ Coulomb term

$b_{\mathrm{v}} = 16\ \mathrm{MeV}$ $b_{\mathrm{s}} = 19\ \mathrm{MeV}$ $b_{\mathrm{sym}} = 45\ \mathrm{MeV}$ $b_{\mathrm{C}} = 0.77\ \mathrm{MeV}$

Density saturation in nuclear equation of state (EOS)

Nuclear EOS has **the state variable δ that represents the ratio of proton and neutron** (isospin).
Constraining EOS is one of the most imortant subject in nuclear physics, but this is another story.

$$E(T,\rho,\delta) = E(T,\rho,\delta=0) + E_{sym}(T,\rho)\delta^2 + O(\delta^4)$$

$$\delta = (\rho_n - \rho_p)/\rho$$

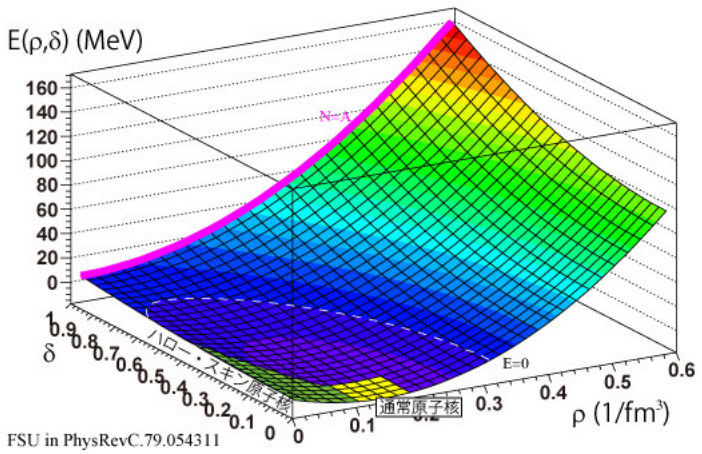

arXiv:1303.0064

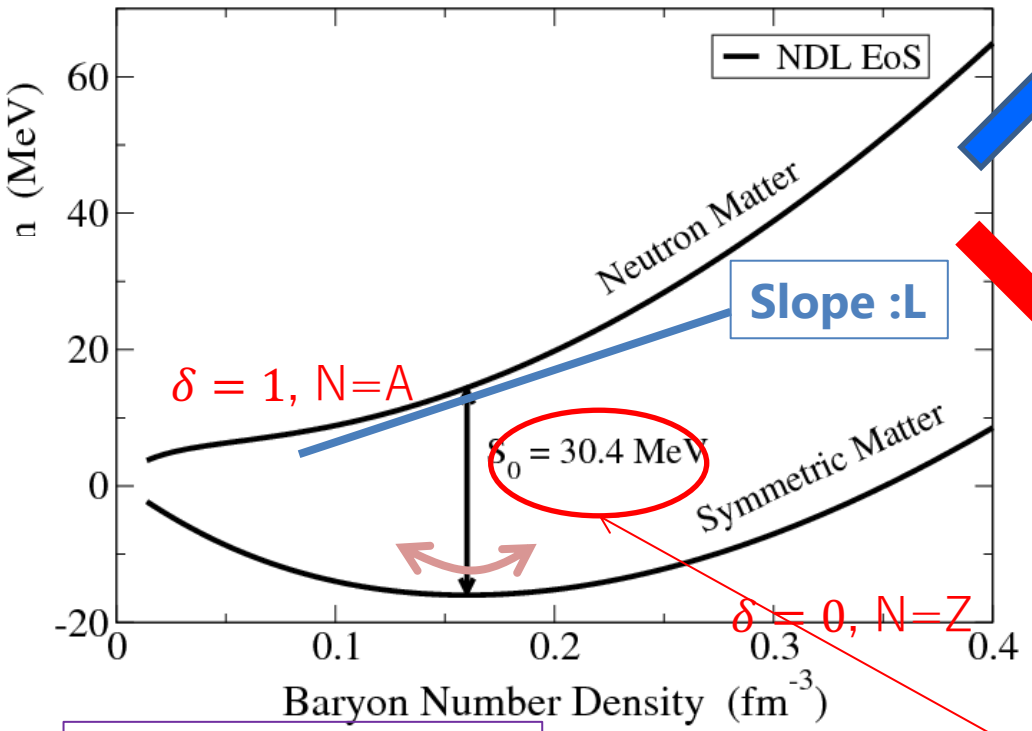

stiff

soft

Incompressibility :K

Symmetry Energy at r=r_0 :S (or J)

Density saturation is not enough to explain magicity

Flat bottom potential can explain N = 2, 8 and 20, but is **not at all effective for N = 28, 50, 82, and 126**.
This indicates that essential effects are missing in the description based on the density saturation.

Woods-saxon potential

$$U(r) = -\frac{V_0}{1+\exp((r-R)/a)}$$

R : radius parameter ($R = r_0 A^{1/3}$, $r_0 = 1.2$ fm)
a : diffuseness (~0.6 fm)

$r < R$ constant depth

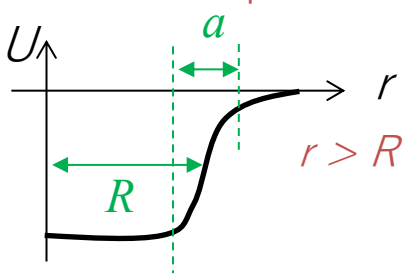

$r > R$ quickly vanishing to zero

The orbitals of the same N split depending on the angular momentum l.

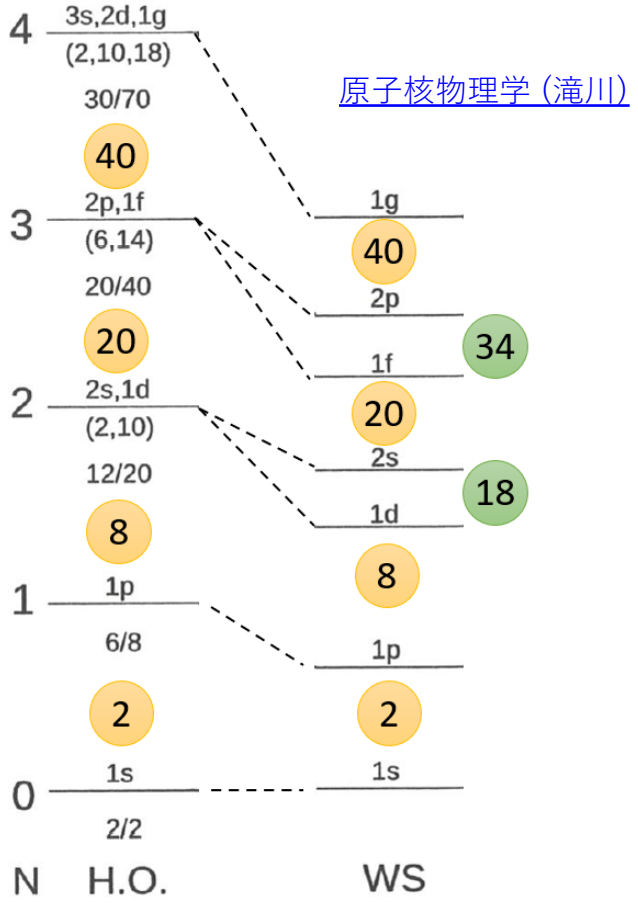

原子核物理学 (滝川)

Spin-orbit coupling

Mayer anad Jensen resolve this issue by introducing the spin-orbit coupling in 1949.

On the "Magic Numbers" in Nuclear Structure

OTTO HAXEL
Max Planck Institut, Göttingen
J. HANS D. JENSEN
Institut f. theor. Physik, Heidelberg
AND
HANS E. SUESS
Inst. f. phys. Chemie, Hamburg

April 18, 1949

A SIMPLE explanation of the "magic numbers" 14, 28, 50, 82, 126 follows at once from the oscillator model of the nucleus,[1] if one assumes that the spin-orbit coupling in the Yukawa field theory of nuclear forces leads to a strong splitting of a term with angular momentum l into two distinct terms $j=l\pm\frac{1}{2}$.

$$U(r) \rightarrow U(r) + W(r)\boldsymbol{l}\cdot\boldsymbol{s}$$

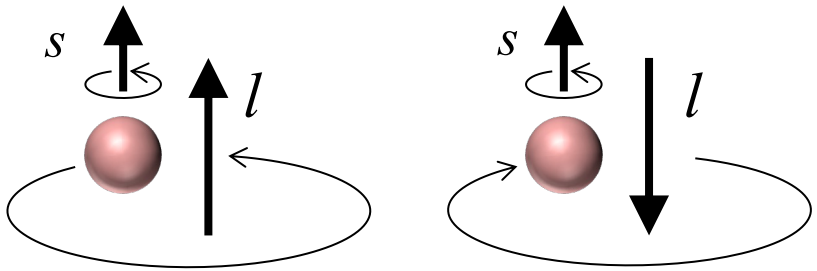

Orbit splits depending on the **parallel or anti-parallel** of spin and angular momentum

The **Nobel Prize in Physics 1963** was divided, one half awarded to Eugene Paul Wigner "for his contributions to the theory of the atomic nucleus and the elementary particles, particularly through the discovery and application of fundamental symmetry principles", the other half jointly to Maria Goeppert Mayer and J. Hans D. Jensen "**for their discoveries concerning nuclear shell structure**"

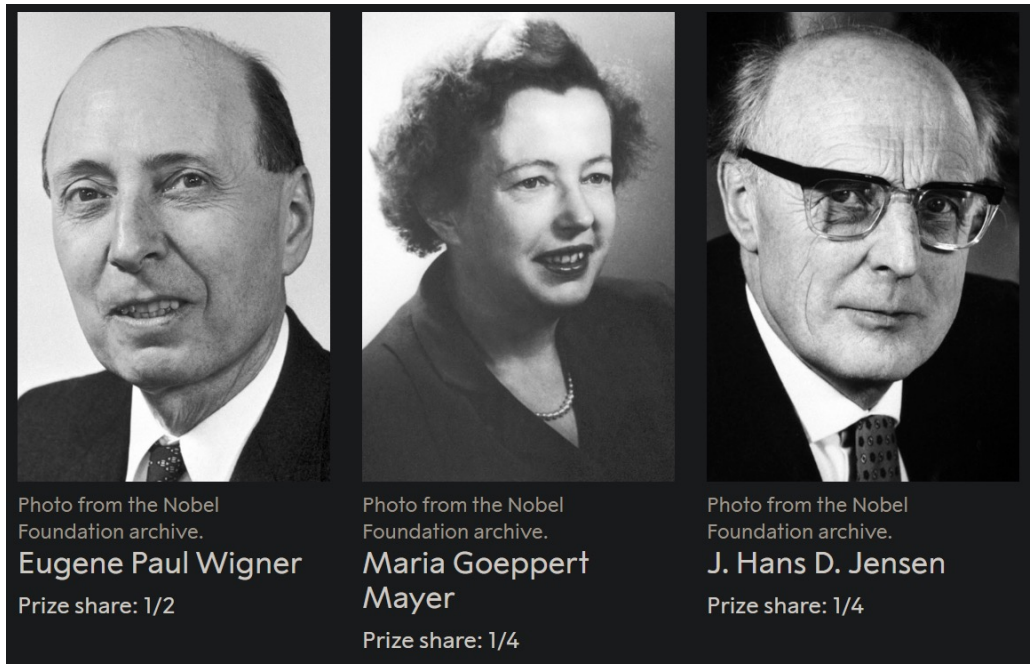

Spin-orbit coupling

$$U(r) \rightarrow U(r) + W(r)\boldsymbol{l}\cdot\boldsymbol{s}$$

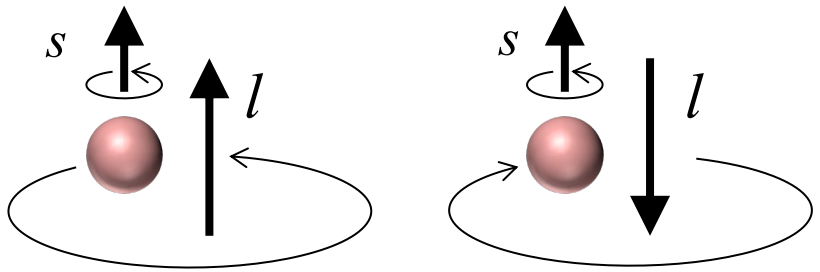

Orbit splits depending on the **parallel or anti-parallel** of spin and angular momentum

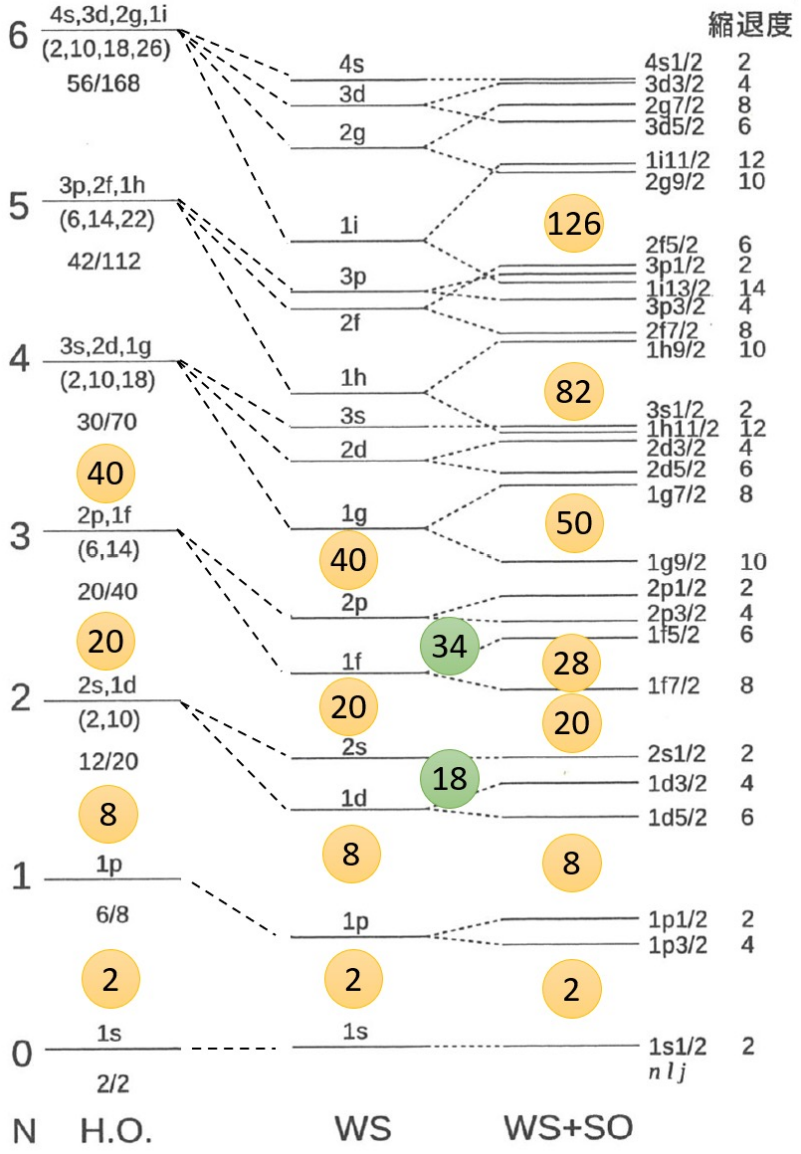

What is the origin of spin-orbit potential?

The spin-orbit term of nuclear force is too weak to account for the spin-orbit splitting.
This was understood as an essential issue of this potential.

The importance of **the tensor force** was pointed out
(Feingold, Wigner, 1950/ Arima, Terasawa, 1960)

Core polarization by tensor force

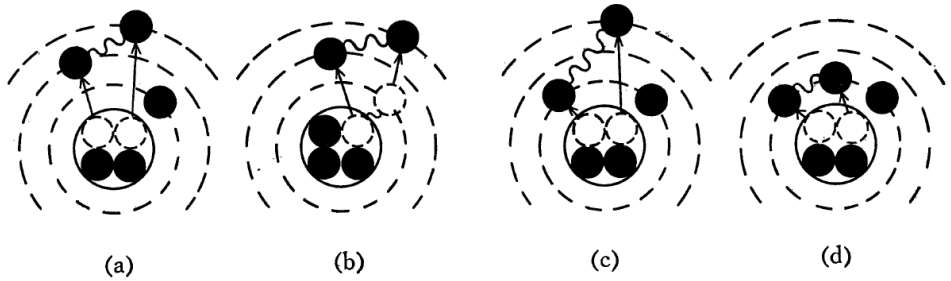

Fig. 1. Figures (a), (b), (c) and (d) show configurations (I), (II), (IIIa) and (IIIb) in He^5, respectively.

$$S_{12} = 2\left[3(\mathbf{S}\cdot\hat{\mathbf{r}})^2 - \mathbf{S}^2\right]$$

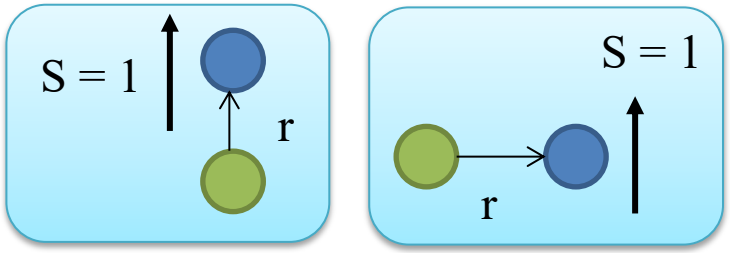

What is the origin of spin-orbit potential?

The three-body force (Fujita, Miyazawa, 1957) is another possible origin.

Spin-Orbit Coupling in Heavy Nuclei

Jun-ichi FUJITA and Hironari MIYAZAWA

Department of Physics, University of Tokyo, Tokyo

(Received October 27, 1956)

In the preceding paper we have calculated the three-body forces in the static approximation. Using the result a strong spin-orbit coupling, compared with the Thomas term, is derived in this paper. Though it is not sufficient to explain the observed spin-orbit coupling for itself, we expect that a considerable part of the nuclear spin-orbit interaction should be due to the many-body forces.

The integration of last equation can be carried out easily and

$$\int_0^\infty E_{\text{eff}}(1)\,dz_1 = \{C\pi(2\pi)^3/4(2\pi^2)^2\}\,\{P_F^3/(P_F^2+1)\}$$
$$\times[8/3-1/P_F^2(2+1/P_F\sqrt{P_F^2+1}\,\log|(\sqrt{P_F^2+1}-P_F)/(\sqrt{P_F^2+1}+P_F)|]$$
$$\cdot(\boldsymbol{P}\times\sigma)_z. \qquad (16)$$

Inserting the numerical values, $P_F=3/2$ and $f^2/4\pi=0.08$,

$$\int_0^\infty E_{\text{eff}}(1)\,dz_1 = -0.94\times10^{-26}(\boldsymbol{l}\sigma)/R \ \text{(Mev.cm)}. \qquad (17)$$

This result is about 4.3 times as large as that of the Thomas term, as seen from the discussion in Sec. 2.

Puzzle of single-particle motion

One-body mean-field potential is much more complex than imagined
due to many-body correlations.

Density saturation

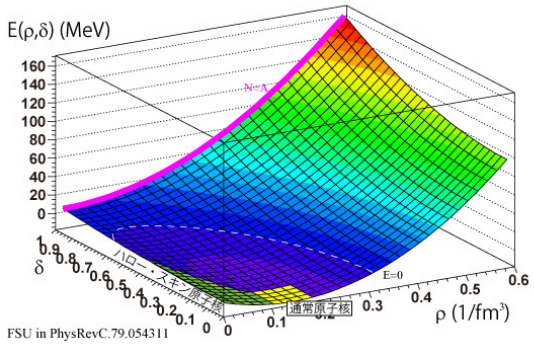

Flat-bottom potential

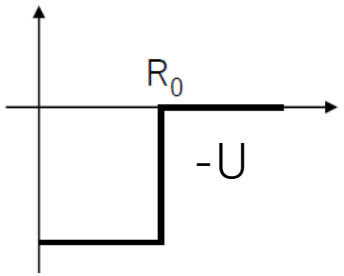

Many-body correlations

Spin-orbit, tensor, three body,
continuum…

Dependence on spin,
isospin, density …

Radioactive isotope beams!

Evolution of nuclear mean-field

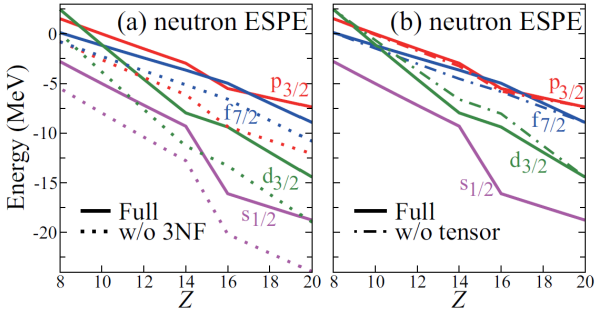

Nuclear physics School for Young Scientists
(NUSYS-2024)

Puzzle of magic number N = 20:

Mutual evolution of single-particle and collective motions

- Historical overview of ^{32}Mg
- Essence of spectroscoy with RI beams
- What is behind mutual evolutions?

Beijing Normal University (Zhuhai, Guangdong)
July 27 to August 2, 2024

Basics of ion beam facility

Before describing RI beam innovations, we need to know **fundamentals related to ion beam acceleration and transport**.

There are three major components

Ion source

Ionize neutral atoms

Accelerator

Accelerate ions

Beam transport

Transport ions

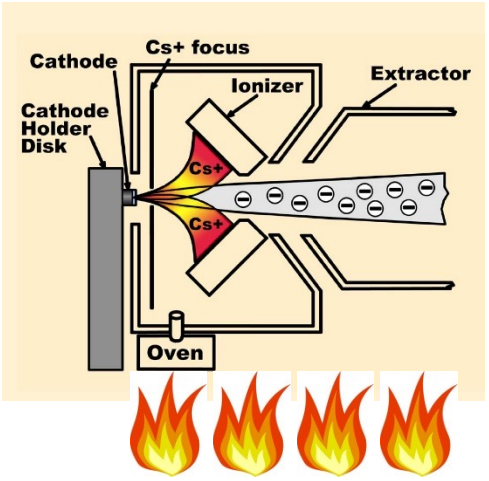

pelletron.com

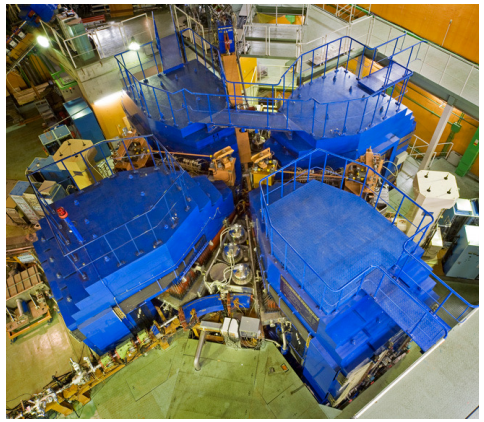

Riken Ring Cyclotron

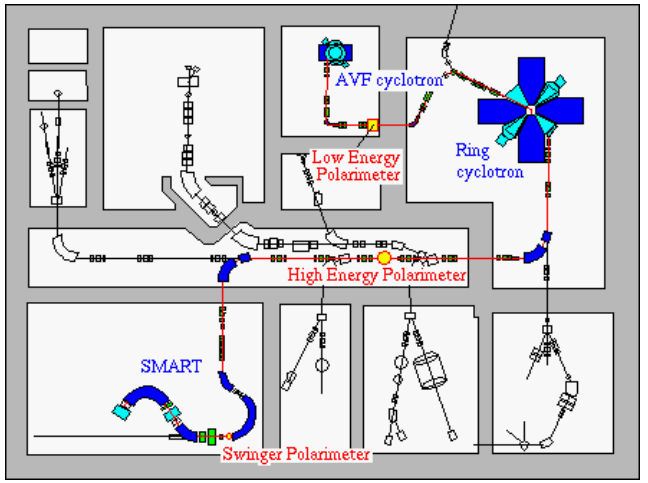

Layout of RARF

To realize RI beam facility

RI beam facilities rely on the same general layout of acelerator facility, **implementing functionalities of RI beam production/separation/identification**. Depending on the implementation, there are two major types: **ISOL and in-flight**.

ISOL

Ion source

Ionize neutral atoms

Accelerator

Accelerate ions

In-flight

Beam transport

Transport ions

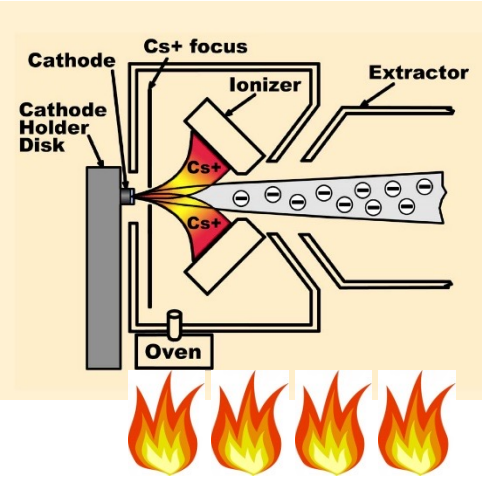

pelletron.com

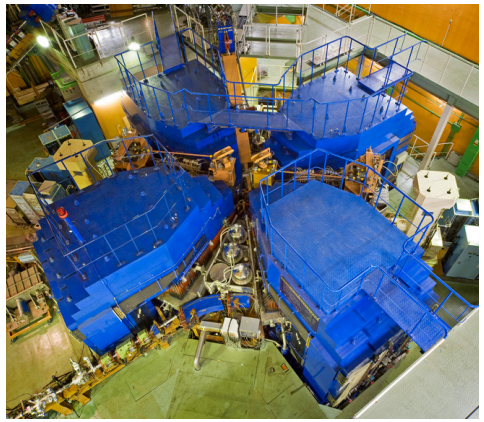

Riken Ring Cyclotron

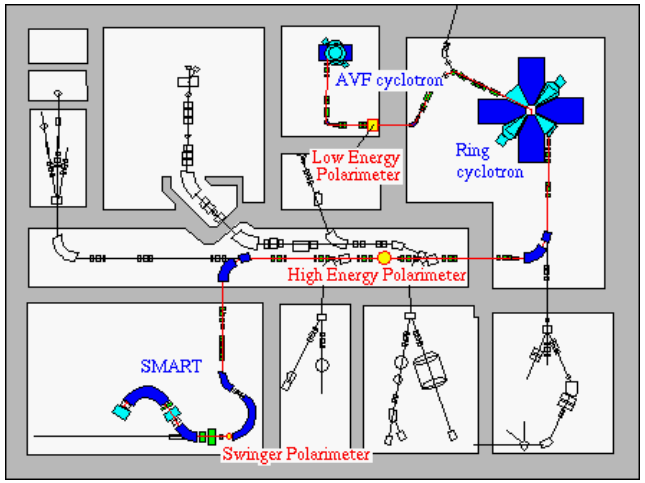

Layout of RARF

ISOL (ISOtope OnLine)

ISOL facility uses **‘online’ ion source**, which generates RI by using a beam. **The same accelerator and beam transport system for a stable beam** is used.

No change

Online ion source

Accelerator
Accelerate ions

Beam transport
Transport ions

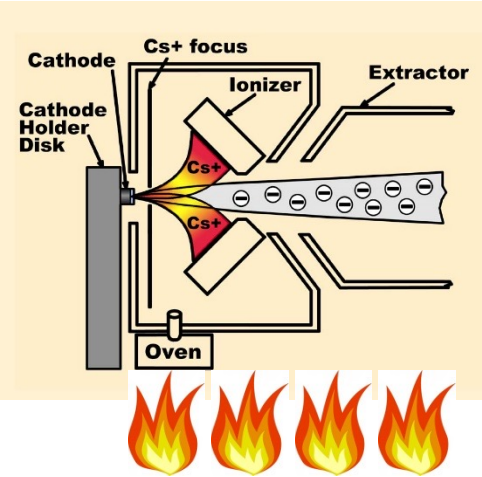

pelletron.com

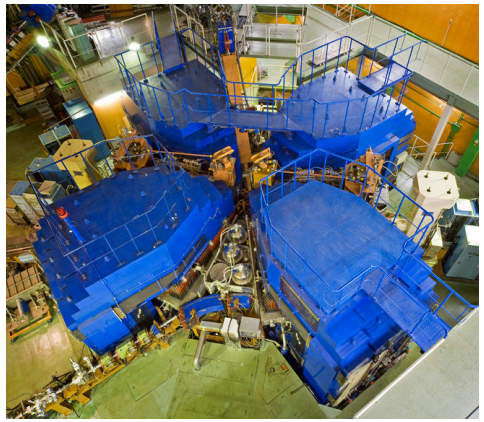

Riken Ring Cyclotron

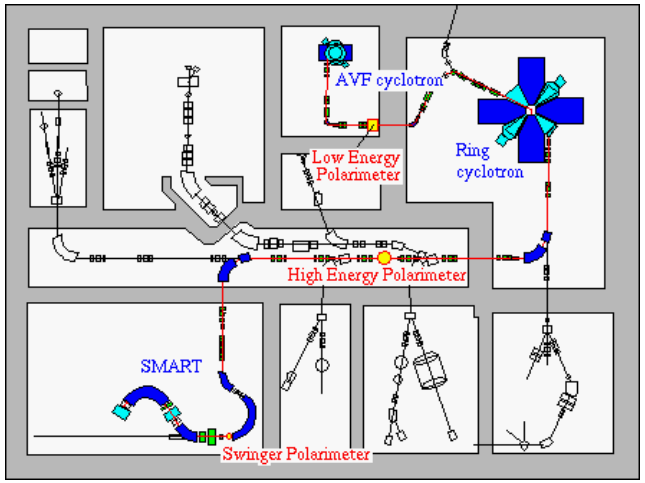

Layout of RARF

ISOL (ISOtope OnLine)

Offline standard source is supplied neutral atoms with stable isotopes from the material input.
For online ion source, the material input is **pipelined to a production target of RI**.

Layout of standard ion source

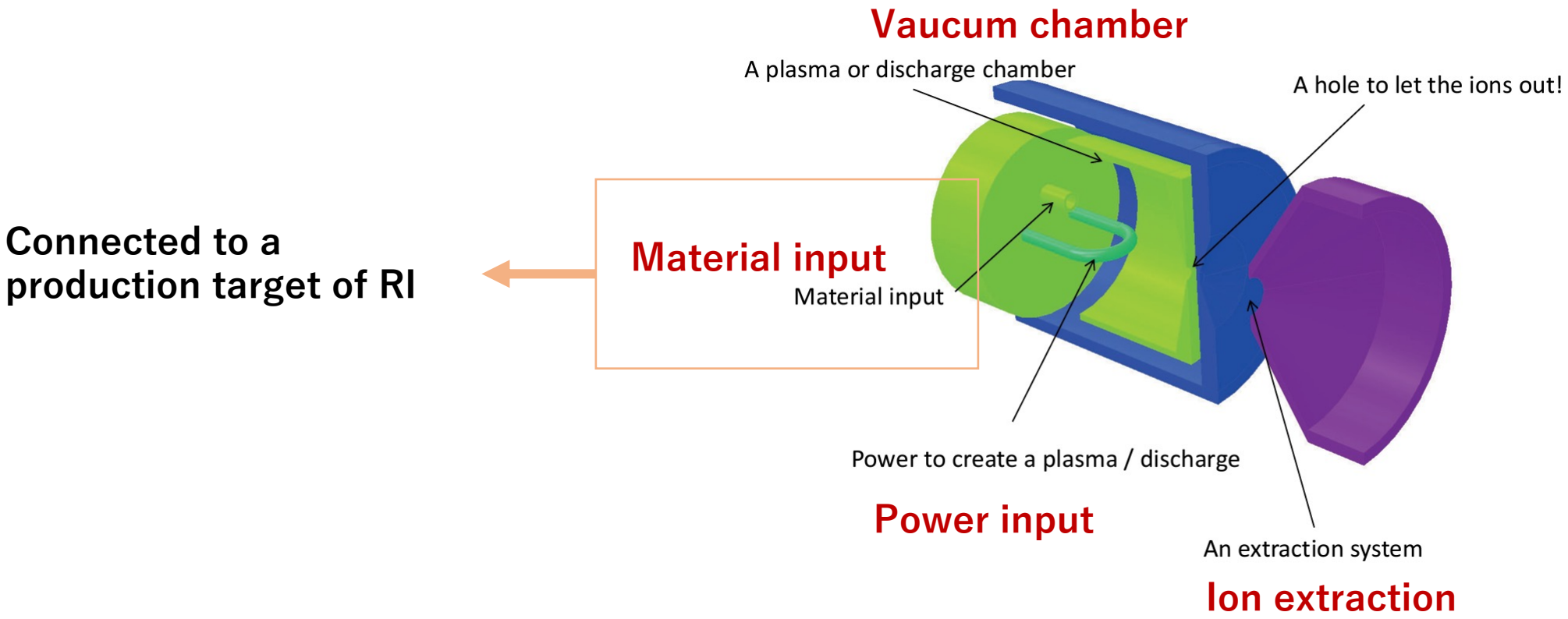

ISOL facility in the world

The ISOL technique was **invented in Copenhagen over 50 years ago** (in 1950s) and eventually migrated to CERN where a suitable proton drive beam was available at the Syncho-Cyclotron.

GANIL SPIRAL

SPIRAL2 (202X-)

Korea RAON (2021-)

TRIUMF

ARIEL (202x-)

CERN ISOLDE

HIE-ISOLDE (2021-)

SPES (2020-)

Magicity loss at $N = 20$: First contact

Mass anomaly was found for **^{31}Na (with N = 20)** and **^{32}Na (N = 21)** at ISOLDE, CERN

C. Thibault+ NPA 1975

Direct measurement of the masses of ^{11}Li and $^{26-32}$Na with an on-line mass spectrometer

C. Thibault, R. Klapisch, C. Rigaud, A. M. Poskanzer,* R. Prieels,† L. Lessard,‡ and W. Reisdorf§

Laboratoire René Bernas du Centre de Spectrométrie Nucléaire et de Spectrométrie de Masse, 91406 Orsay, France

(Received 17 March 1975)

The use of an on-line mass spectrometer to make direct mass measurements of short-lived isotopes far from the stability line has been improved to yield more accurate mass measurements for $^{27-30}$Na, new mass measurements for ^{11}Li, $^{31, 32}$Na, and to remove a discrepancy between existing mass measurements of ^{26}Na. The mass excesses (keV) measured are: ^{11}Li, 40940 ± 80; ^{26}Na, −6901 ± 25; ^{27}Na, −5620 ± 60; ^{28}Na, −1140 ± 80; ^{29}Na, 2650 ± 100; ^{30}Na, 8370 ± 200; ^{31}Na, 10600 ± 800; ^{32}Na, 16400 ± 1100. The ^{11}Li value indicates that it is bound by only 170 ± 80 keV. The masses of ^{31}Na and ^{32}Na imply that these nuclei are more tightly bound than expected from theoretical predictions.

Magicity loss at $N = 20$: First contact

The mass was measured by using the **mass separator**.

CERN Proton Synchrotron

24 GeV

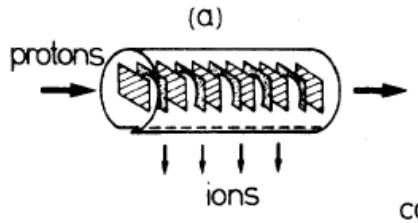

100 foils of graphite foils (70 μm),
where uranium (5~10 mg/cm^2) is evaporated.

C. Thibault+ NPA 1975

1.5 $\times 10^{12}$ protons/burst
Every 10 sec.
Lasting 2 μs

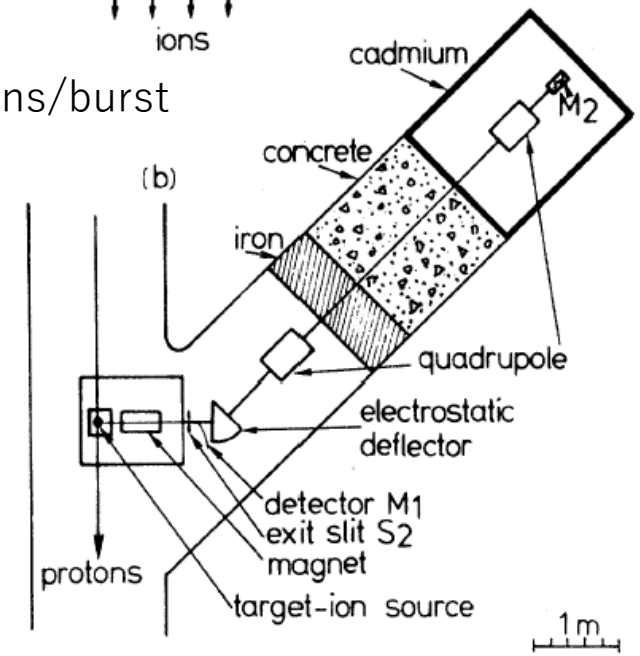

FIG. 1. (a) The target-ion source made of an array of foils wrapped in a rhenium envelope. (b) Setup of the mass spectrometer in the fast extracted beam of 24 GeV protons produced by the CERN synchrotron. The mass spectrometer magnet bends in the vertical plane.

$$\frac{M_A}{M_B} = \frac{V_B}{V_A}.$$

Accelerating voltage
from S1 to S2 (to keep the same trajectory)

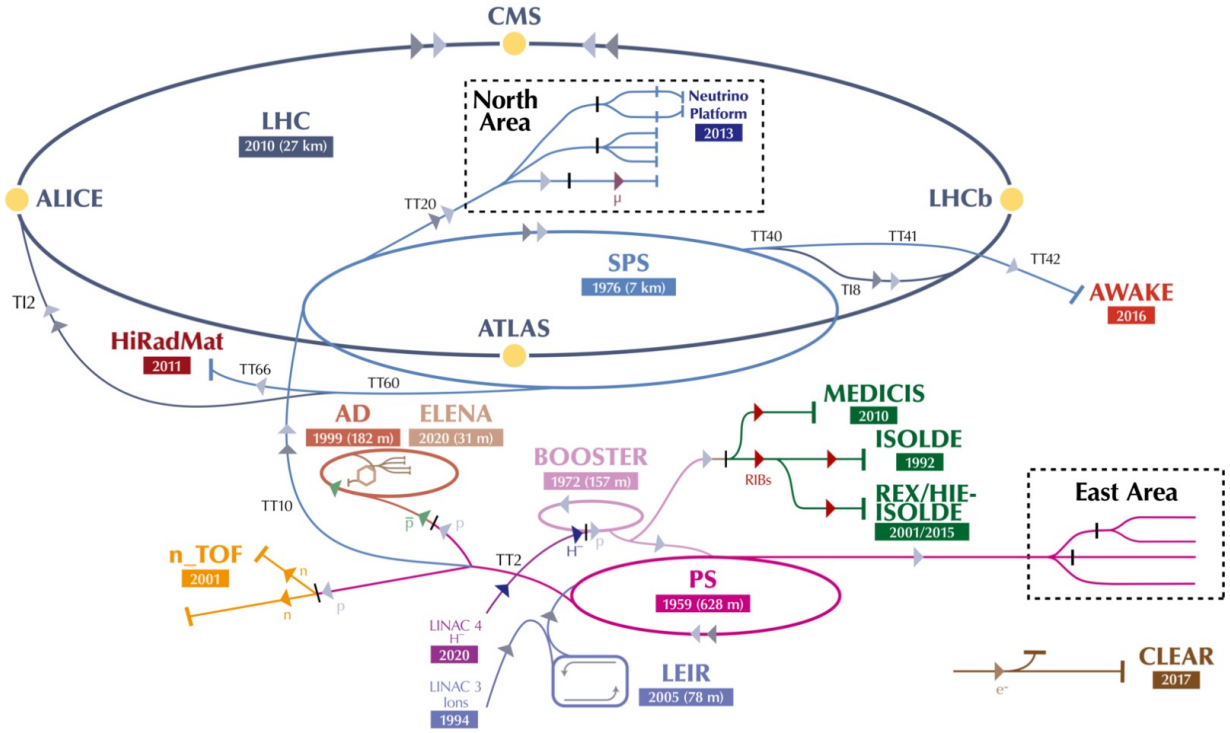

Magicity loss at $N = 20$: First contact

Systematics of 2n separation energies shows a hump at N = 20 in Na isotopes, which conflicts with theories.

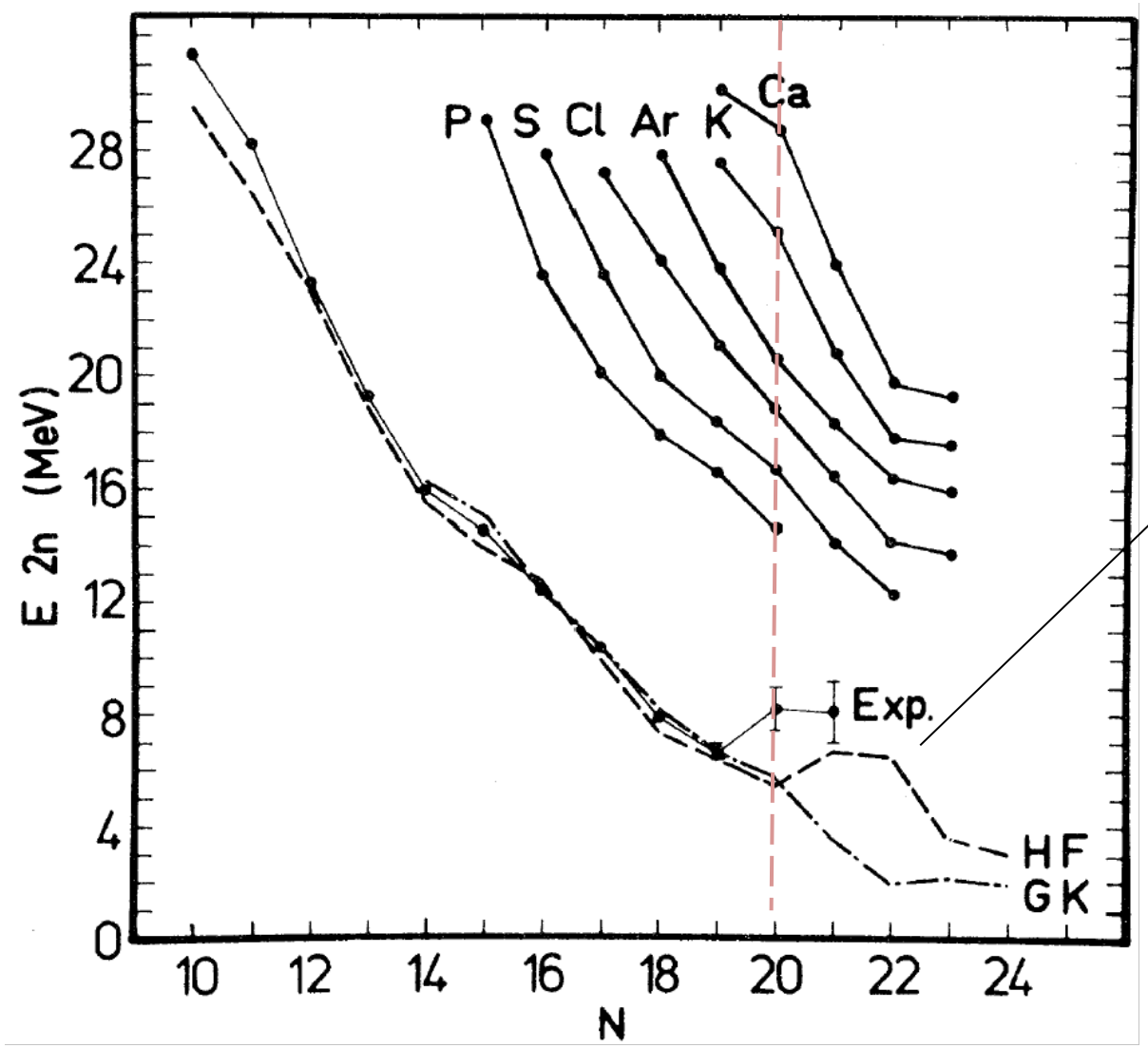

proached, the Hartree-Fock calculations of Ref. 46 yield two possible prolate solutions corresponding to two minima of comparable energy. Whereas the first minimum corresponds to a more spherical shape, a rather large deformation (Q_p ~ 56 fm^2 for ^{31}Na and ^{32}Na) is associated with the second solution. That solution is definitely the stablest when special care is taken to add the rotation energy. It is seen in Fig. 10 that it reproduces well the upward trend of the two-neutron separation energy around $N = 20$.[47] The reason

Magicity loss at $N = 20$

The 2^+ excited state in ^{32}Mg was found **anomalously at low energy** in a β -decay study at CERN, ISOLDE

D. Guillemaud-Muller+ NPA 1984

β-DECAY SCHEMES OF VERY NEUTRON-RICH SODIUM ISOTOPES AND THEIR DESCENDANTS

D. GUILLEMAUD-MUELLER*, C. DETRAZ*, M. LANGEVIN and F. NAULIN

Institut de Physique Nucléaire, BP 1, F-91406 Orsay, France

M. DE SAINT-SIMON, C. THIBAULT and F. TOUCHARD

Laboratoire René Bernas du Centre de Spectrométrie Nucléaire et de Spectrométrie de Masse, BP 1, F-91406 Orsay, France

and

M. EPHERRE

Laboratoire René Bernas and CERN, Division EP, CH-1211 Geneva 23, Switzerland

Received 6 February 1984

Abstract: The γ-activities from the β-decay of Na isotopes up to ^{34}Na, formed in high-energy fragmentation and analysed through mass-spectrometry techniques, are observed as well as those from their Mg descendants. The I_γ intensities, the β-delayed one- and two-neutron probabilities and the I_β intensities are measured. Decay schemes are proposed. We confirm, from the low location of the first 2^+ level of ^{32}Mg, the occurrence of a nuclear deformation at $Z \simeq 11$, $N \simeq 20$.

Magicity loss at $N = 20$

The experiment was performed using an ISOL beam with a simple, but typical β-decay setup.

Neutron-rich Na isotopes were produced by the fragmentation of a **30 g/cm^2 iridium target by 10 GeV protons** from the CERN PS

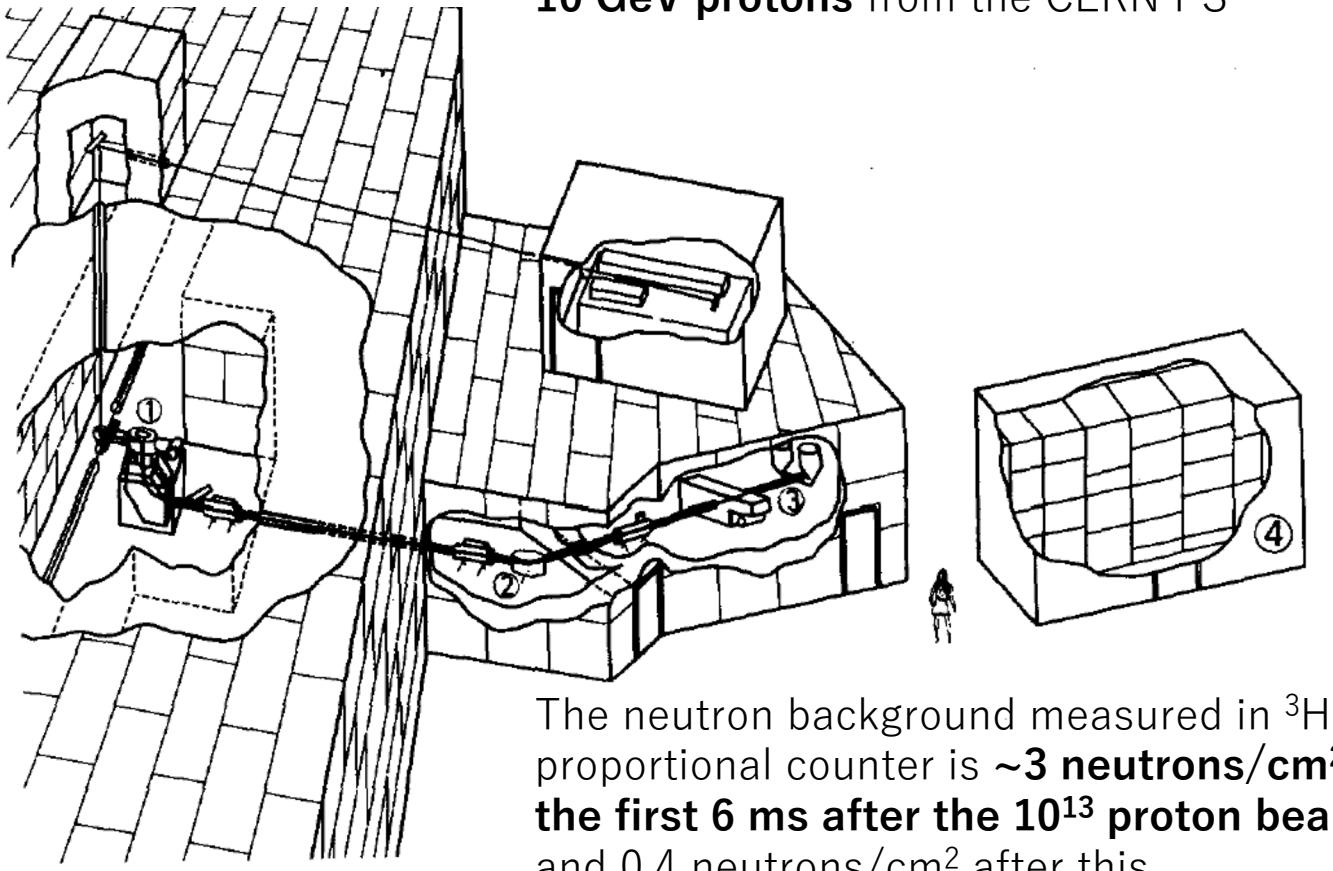

The neutron background measured in ^{3}He proportional counter is **~3 neutrons/cm^2 during the first 6 ms after the 10^{13} proton beam burst** and 0.4 neutrons/cm^2 after this.

Fig. 1. General view of the mass-spectrometer lay-out: 1 – mass spectrometer; 2 – electrostatic deflector; 3 – cadmium clothed detecting area; 4 – experimental control room.

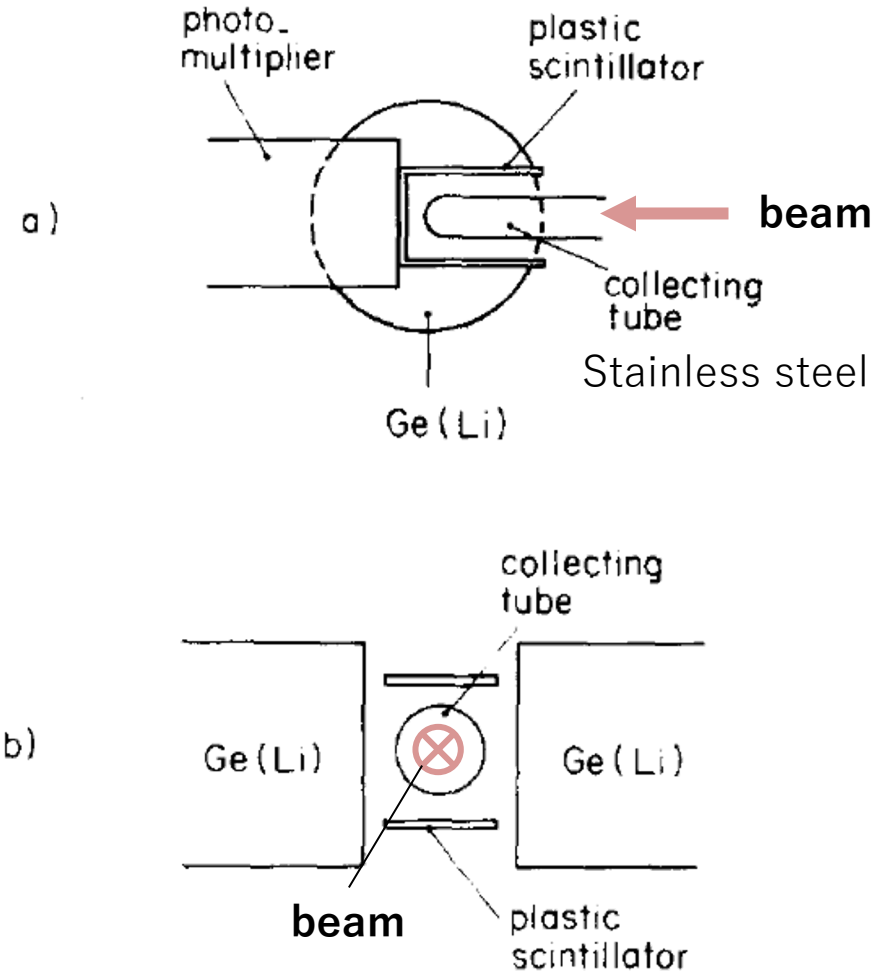

Magicity loss at $N = 20$

For the analysis of β decay, the time of γ-ray emission is delayed by the timescale of lifetime.
It is often called **delayed coincidence**.

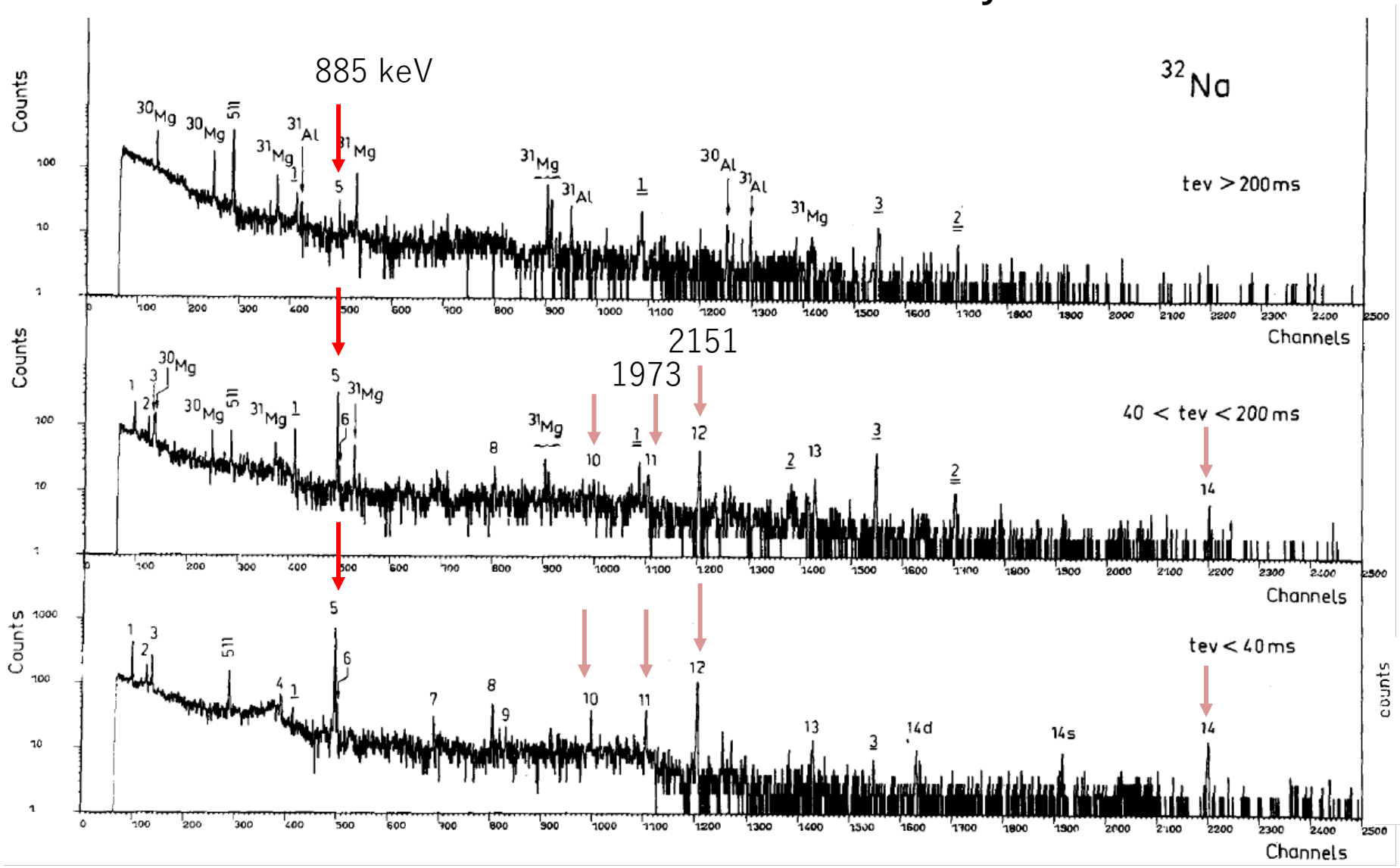

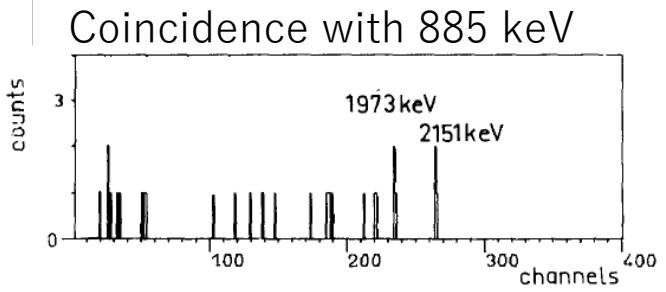

Magicity loss at $N = 20$

The first 2^+ state in ^{32}Mg was found at 886 keV. The energy is lower than expected for the magicity N = 32, suggesting **a new region of deformation at Z ~11 and N = 20**.

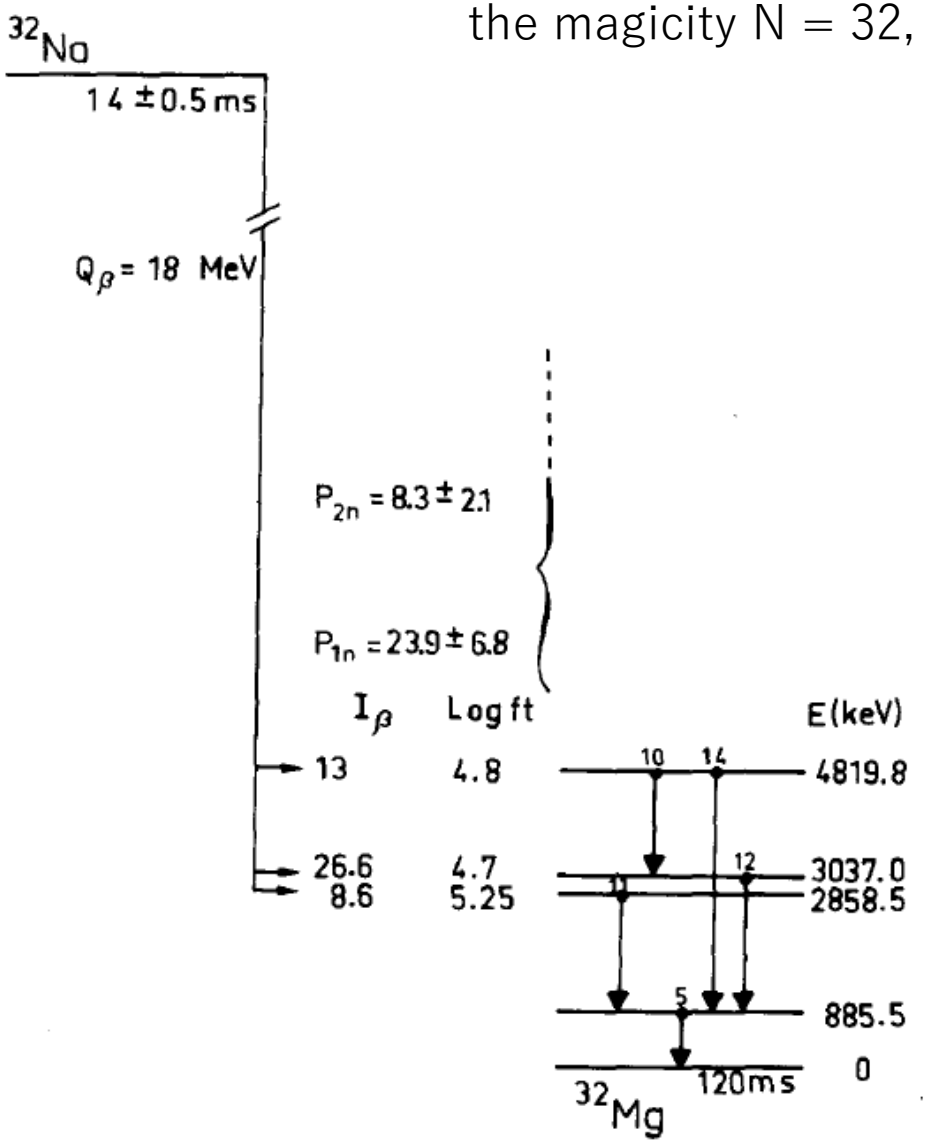

$$E(2^+) = \frac{3\hbar^2}{J} = 1224(\langle\beta^2\rangle A^{\frac{7}{3}})^{-1},$$

β : deformation parameter

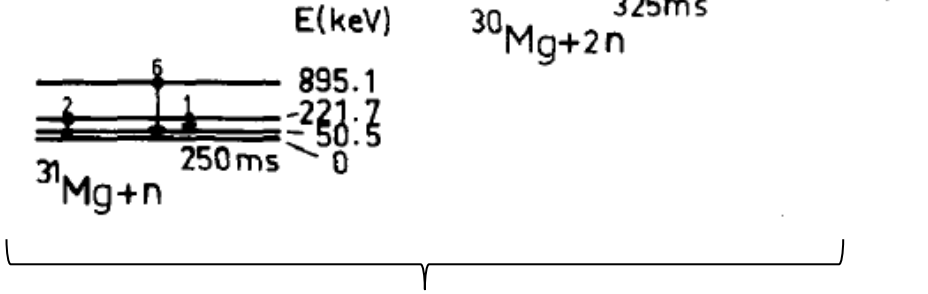

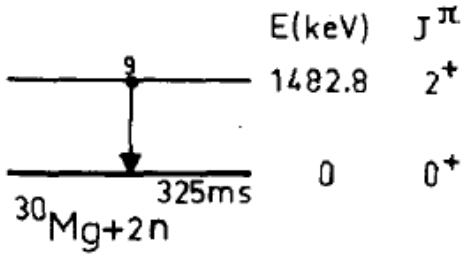

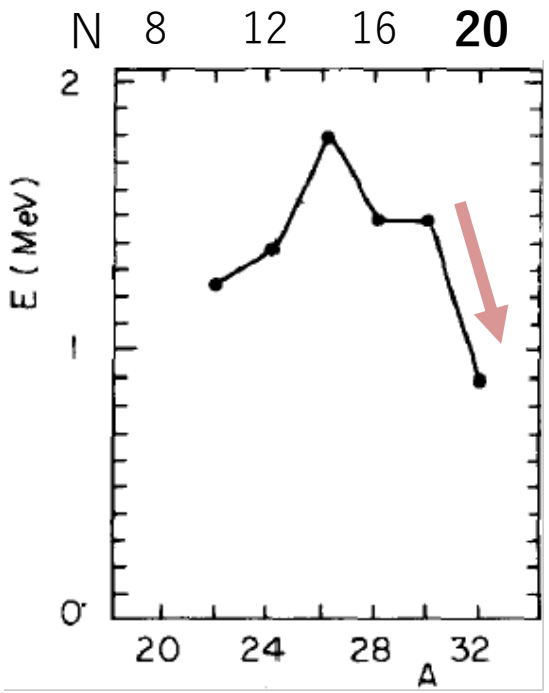

Observation of **delayed neutron emissions** are another important finding as characteristics of neutron-rich nuclei.

ISOLDE yield database

Figure from Gottberg NIMB 2016

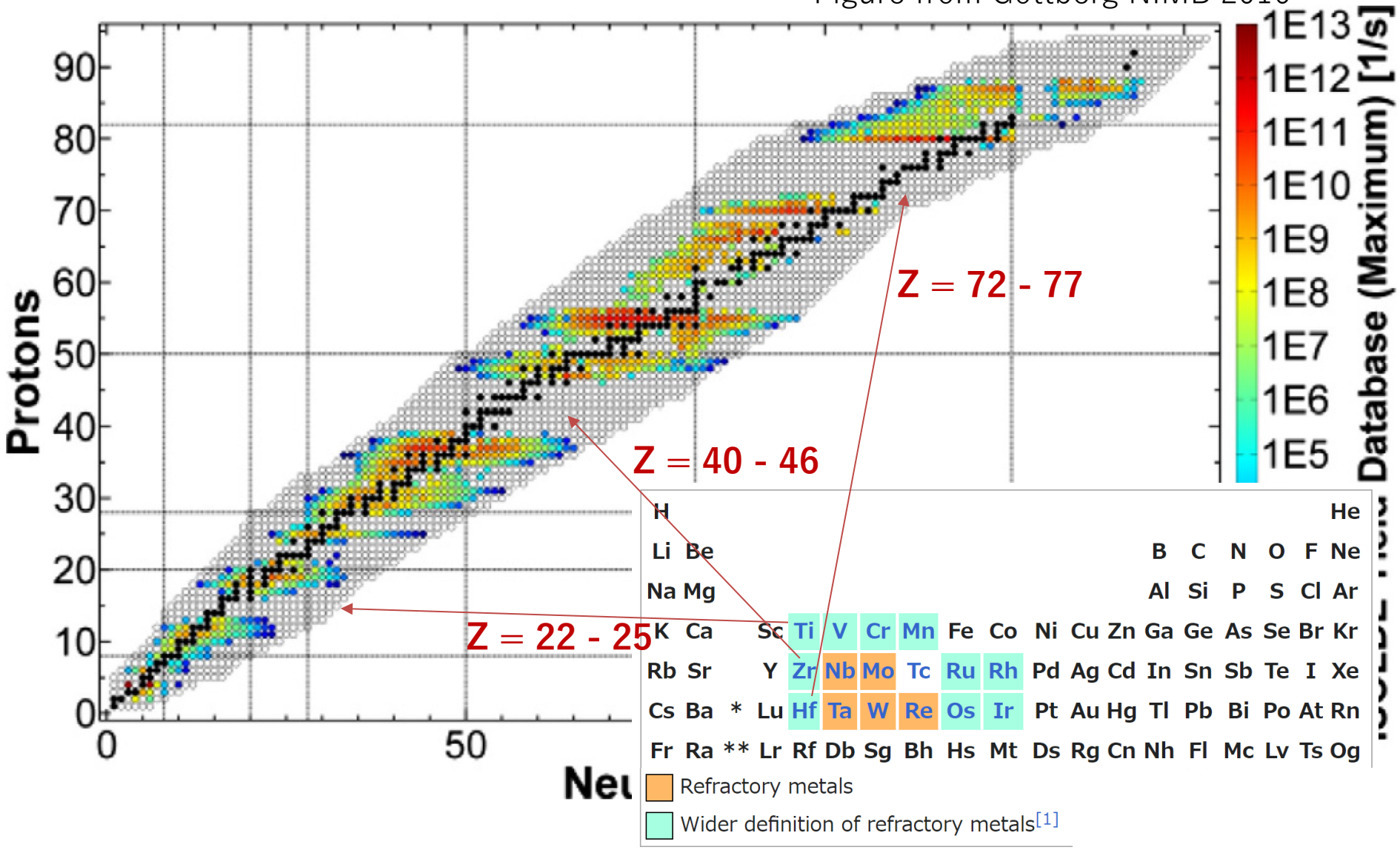

Chemical dependence

There are a number of elements that have never been produced at ISOLDE.

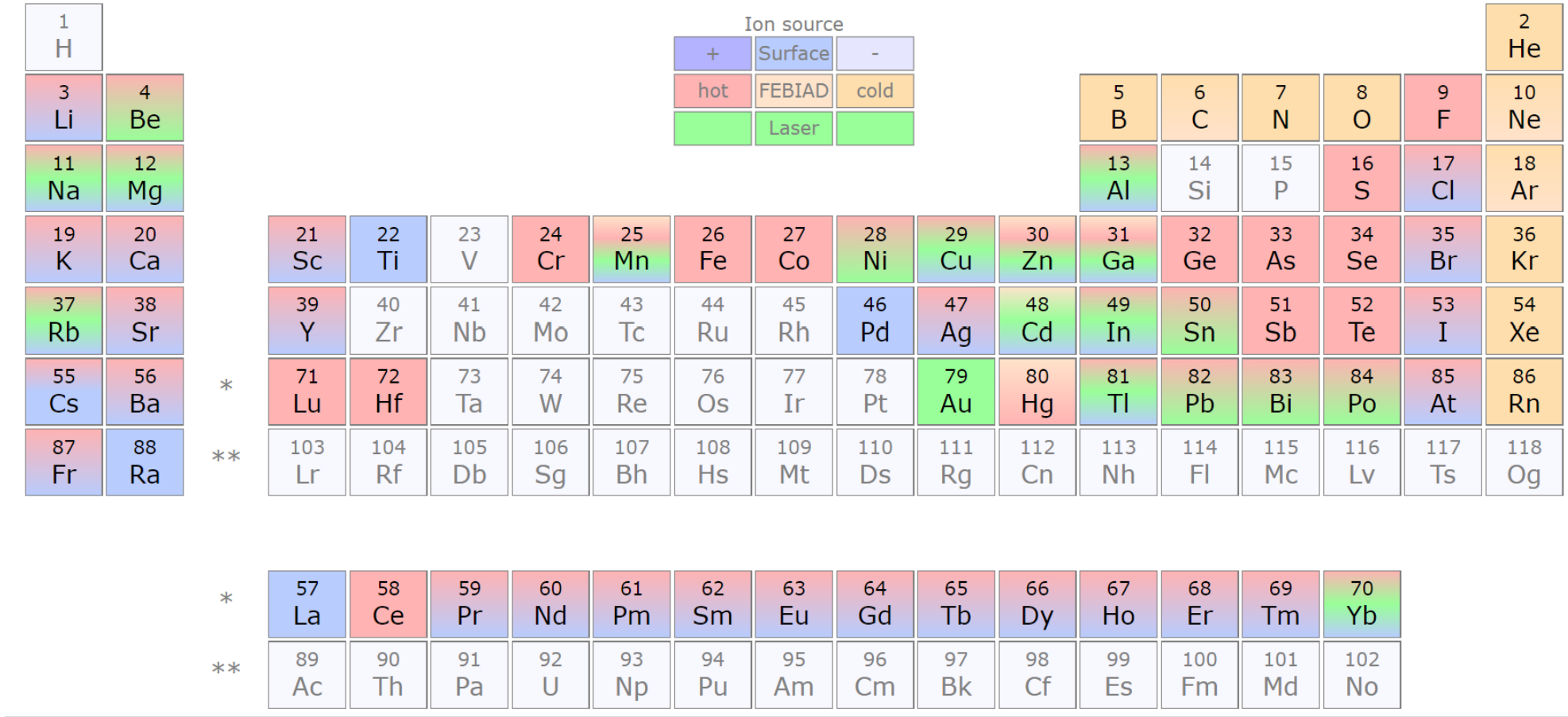

Beam intensity toward the dripline

Ne isotopes

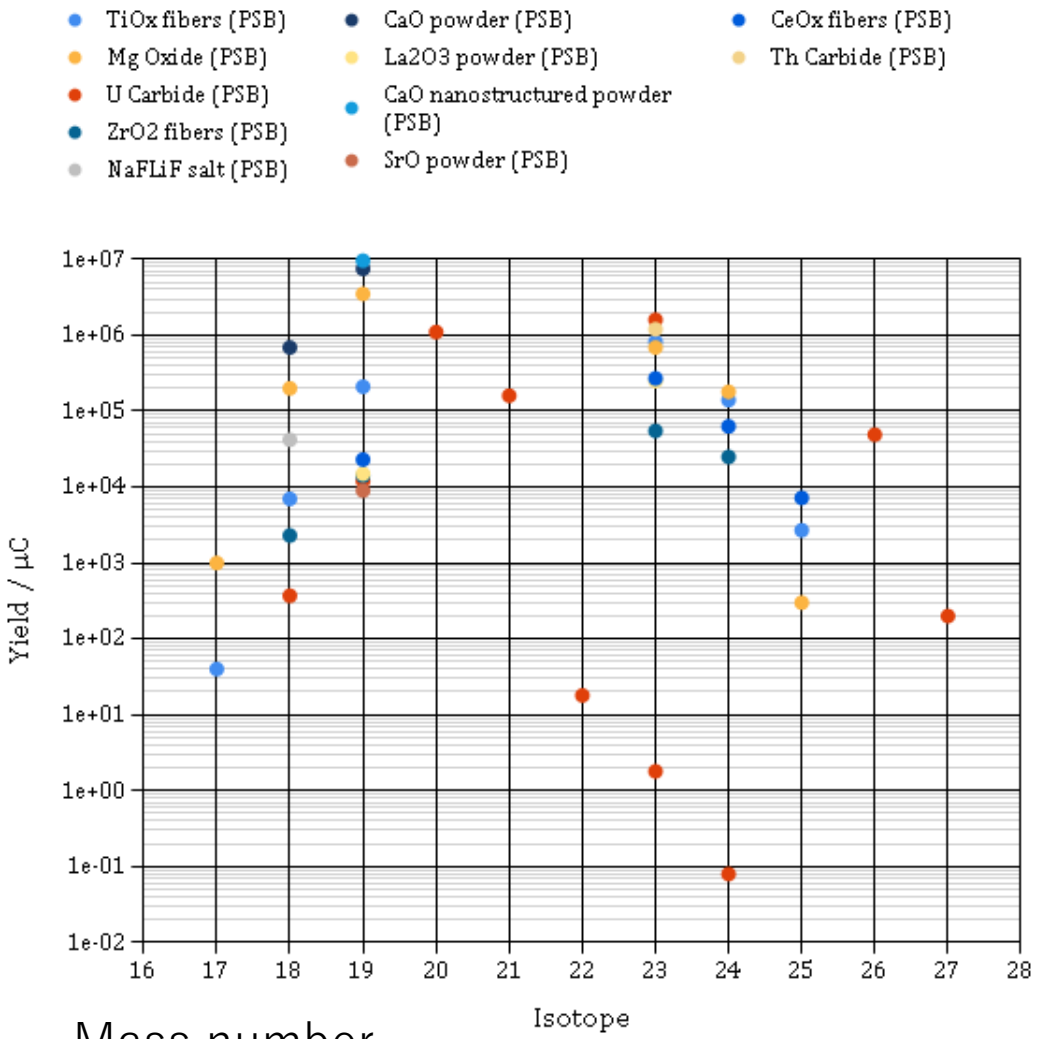

Mass number

Ne is rare gas with chemical properties favorable for the ISOL technique.

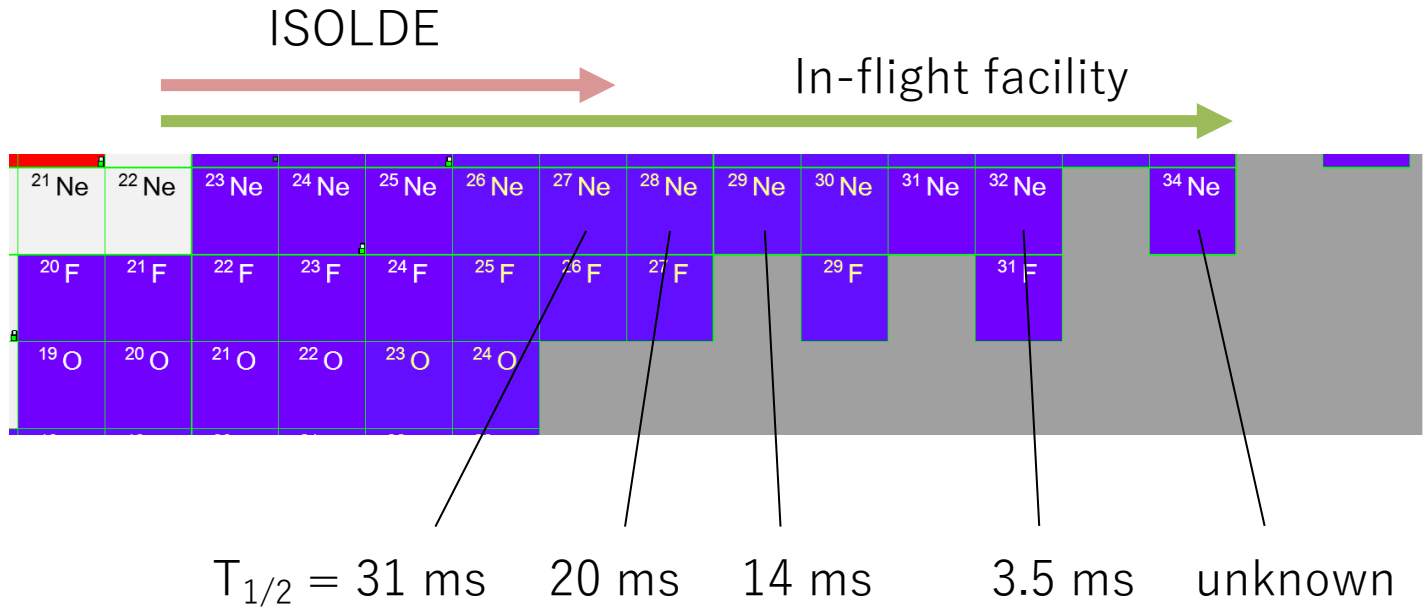

$T_{1/2}$ = 31 ms 20 ms 14 ms 3.5 ms unknown

No isotopes beyond ^{27}Ne have been produced.
The lifetime shorter than 30 ms seems constrain the extraction of Ne from the ion source.

In-flight method

ISOL technique has inherent limits in terms of species in RI beam production.
The in-flight method, invented in 1980s, overcame the shortcomings of ISOL.

No change

ion source | **Accelerator** Accelerate ions | **Beam transport** Transport ions

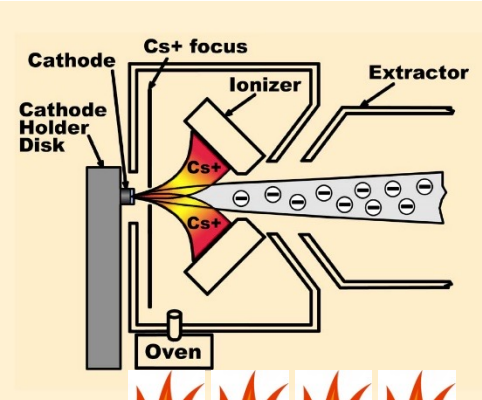

pelletron.com

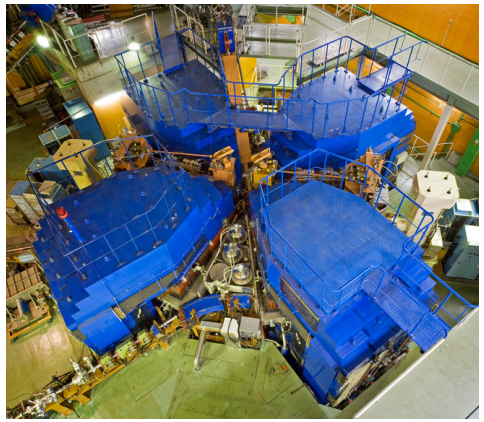

Riken Ring Cyclotron

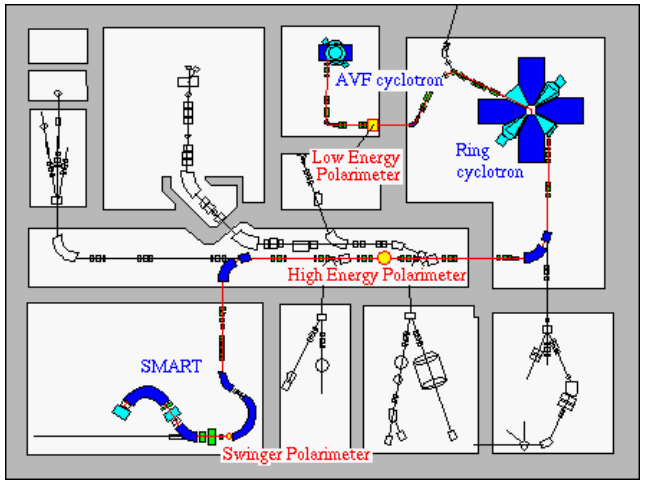

Layout of RARF

In-flight method

The in-flight method encompasses an RI production station after the accelerator, where RIs are produced by interactions of a heavy ion beam with a target. Reaction residues, so-called '**fragments**' are collected, separated and identified by a **magnetic fragment spectrometer**.

Ion source

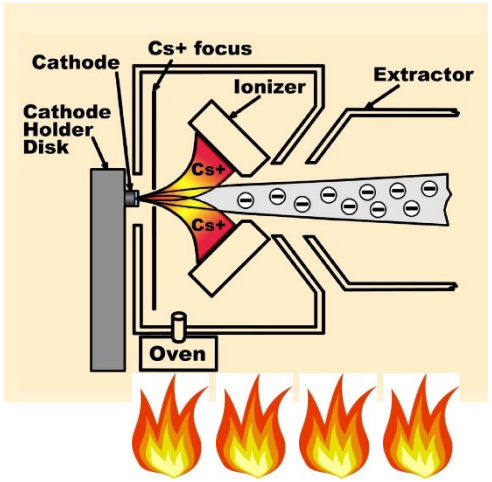

Accelerator

Beam transport

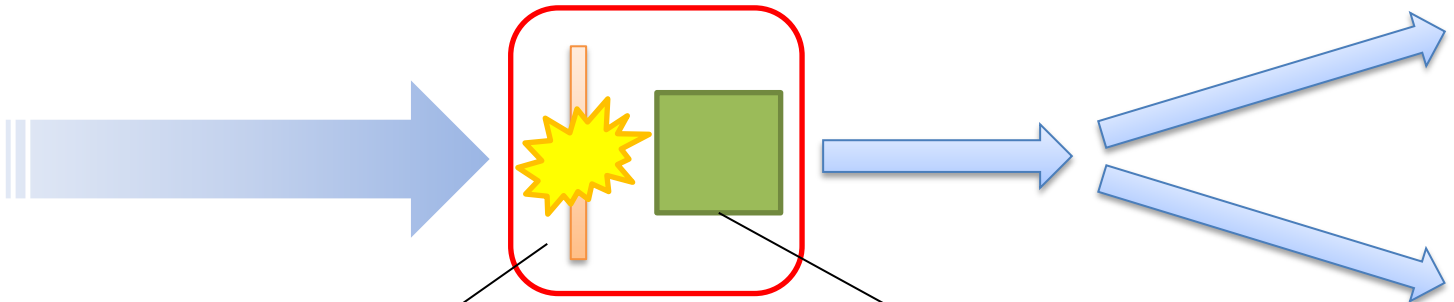

Production target

Fragment separator

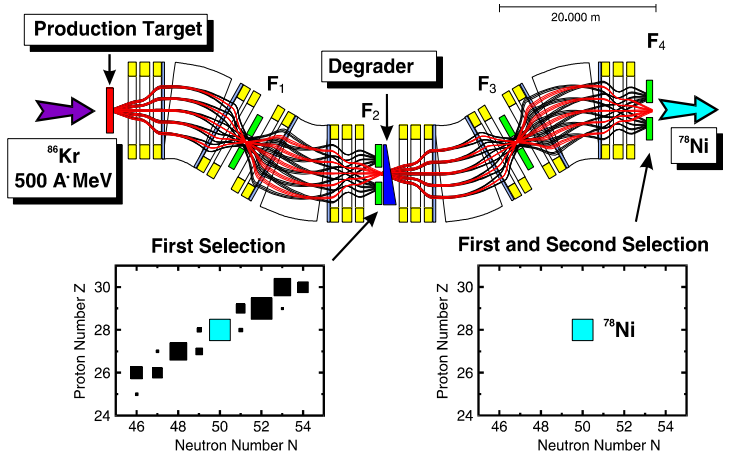

Characteristics of in-flight method

Pros and cons of the in-flight method are in contrast with the ISOL technique.

Reaction, beam and target

- Reactions should be **peripheral collisions**, where fragments are emitted at far forward angles.
- **Intermediate energies or higher** (>several tens of MeV/u, β >0.3)
- So far, **projectile-fragmentation reactions** and **in-flight fission of ^{238}U** are only applications.

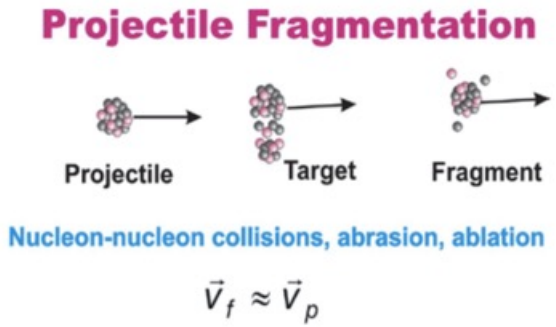

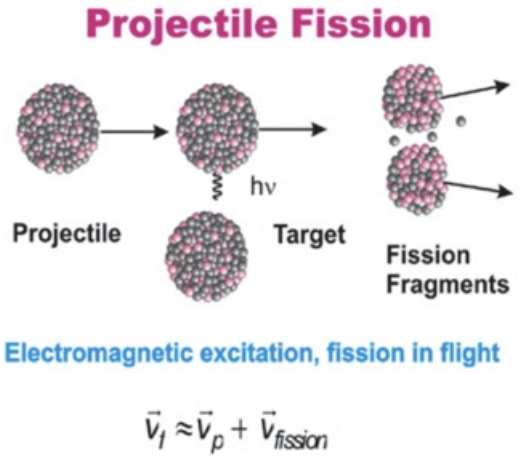

Pros

- Physical separation and identification. **No chemical dependence**.
- **Applicability to very short-lived nuclei**. No constraint by lifetime down to ~ 1 μ s.

Cons

- **Emittance growth** at the production target.
- **Purity**. Kinematical separation is increasingly difficult for heavier isotopes.
- **Particle identificaiton only from kinetic properties** (no chemical information).

Fragment separator

A magnetic serapartor to separate fragments is crucial element of the in-flight method.

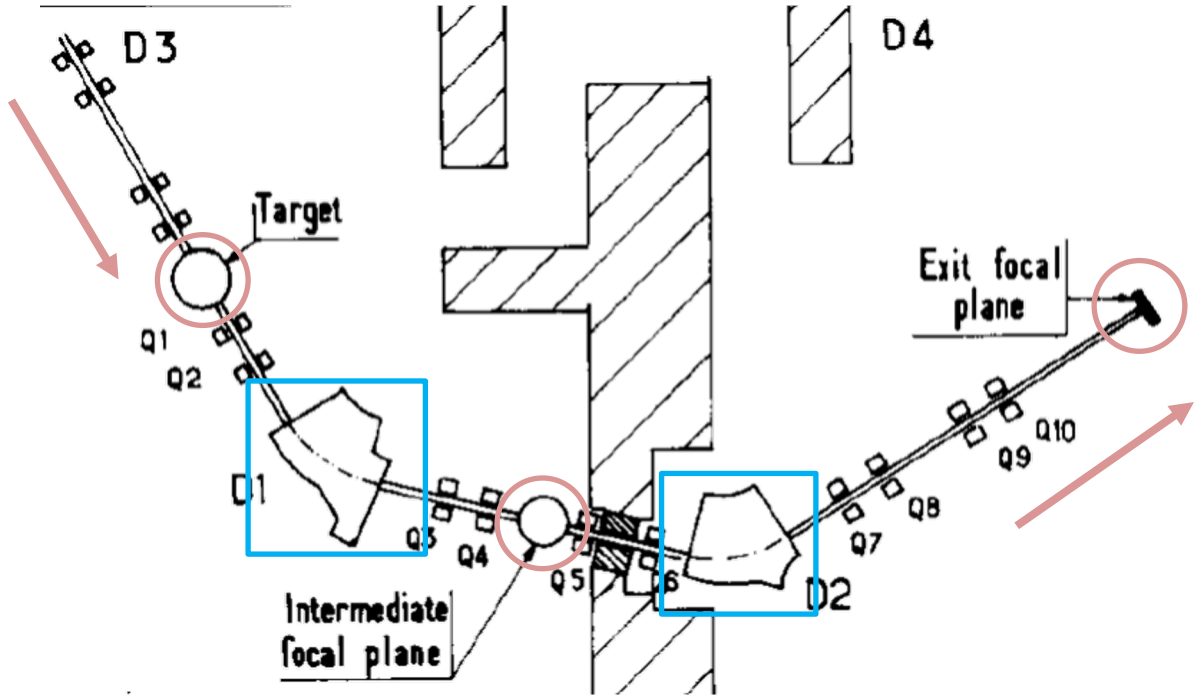

J.P. Dufour+ NIM A 1986

K.-H. Schmidt+ NIM A 1987

The spectrometer layout consists of

- **Three focal points**: (1) **production target** at the starting point, (2) intermediate plane, and (3) the **experimental station** at the exit point.
- **Two dipole deflecting magnets** are connecting the focal plane.
- **Several quadrupole focusing magnets** are installed.

Acromaticity with energy degrader

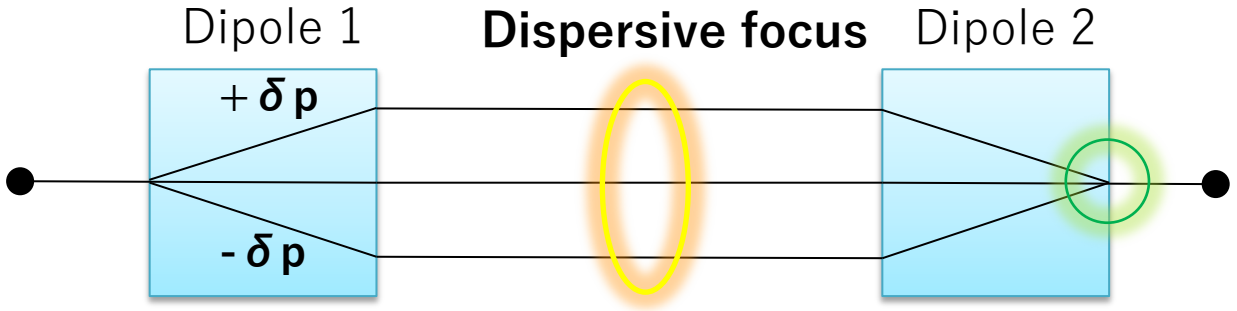

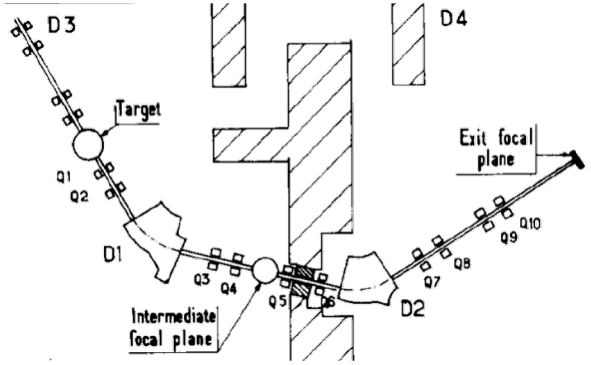

A/Q selection
if the velocity is constant

'**Achromaticity**' (symmetry in ion optics)
Same focus for different momenta

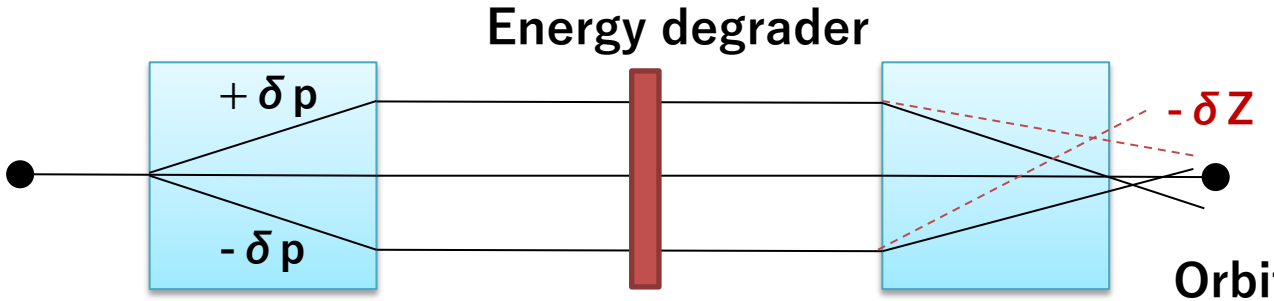

Orbital splits for different Z,
but '**achromaticity**' is broken.

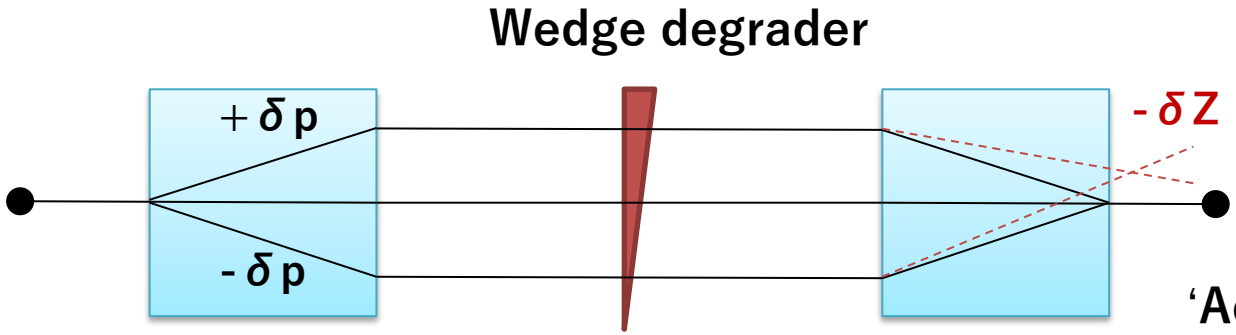

'**Achromaticity**' is restored
(**only for nucleus of interest**).

Purification by projectile-fragment separator

Magnetic rigidity ($B\rho$) analysis by a pair of **dipole magnets**

^{70}Zn beam to produce ^{52}Ca (simulation)

^{70}Zn (345 MeV/u) + Be (1.48 g/cm^2)

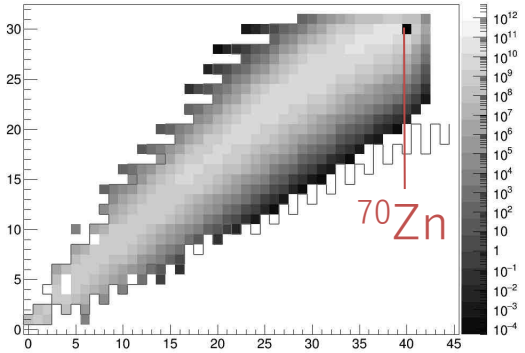

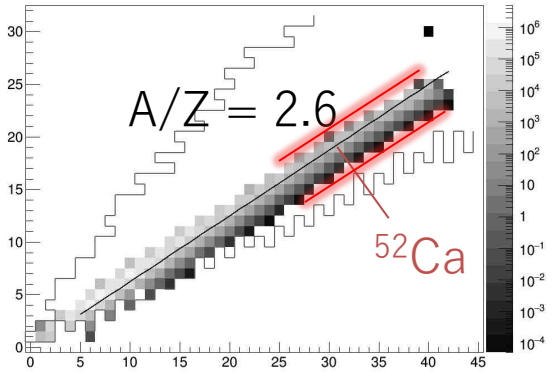

*Q = Z (full strip)

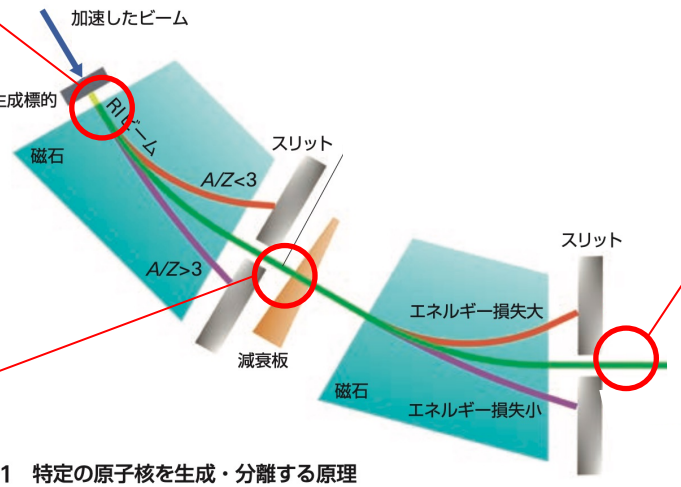

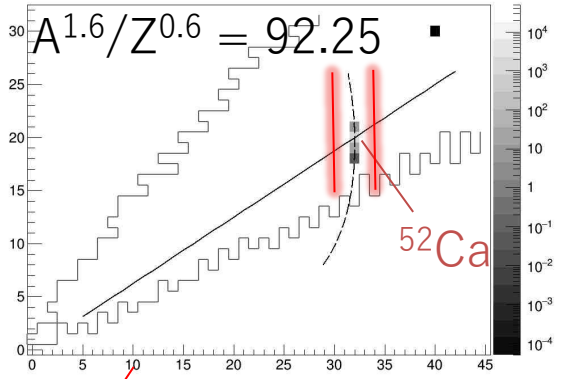

Courtesy N. Fukuda

図1　特定の原子核を生成・分離する原理

磁石による曲げられにくさ（磁気剛性）は、質量数と陽子数（荷電数）の比に速度を掛けた値に比例する。ウランなどのビームが標的に当たり生成されたRIビーム中のさまざまな原子核の速度はほぼ一定なので、磁石で曲げることで質量数と陽子数（荷電数）の比が同じものを、さらに減衰板に通すことで特定の陽子数の原子核だけを分離することができる。なお、RIBFで加速して生成標的に当てるビームの原子核には、ウラン238、キセノン124、クリプトン78、亜鉛70、カルシウム48、酸素18、窒素14などがある。

RIKEN NEWS 2018 May, p.6-9
「原子核のフロンティアをBigRIPSで開拓する」

Coulomb excitation of ^{32}Mg

Disappearance of Magic number N = 20 from E2 transition probability.

T. Motobayashi *et al.*, Phys. Lett. B 346, 9 ('95).

Large deformation of the very neutron-rich nucleus ^{32}Mg from intermediate-energy Coulomb excitation

T. Motobayashi [a,1], Y. Ikeda [a], Y. Ando [a], K. Ieki [a], M. Inoue [a], N. Iwasa [a], T. Kikuchi [a], M. Kurokawa [a], S. Moriya [a], S. Ogawa [a], H. Murakami [a], S. Shimoura [a], Y. Yanagisawa [a], T. Nakamura [b], Y. Watanabe [b], M. Ishihara [b,c], T. Teranishi [c], H. Okuno [c], R.F. Casten [d]

[a] *Department of Physics, Rikkyo University, Nishi-Ikebukuro, Toshima, Tokyo 171, Japan*
[b] *RIKEN (Institute of Physical and Chemical Research), Hirosawa, Wako, Saitama 351-01, Japan*
[c] *Department of Physics, University of Tokyo, Hongo, Bunkyo, Tokyo 113, Japan*
[d] *Physics Department, Brookhaven National Laboratory, Upton, N.Y. 11973, USA*

Received 21 November 1994
Editor: R.H. Siemssen

Abstract

The Coulomb excitation of a very neutron-rich nucleus ^{32}Mg to its 2^+ state was studied using an unstable nuclear beam of ^{32}Mg at 49.2 MeV/u with a ^{208}Pb target. The $B(E2)$ value of 454 ± 78 e^2fm^4 was extracted by a coupled channel analysis. The value is in good agreement with recent predictions. It confirms a large deformation for ^{32}Mg suggested by the low excitation energy of the 2^+ state, and points to the vanishing of the $N = 20$ shell gap.

- First application of **in-beam gamma-ray spectroscopy with RI beam**.
- First measurement of **B(E2) using Coulomb excitation with RI beam**.
- Shell model calculations with **wider model space to account for quenching N = 20 shell gap**.

B(E2) and magicity

Electromagnetic transition probability

- Long-range approximation: Selective for spin and parity.
- Well defined EM operator: Access to wavefunctions.

$$B(EI; I_i \to I_f) = \frac{1}{2I_i+1}|\langle f||\hat{Q}_I||i\rangle|^2,$$

$$B(MI; I_i \to I_f) = \frac{1}{2I_i+1}|\langle f||\hat{M}_I||i\rangle|^2$$

$$\hat{\mathcal{M}}(E, kIM) \approx \int \rho r^I Y_{IM} d\mathbf{r} = \hat{Q}_{IM},$$

$$\hat{\mathcal{M}}(M, kIM) \approx \frac{1}{c(I+1)} \int (\mathbf{r} \times \mathbf{j}) \cdot \boldsymbol{\nabla}(r^I Y_{IM}) d\mathbf{r} = \hat{M}_{IM}.$$

型	角運動量の選択則	パリティ変化	遷移確率 $T(\mathrm{sec}^{-1})$
E1	$\lvert I_i - I_f\rvert \le 1 \le I_i + I_f$	yes($\Pi_i \neq \Pi_f$)	$\mathrm{T(E1)} = 1.59 \cdot 10^{15} \cdot E^3 \cdot \mathrm{B(E1)}$
E2	$\lvert I_i - I_f\rvert \le 2 \le I_i + I_f$	no($\Pi_i = \Pi_f$)	$\mathrm{T(E2)} = 1.22 \cdot 10^{9} \cdot E^5 \cdot \mathrm{B(E2)}$
E3	$\lvert I_i - I_f\rvert \le 3 \le I_i + I_f$	yes($\Pi_i \neq \Pi_f$)	$\mathrm{T(E3)} = 5.67 \cdot 10^{2} \cdot E^7 \cdot \mathrm{B(E3)}$
M1	$\lvert I_i - I_f\rvert \le 1 \le I_i + I_f$	no($\Pi_i = \Pi_f$)	$\mathrm{T(M1)} = 1.76 \cdot 10^{13} \cdot E^3 \cdot \mathrm{B(M1)}$
M2	$\lvert I_i - I_f\rvert \le 2 \le I_i + I_f$	yes($\Pi_i \neq \Pi_f$)	$\mathrm{T(M2)} = 1.35 \cdot 10^{7} \cdot E^5 \cdot \mathrm{B(M2)}$
M3	$\lvert I_i - I_f\rvert \le 3 \le I_i + I_f$	no($\Pi_i = \Pi_f$)	$\mathrm{T(M3)} = 6.28 \cdot 10^{0} \cdot E^7 \cdot \mathrm{B(M3)}$

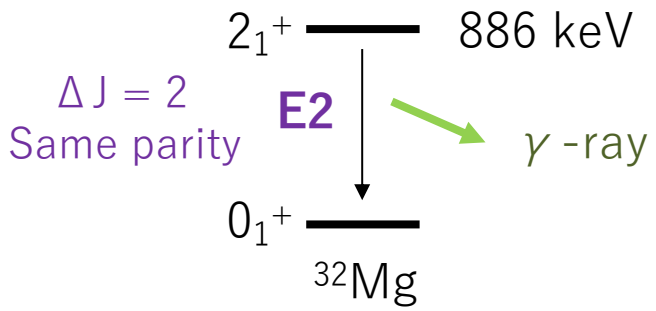

B(E2) and magicity

At magicity, B(E2) is small and close to single-particle unit.
Small B(E2) validates magicity, while **large B(E2) indicates magicity loss**.

$$B(E2; 2_1^+ \to 0_{g.s.}^+) = \frac{1}{5}\left(\frac{3}{4\pi} Z e R_0^2\right)^2 \beta^2$$

$\lambda = 2$

Multipole expansion of charge density

$$\hat{Q}_{\lambda\mu} = e\int_V \hat{\rho}_p(\mathbf{r}) r^\lambda Y_{\lambda,\mu}(\theta,\varphi) d^3r \sim eZ\frac{3}{4\pi} R_0^\lambda \hat{\alpha}_{\lambda\mu}$$

Single particle transition strength

$$B_{sp}(E\lambda; I_i \to I_f) = \frac{1}{2I_i+1}|\langle (n\ell j)_f || e_{eff} r^\lambda Y_\lambda || (n\ell j)_i \rangle|^2$$

shell orbital

$j_i = I + 1/2, j_f = 1/2$

$$B_W(EI) = e^2 \frac{1}{4\pi}\left(\frac{3}{I+3}\right)^2 R_0^{2I}$$

Weisskopf unit (W.u.)

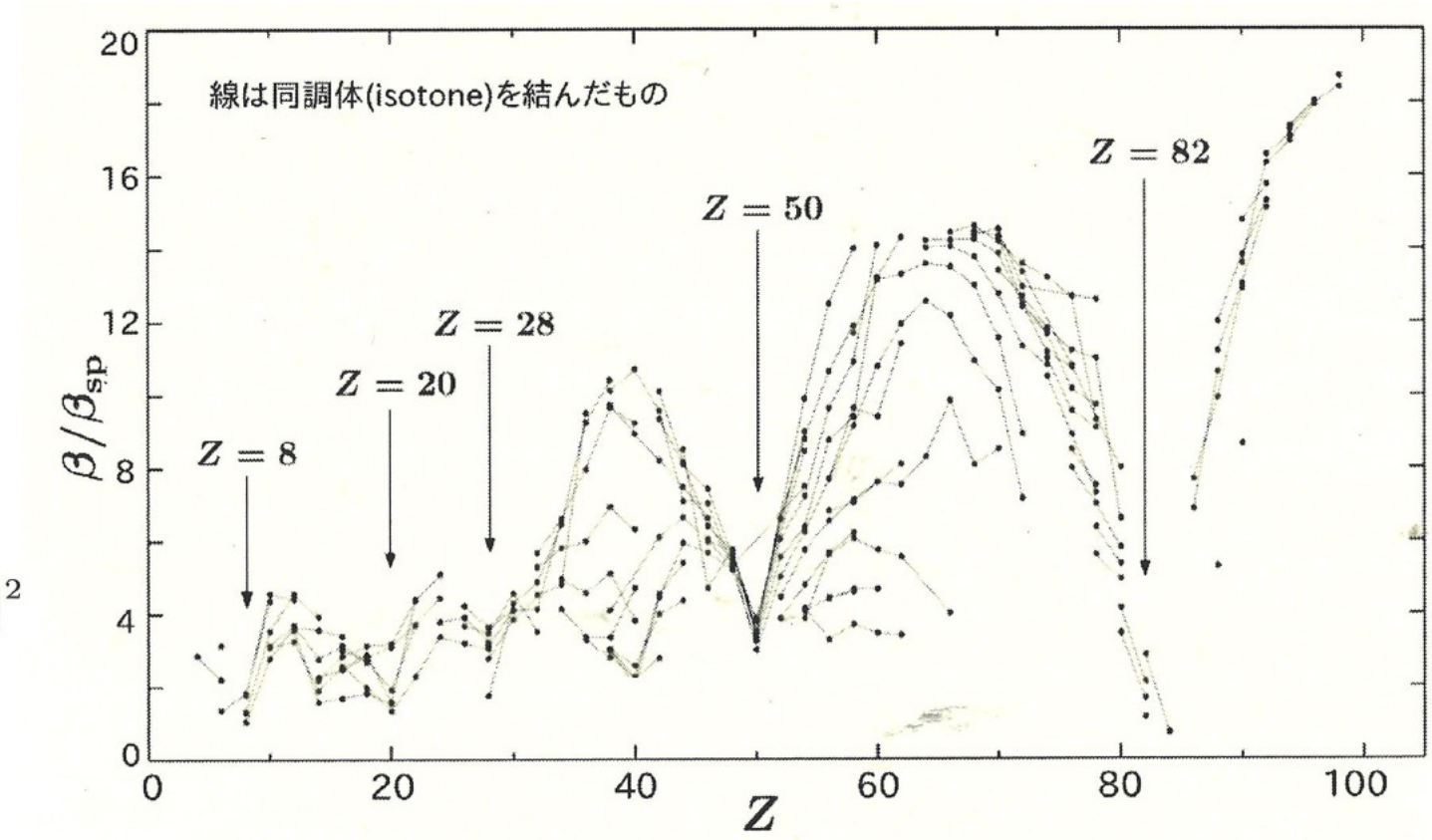

How ^{32}Mg beam was produced

Experiment was performed at RIPS by projectile fragmentation region providing a ^{32}Mg beam of 54 MeV/u

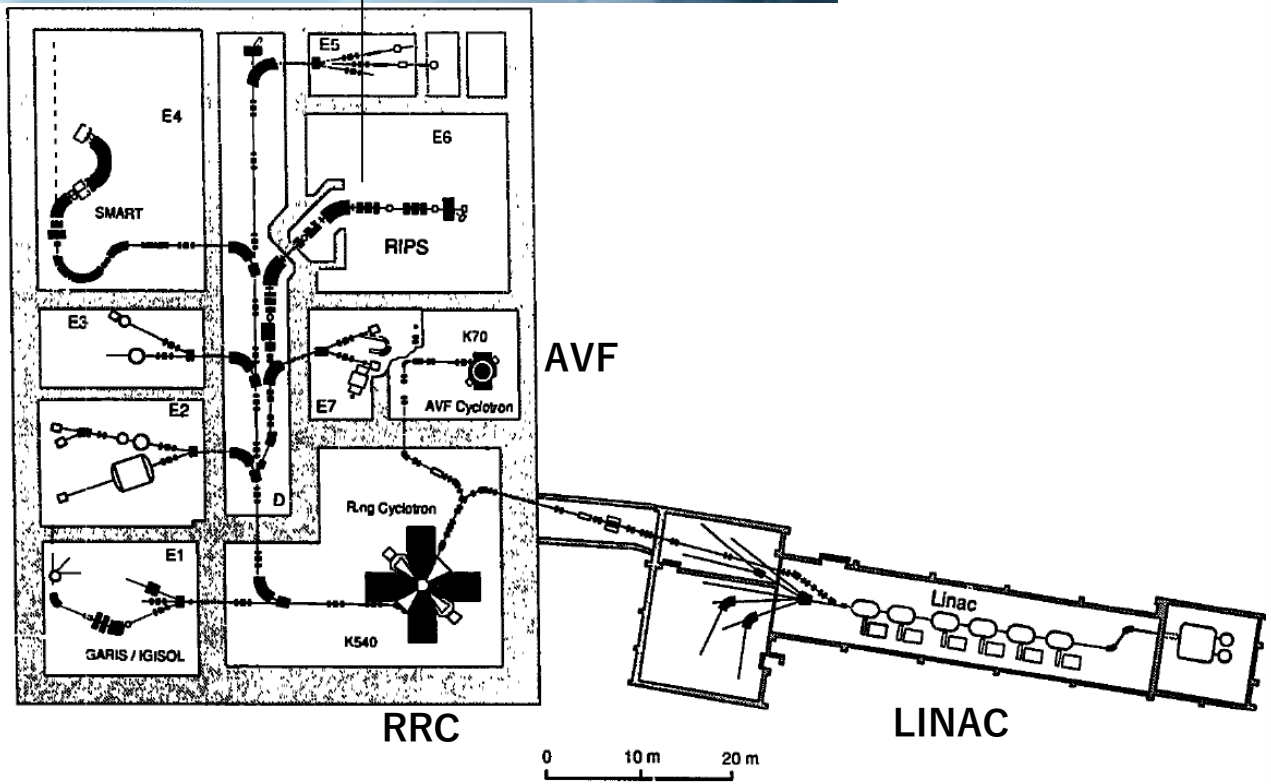

^{32}Mg 300 pps purity 50%

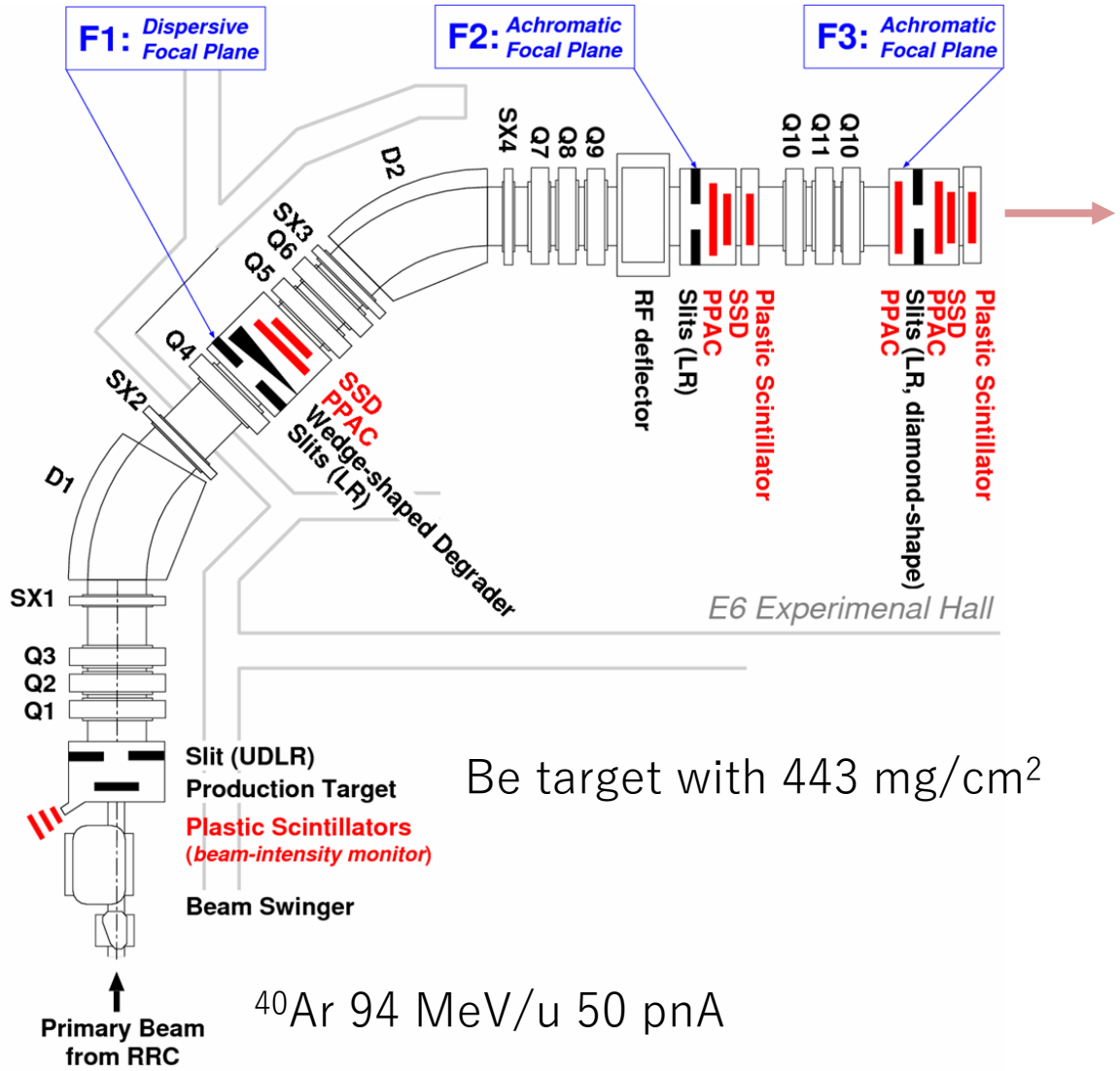

Be target with 443 mg/cm^2

^{40}Ar 94 MeV/u 50 pnA

Coulomb excitation of ^{32}Mg beam

The first 2^+ state of ^{32}Mg is excited by virtual photons of Coulomb field of Pb + Mg collision.

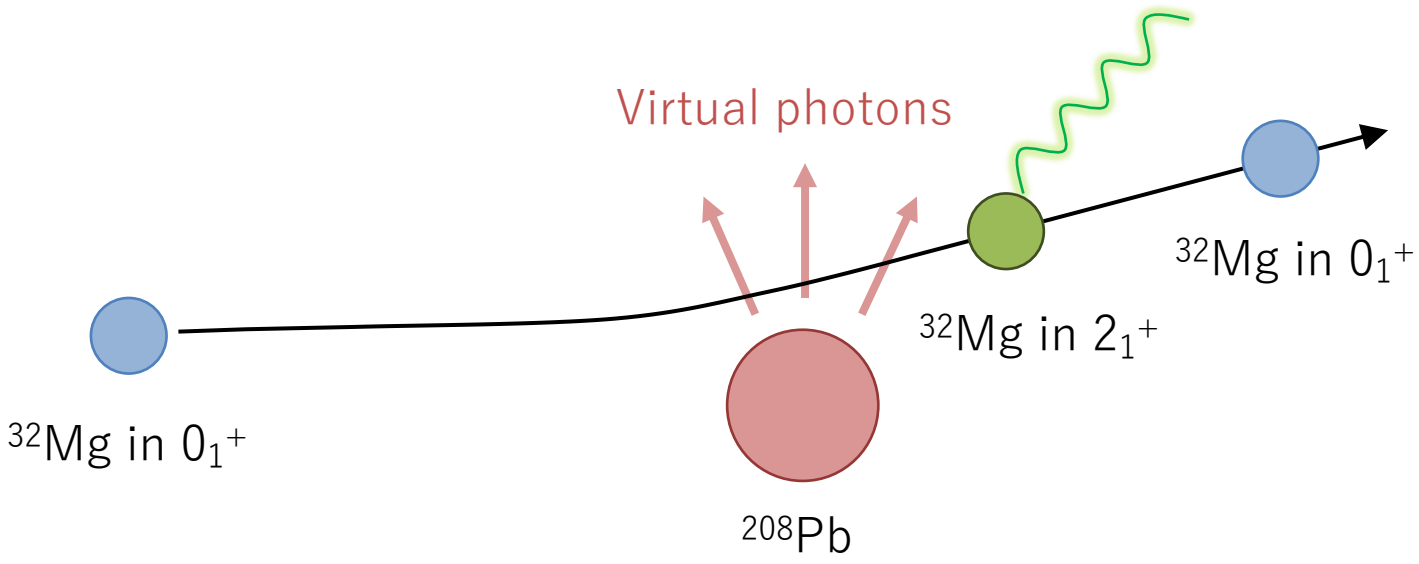

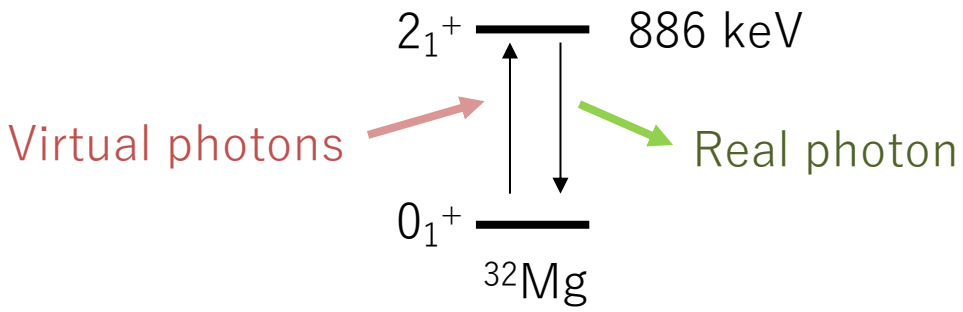

From photon energy to excitation energy

To translate measured photon energy to excitation energy, a few kinematical effects should be considered.

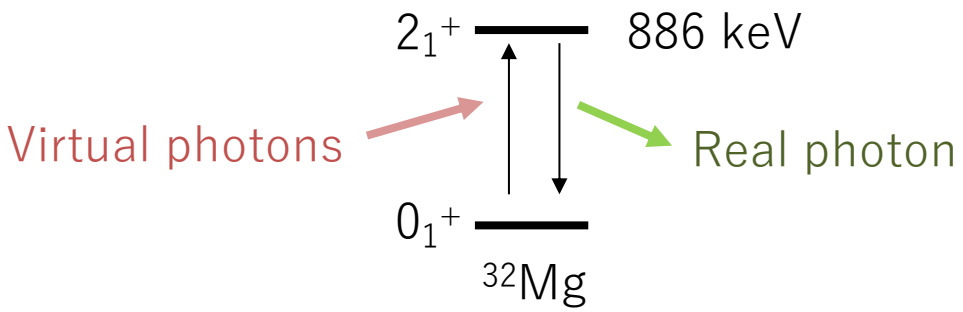

(1) Doppler shift

The photon energy is shifted in the laboratory frame (observer) if the emitter is moving.

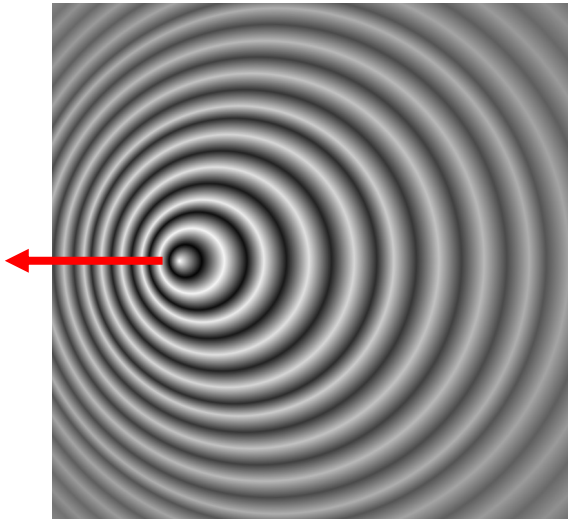

Waves emitted from a moving source

The Lorentz tranformation reads:

$$E_{\mathrm{c.m.}} = \gamma E_{\mathrm{lab}} \left(1 - \beta \cos\theta\right)$$

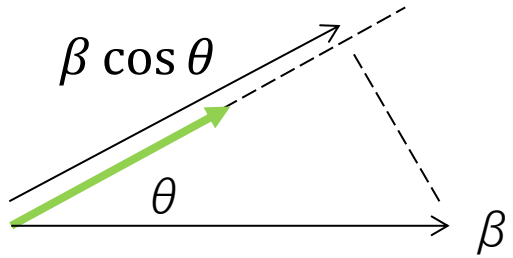

(2) Recoil shift

The photon leaves a recoil energy to the nucleus (**momentum conservation**).

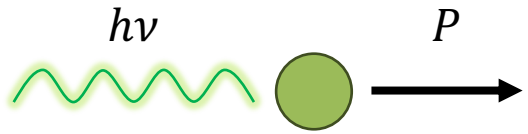

For most cases, this effect is negligibly small due to massless photon.

$$P \ll h\nu$$

* The recoil shift is crucial in measurements of Mössbauer effect (Nobel Prize in Physics 1961).

Setup for Coulomb excitation of ^{32}Mg beam

NaI(Tl) detectors array DALI was developped for **Doppler-shifted gamma-ray measurements.**

To correct for Doppler shift, **emission angle of photon is needed.**
For this aim, DALI consists of many crystals.

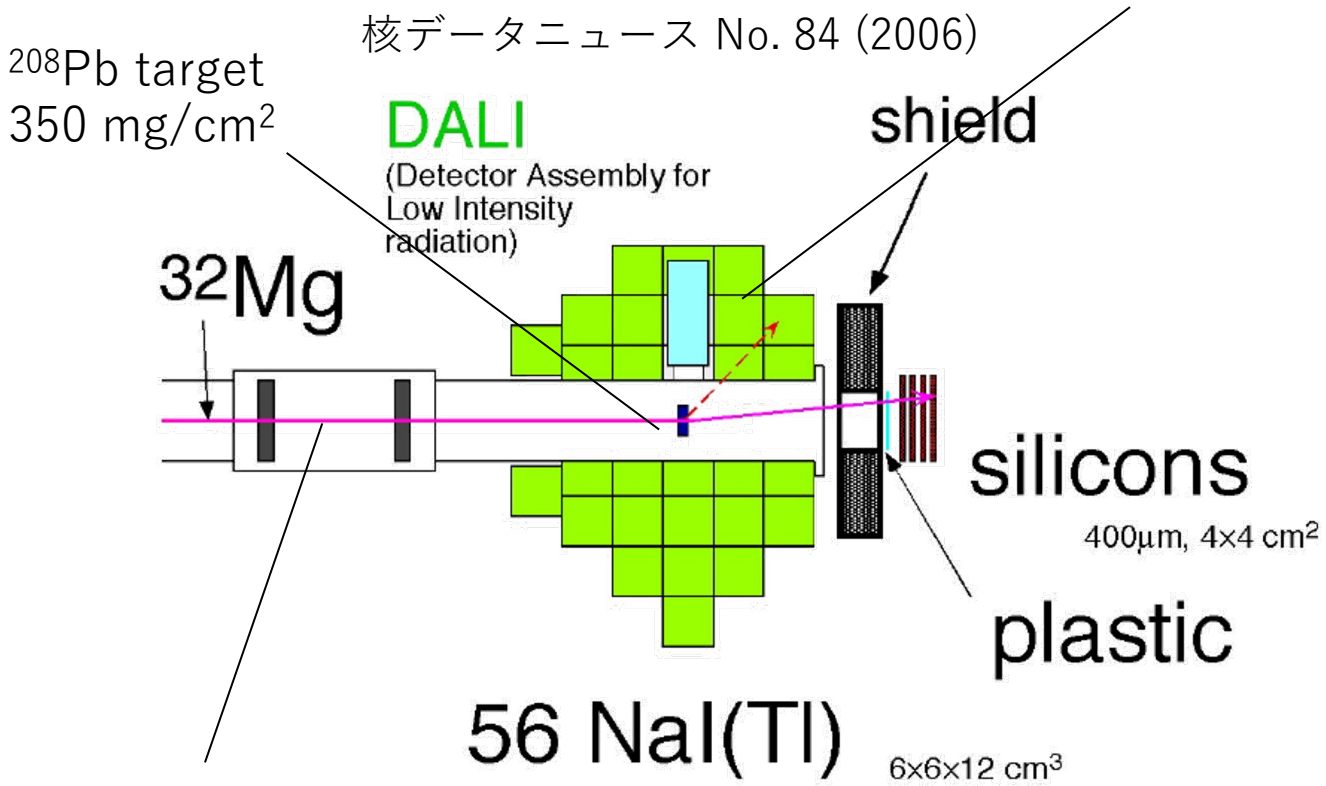

NaI(Tl) 検出器　DALI2 (RIKEN)

Signal readout

Bias voltage

Enclosure of NaI crystal

光電子増倍管
Photomultiplier

The trajectory of beam particles is measured by a pair of 2-dim position detectors PPACs.
The incident angle and position on the target are considered to obtain the photon emission angle.

Coulomb excitation of ^{32}Mg

The excitation is dominated by Coulomb scattering rather than by nuclear scattering, according to the reaction calculation.

After correcting for the Doppler shift

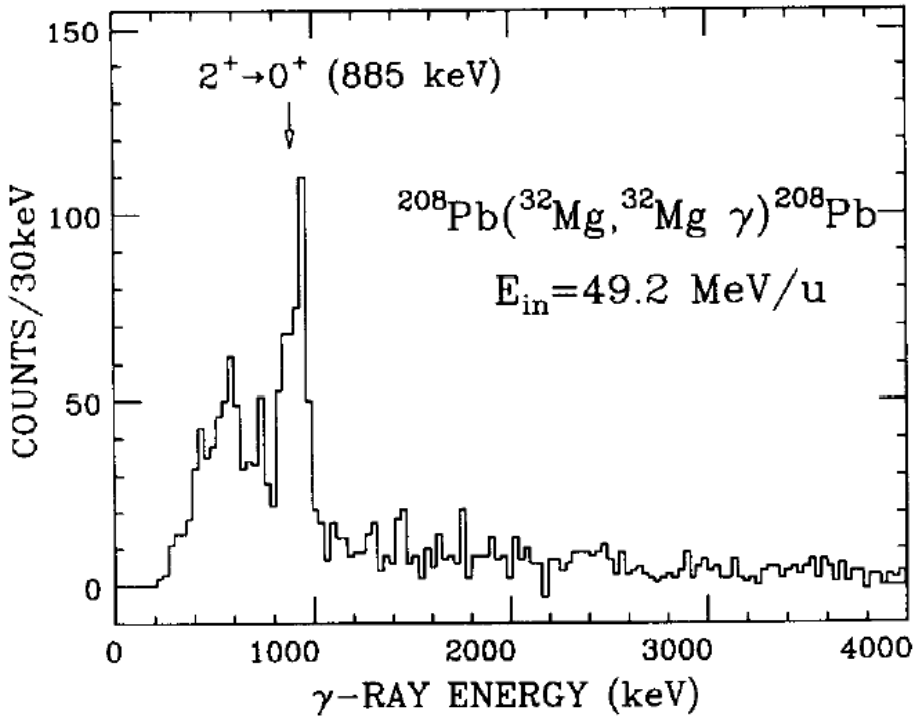

Coupled-channel calculation by ECIS79

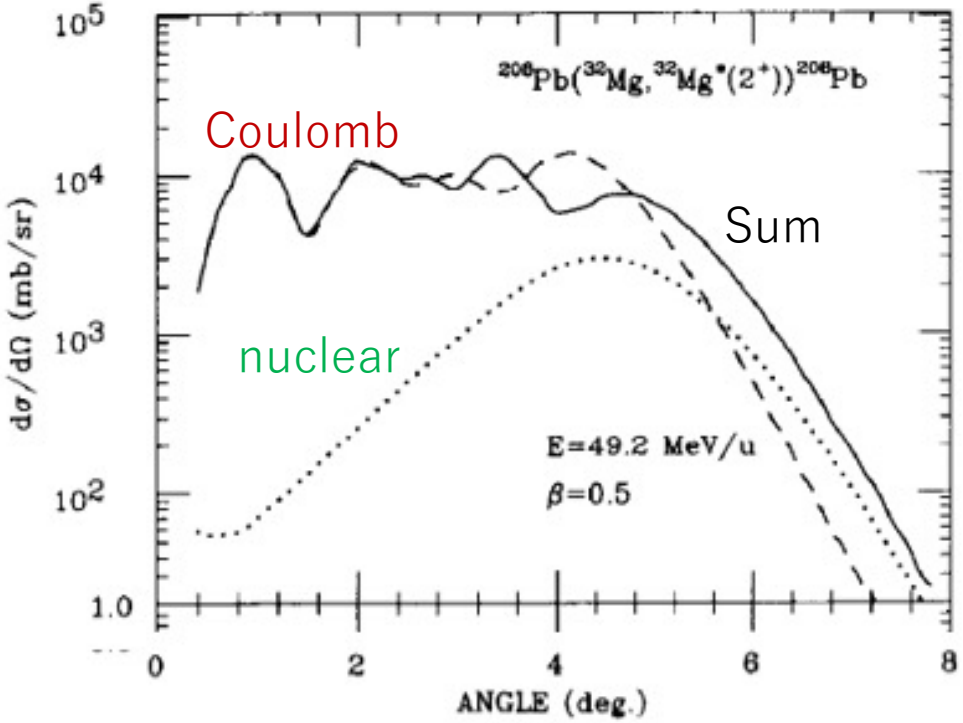

Optical potential: ^{17}O +^{208}Pb at 84 MeV/u
Form factor: deformation model

$$\beta = \beta_N = \beta_C = \frac{4\pi\sqrt{B(E2)}}{3ZeR^2}$$

Large B(E2) of ^{32}Mg

Systematics of isotones show **enhancement of B(E2) at N = 20** with ^{32}Mg, which is **reproduced by shell model calculations with sd+pf model space**. First case of magicity loss is estalished.

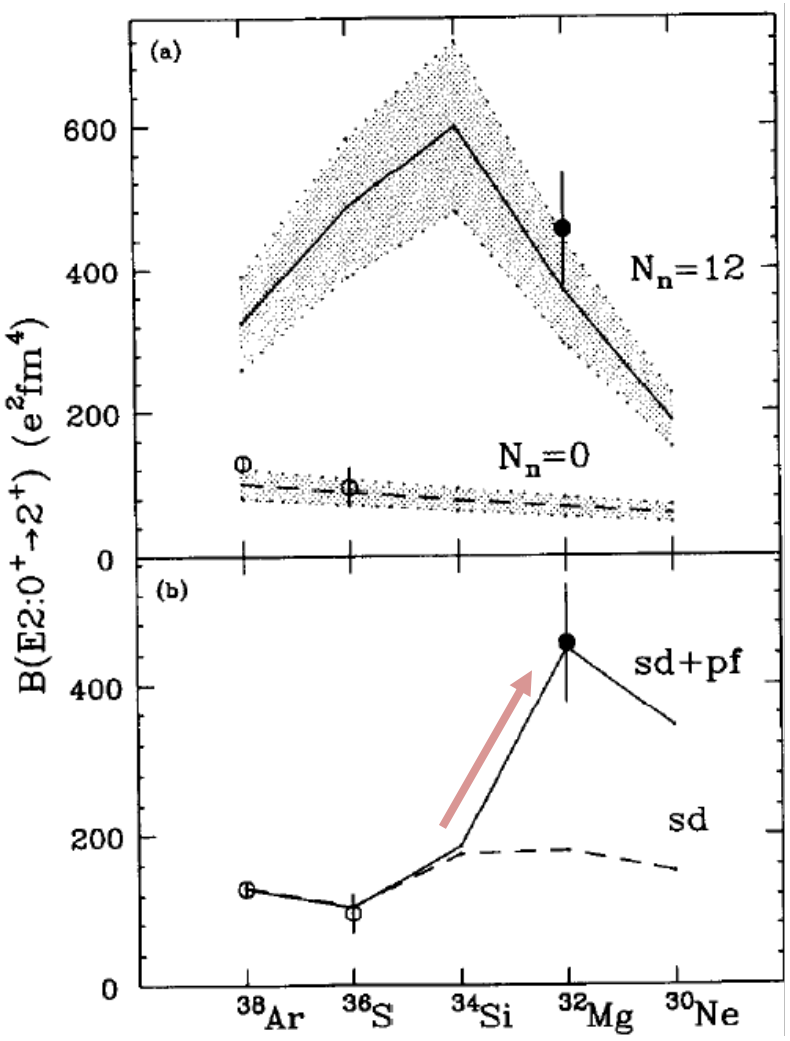

N = 20 isotones

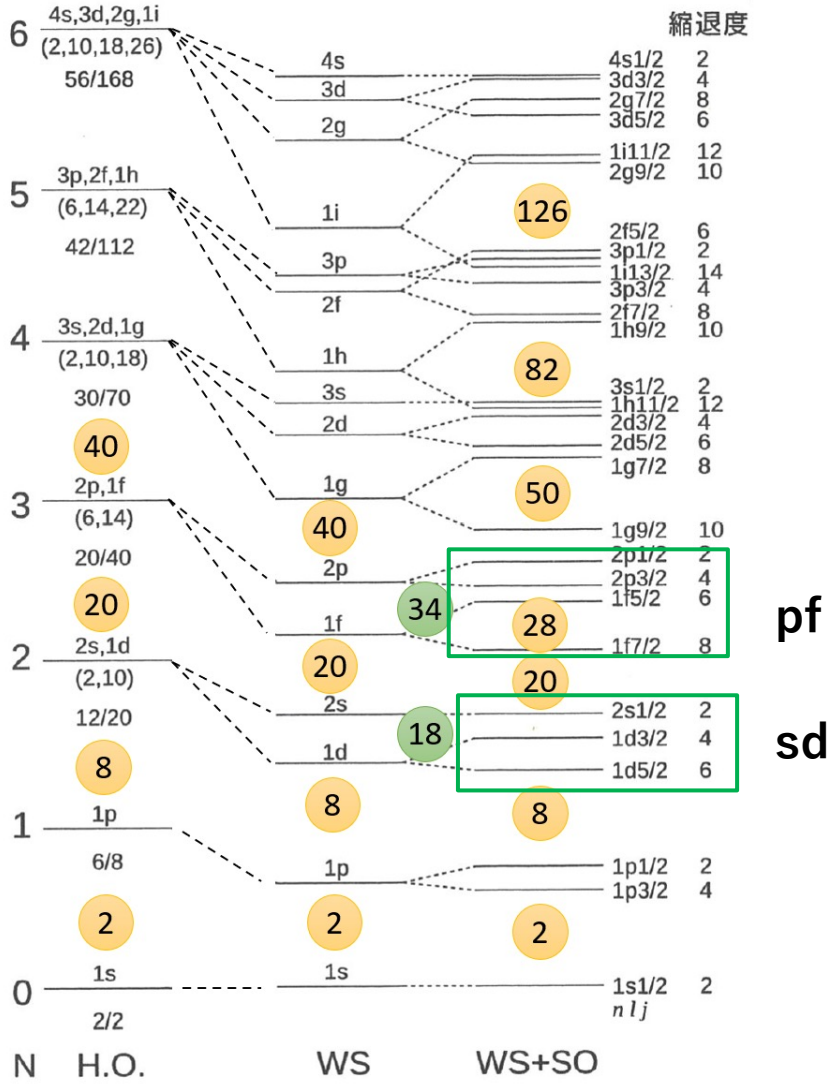

Island of inversion

The ground states are deformed **in a group of nuclei beyond ^{32}Mg**. The region of deformation on the nuclear chart is called ‘Island of inversion’.

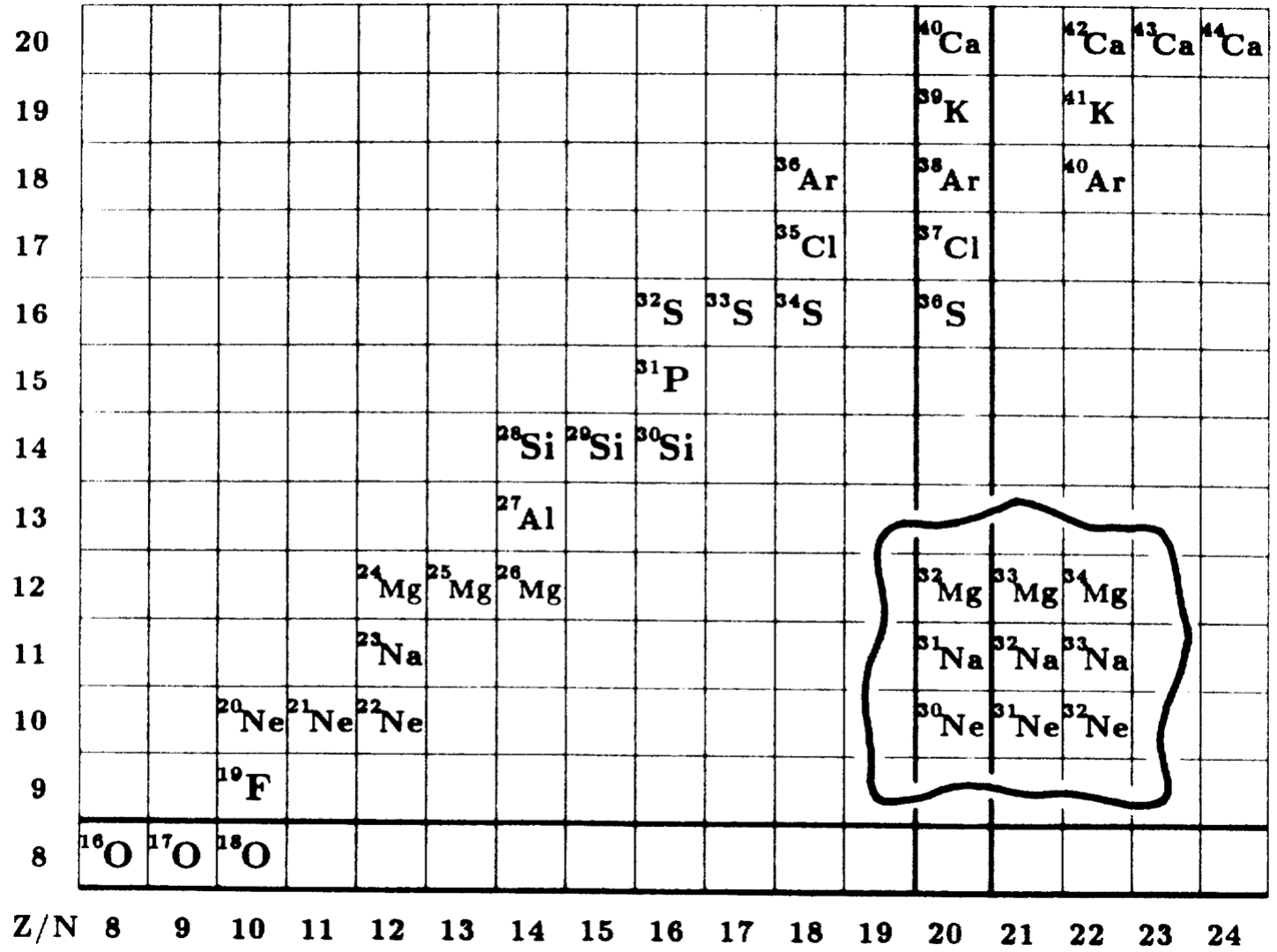

E.K. Warburton+ PRC 1990

Status of magicity

Magicity loss / emergence is found universally over the nuclear chart.

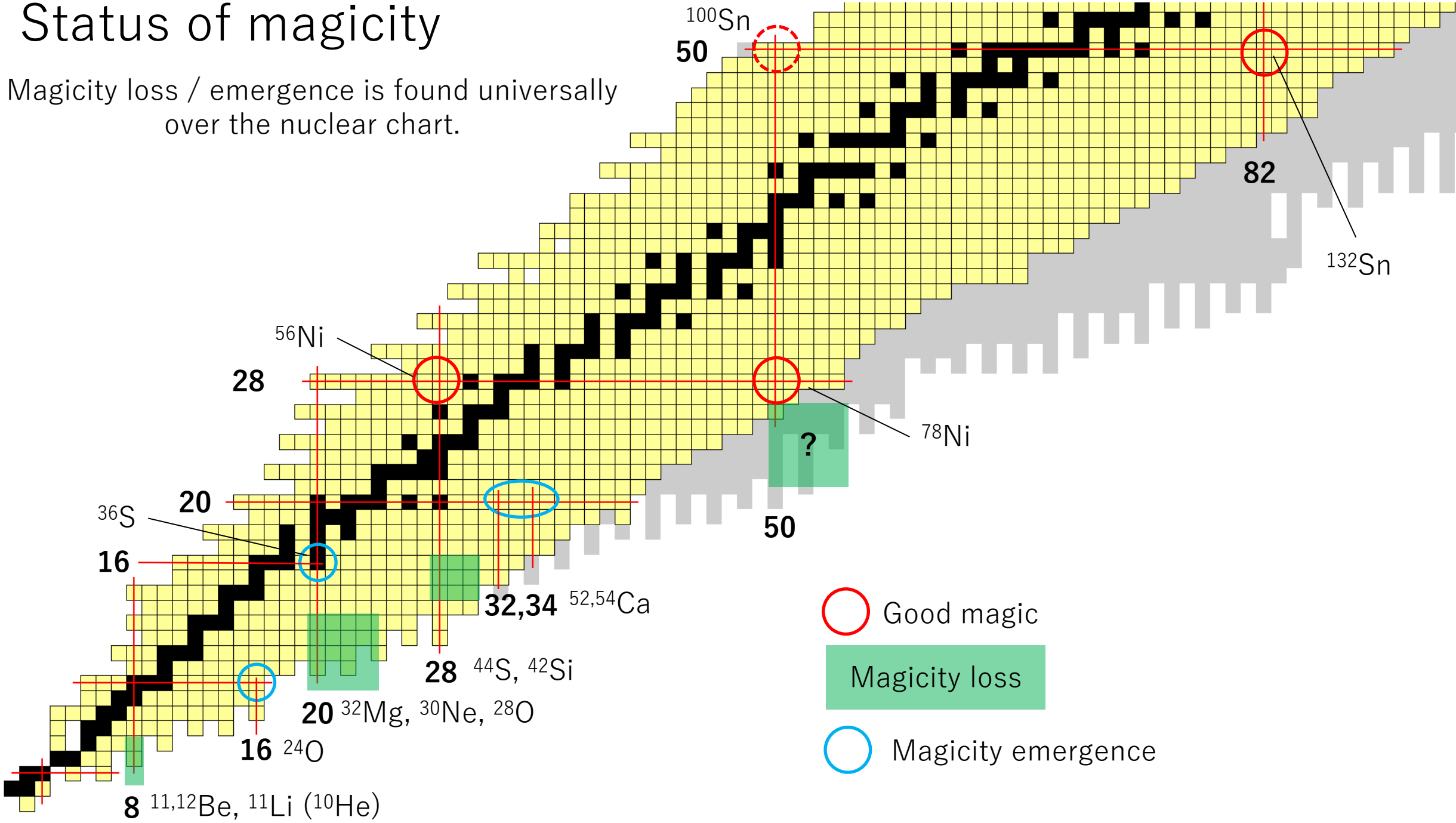

Emergent mean-field from nuclear force

N. Tsunoda+ 2017

Conventional shell model calculations using **fitted interactions**

Cutting-edge calculations using **effective interaction obtained from QCD-based interaction and three-body force**.

Extended Kuo-Krenciglowa (EKK) theory + Entem-Machleidt **QCD-based χN$_3$LO interaction** + **Fujita-Miyazawa three-body force**

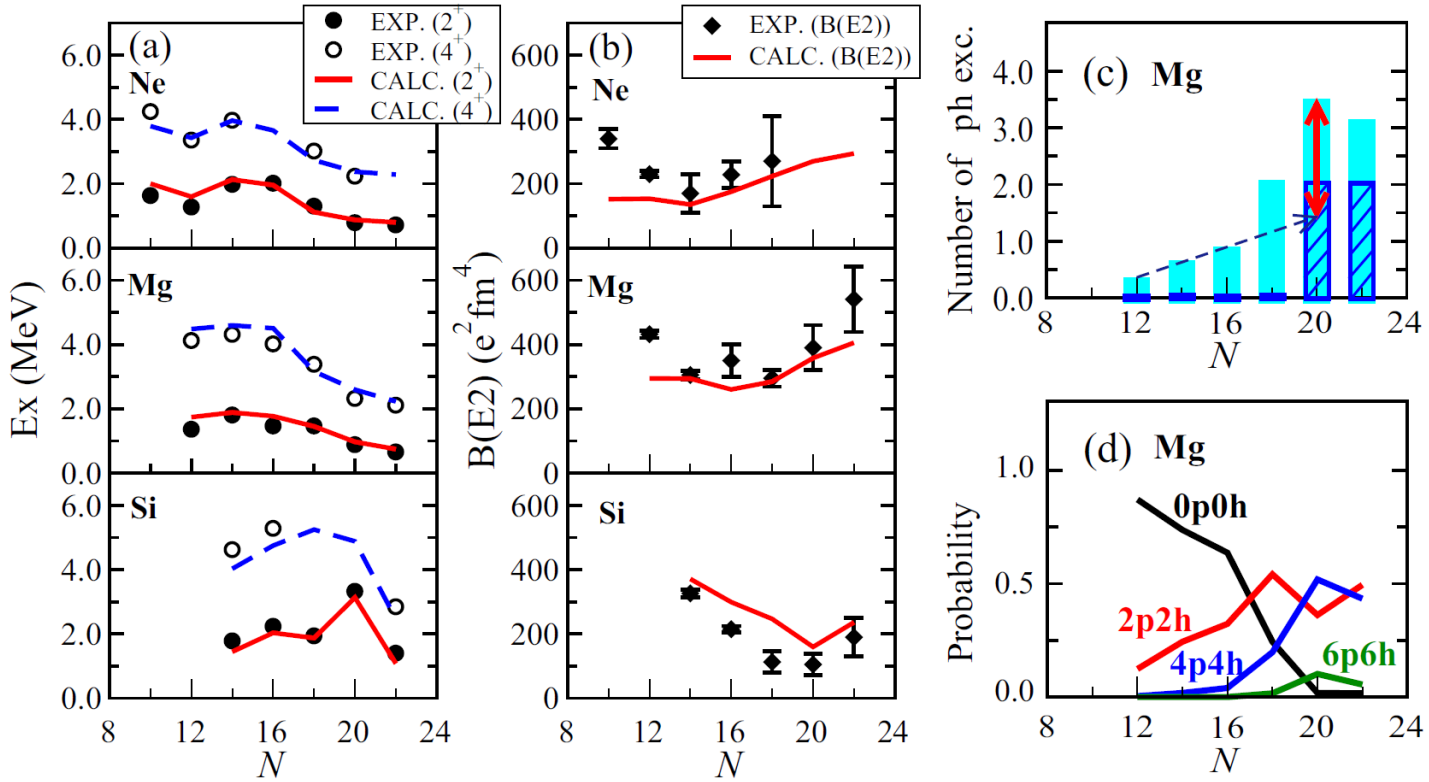

Emergent mean-field from nuclear force

Three body force acts repulsively to decrease binding energies for all orbitals.
Tensor force has stronger orbital dependence.

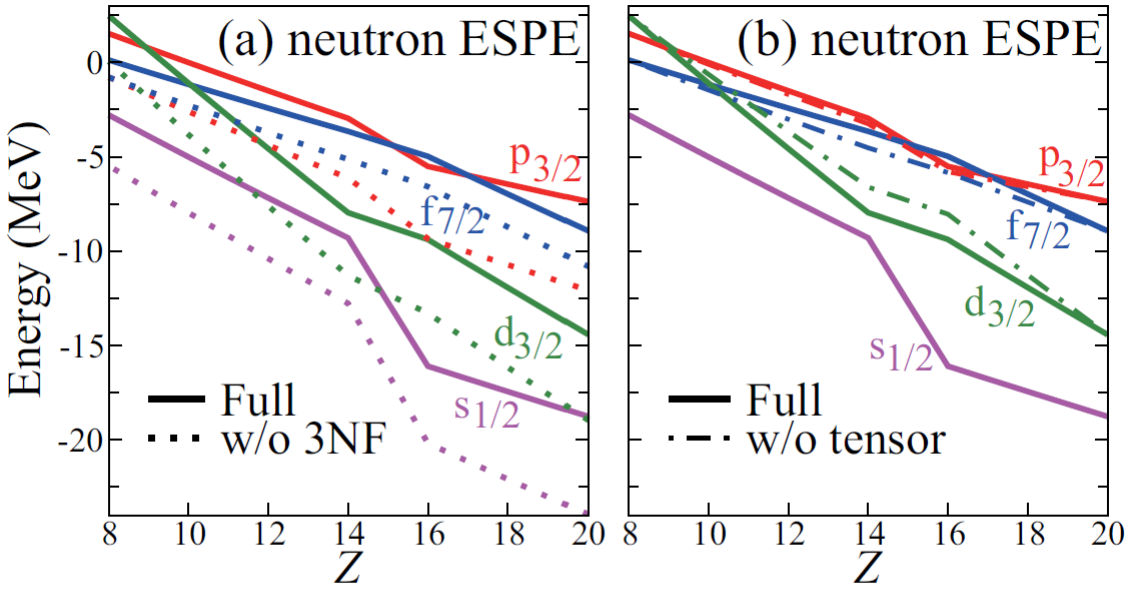

FIG. 5. ESPEs of $N = 20$ isotones for neutrons obtained in the normal filling scheme. (a) The case with and without three-nucleon forces. (b) The case with and without the tensor force.

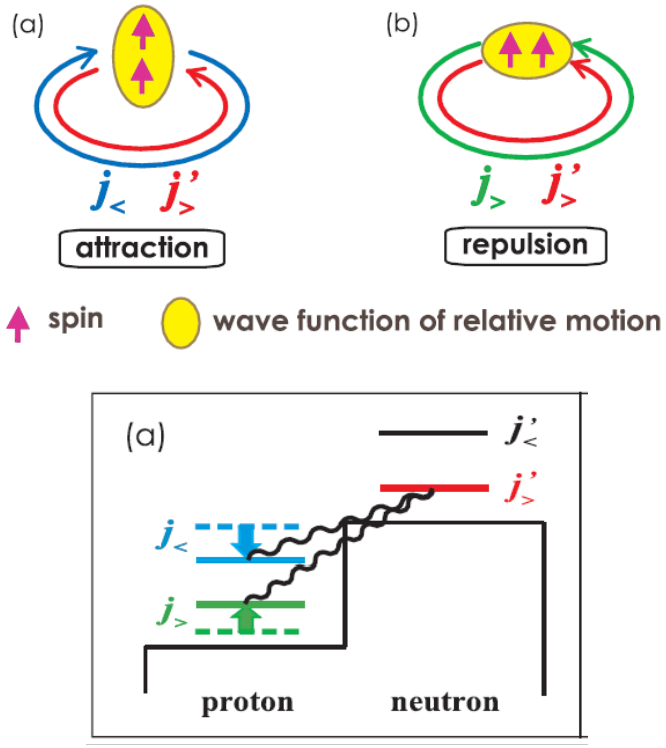

T. Otsuka+ PRL 2005

Antisymmetrized molecular dynamics (AMD)

The large β from B(E2) is in line with **large deformation predicted for the ground state**.
The ground state is dominated by 2p2h configurations, while spherical 0p0h goes to an excited state.

Courtesy M. Kimura

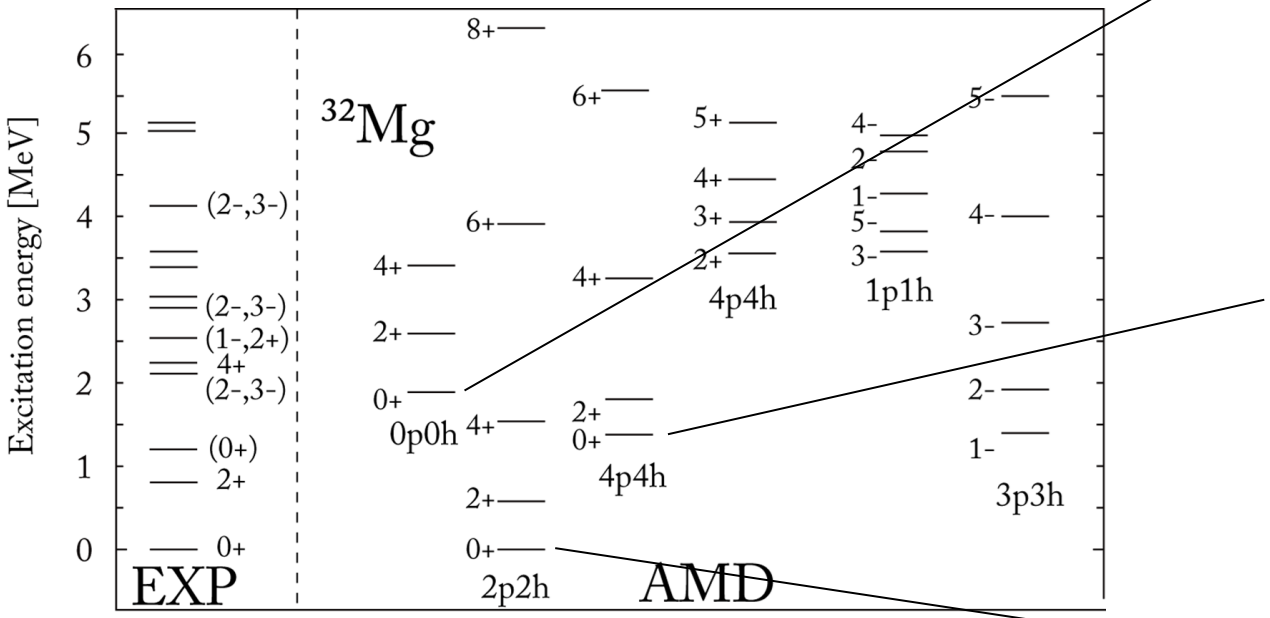

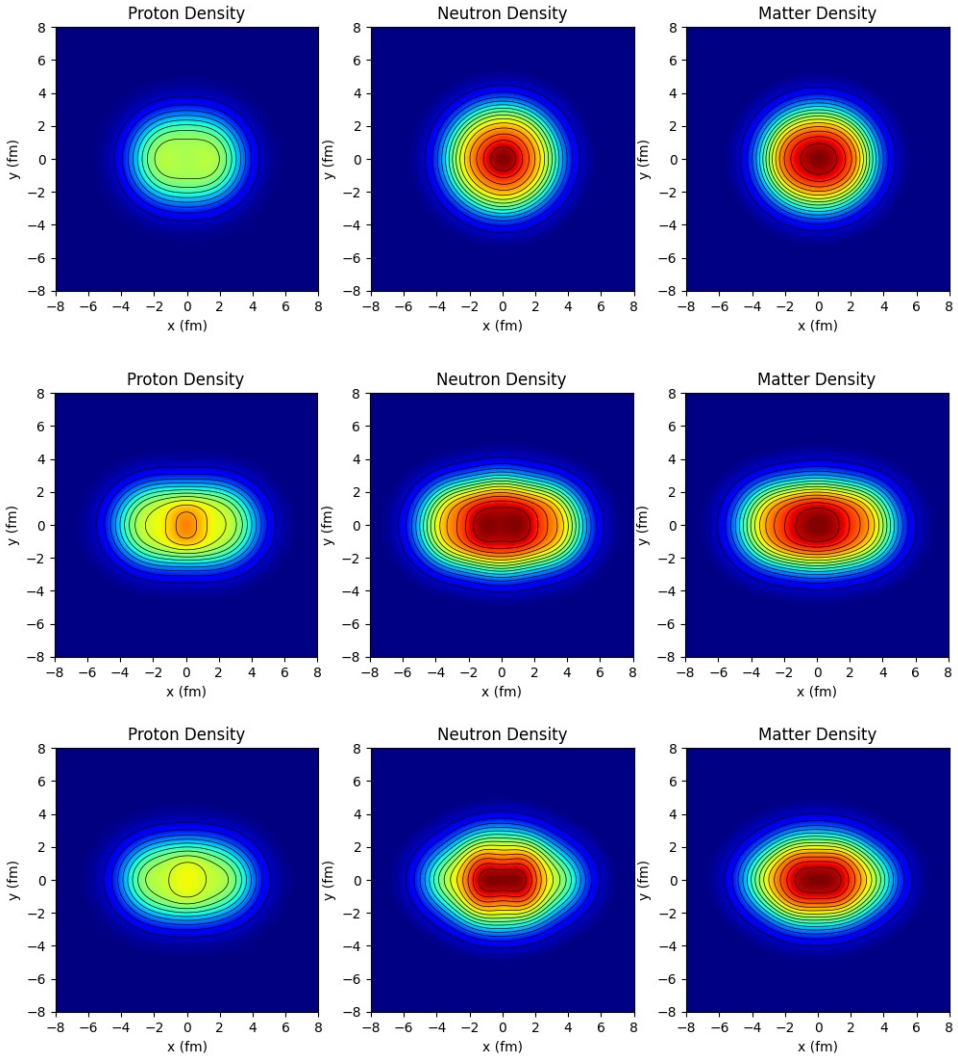

Single particle motion and collective motion

The case of ^{32}Mg illustrates how closely the single particle motion (shell evolution) is related to the collective motion (deformation). Only addition of a few nucleons drastically change the shape of nucleus.

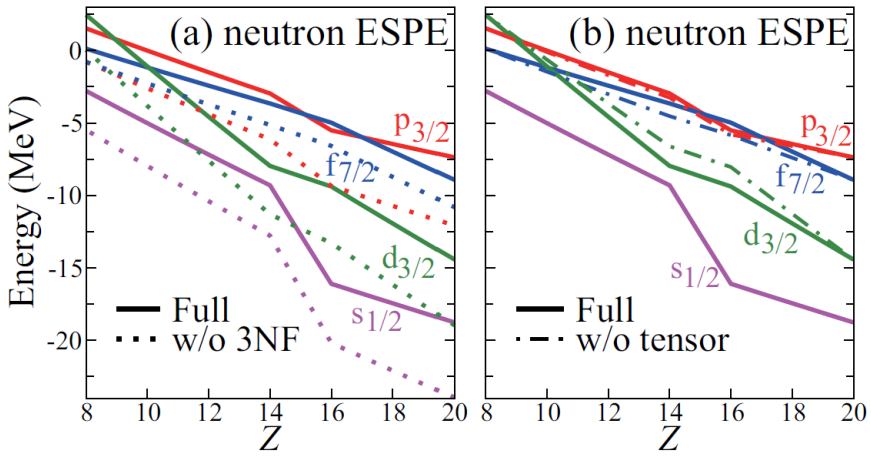

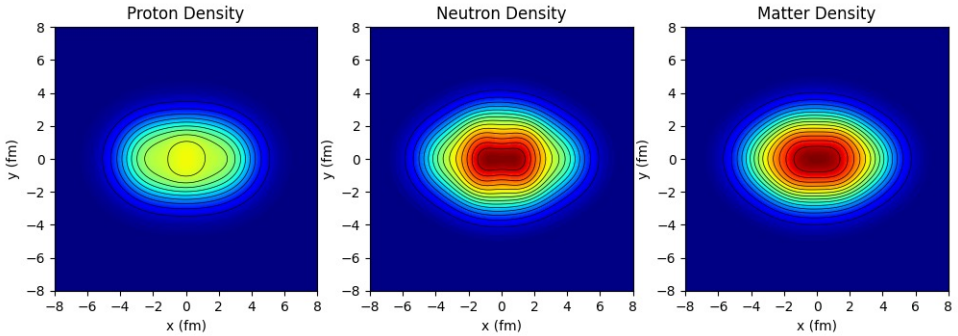

What is the mechanism
to link the two motions
of fundamentally
different nature?

Deformation of liquid drop

Let's brainstorm with a simple classical picture.
Liquid droplet is an example of density-saturated object.

Surface tension keeps the surface to be spherical.

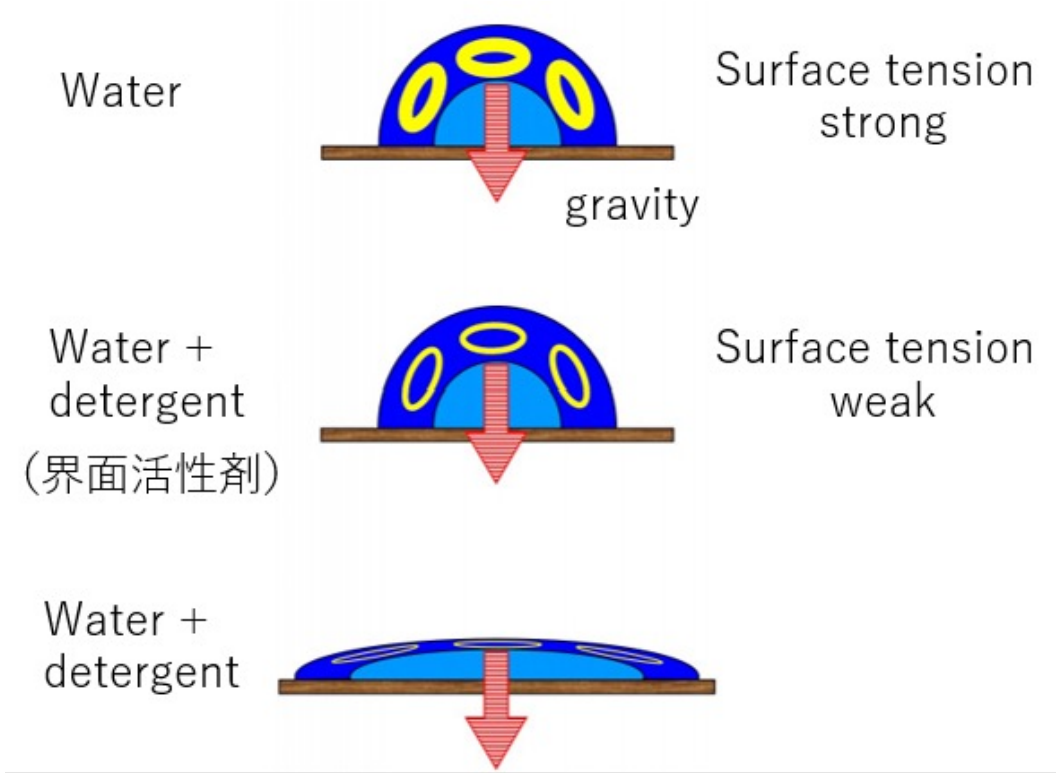

Surface tension, or surface free energy are quantified in **mN/m** or in **mJ/m²**

Liquid	℃	mJ/m²
Water	0	75.64
Water	25	71.97
Water	50	67.91
Water	100	58.85
Ethanol	20	22.27
Ethanol (11.1%) + water	25	46.03
Sucrose (55%) + water	20	76.45
Blood	22	55.89
Liquid nitrogen	−196	8.85
Liquid helium II	−273	0.37
Mercury	15	487.00

Surface tension vs. Volume energy

To quantify whether the surface tension is strong or weak, take the ratio of surface tension (free energy) with respect to the volume energy.

Surface tension of water droplet

Water:
Surface free energy: 73 mJ/m^2 = 7.3 × 10^{-5} J/cm^2
Latent heat: 2.25 kJ/cm^3

$$R_{surf} = \frac{SFE \times 4\pi r^2}{LH \times \frac{4\pi}{3} r^3} = \frac{3\,SFE}{r\,LH} = \frac{10^{-8}}{r\ (\mathrm{cm})}$$

Water droplets of typical size (~1 mm) has **extremely small fraction of energy in the surface.**

Soft and deformative surface.

Surface tension of atomic nuclei

^{24}Mg:
Volume: 16 MeV × 24 = 384 MeV
Surface: -19 MeV × 24$^{2/3}$ = -158 MeV

$$B(A,Z) = b_v A - b_s A^{2/3} - \frac{1}{2} b_{\mathrm{sym}} \frac{(N-Z)^2}{A} - b_C \frac{Z^2}{A^{1/3}} + \delta(A)$$

$b_{\mathrm{v}} = 16$ MeV $b_{\mathrm{s}} = 19$ MeV $b_{\mathrm{sym}} = 45$ MeV $b_{\mathrm{C}} = 0.77$ MeV

Surface of ^{24}Mg contains an energy corresponding to about **half of the volume energy.**

Extremely stiff surface unfavorable for deformation.

* If the droplet size is **~ 0.1 nm**, R_{surf} ~ 1 similar to the situation of atomic nuclei.

Density saturation, shape and shell

Density saturation constrains **coordinate space (shape) and momentum space (shell).**

Spherical symmetry

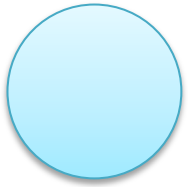

Surface energy

Density saturation

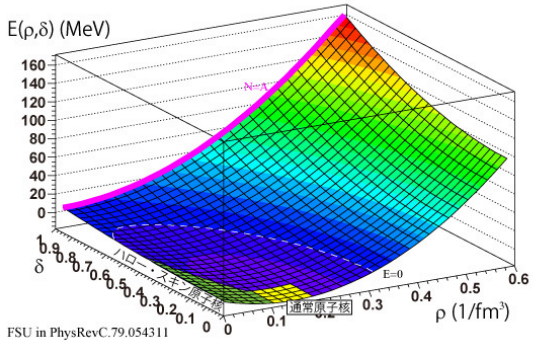

Flat-bottom potential

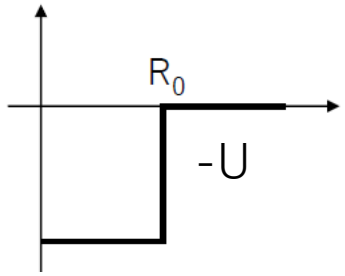

Spin-orbit
Tensor force
Three-body force

Shape deformation

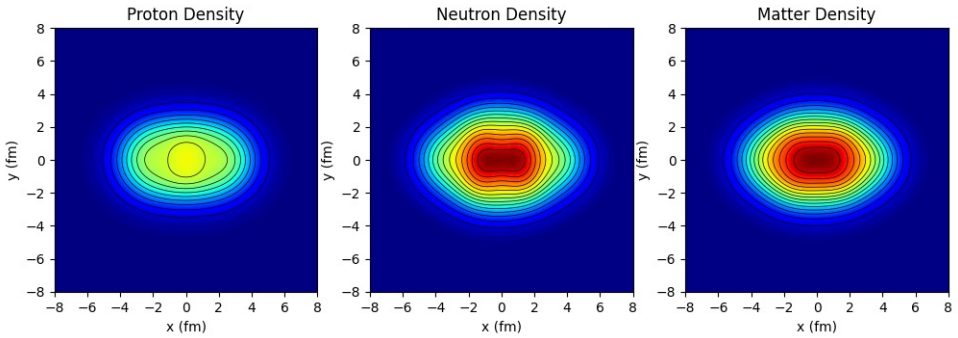

Shell evolution

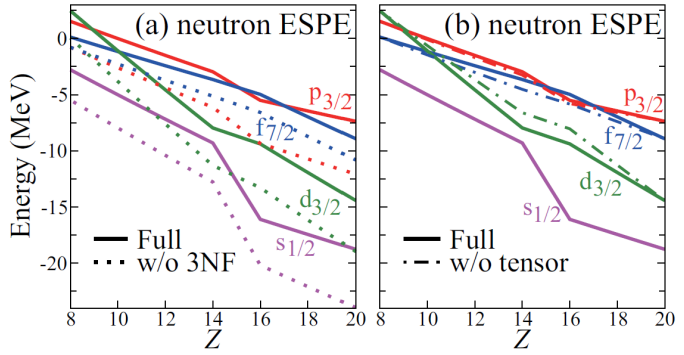

Jahn-Teller effect (or distortion)

A **universal mechanism of spontaneous symmetry breaking** in quantum many-body systems.
A quantum state can stabilize by **breaking the symmetry**, or by **breaking the degeneracy.**

H. Jahn and E. Teller (1937), “Stability of Polyatomic Molecules in Degenerate Electronic States. I. Orbital Degeneracy”, Proceedings of the Royal Society of London 161, 220.

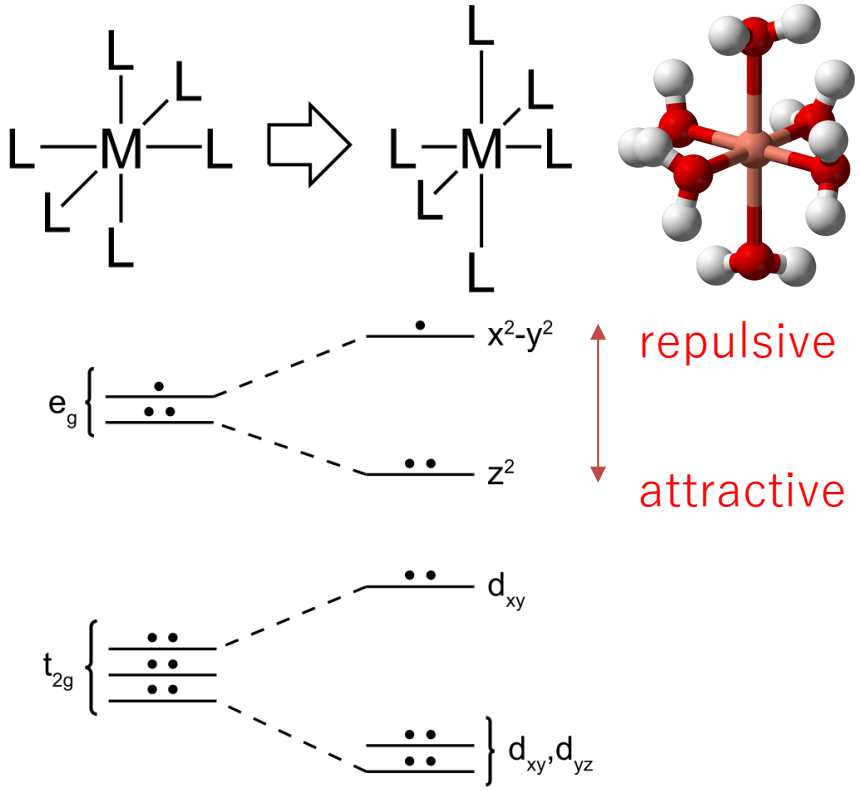

ヘキサアクア銅(II)イオン
$[Cu(OH_2)_6]^{2+}$

Often occurs for octahedral complexes of the transition metals.

Nilsson diagram

Breaking of spherical symmetry leads to splitting of single particle states (Nilsson orbitals).
Deformation leads to energy gain by Jahn-Teller effect.

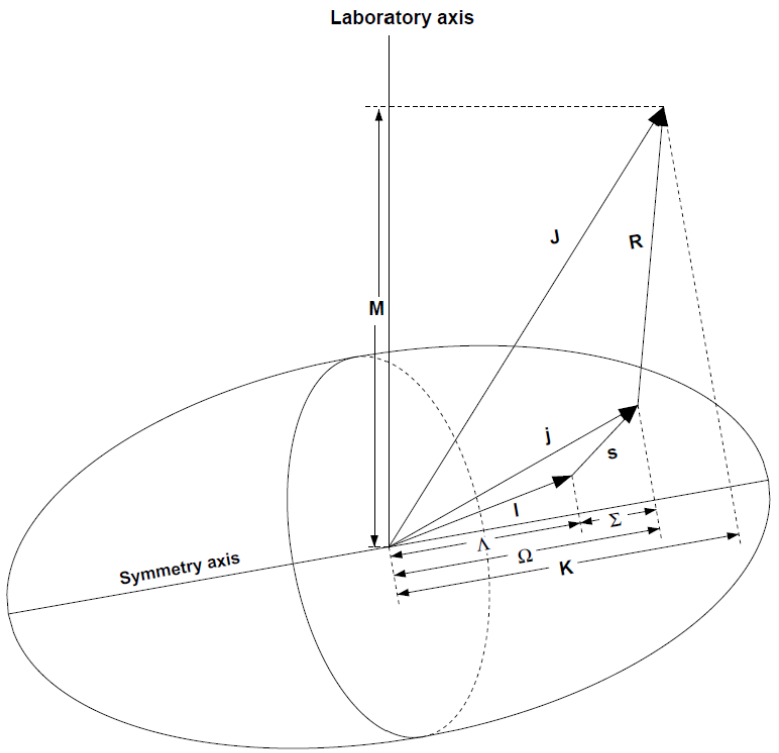

Figure 2. Asymptotic quantum numbers for the deformed shell model

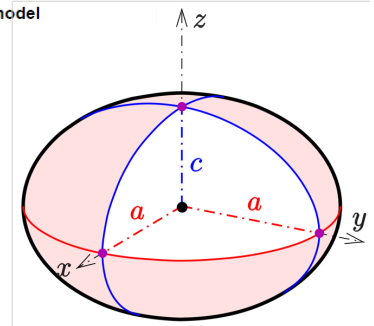

oblate

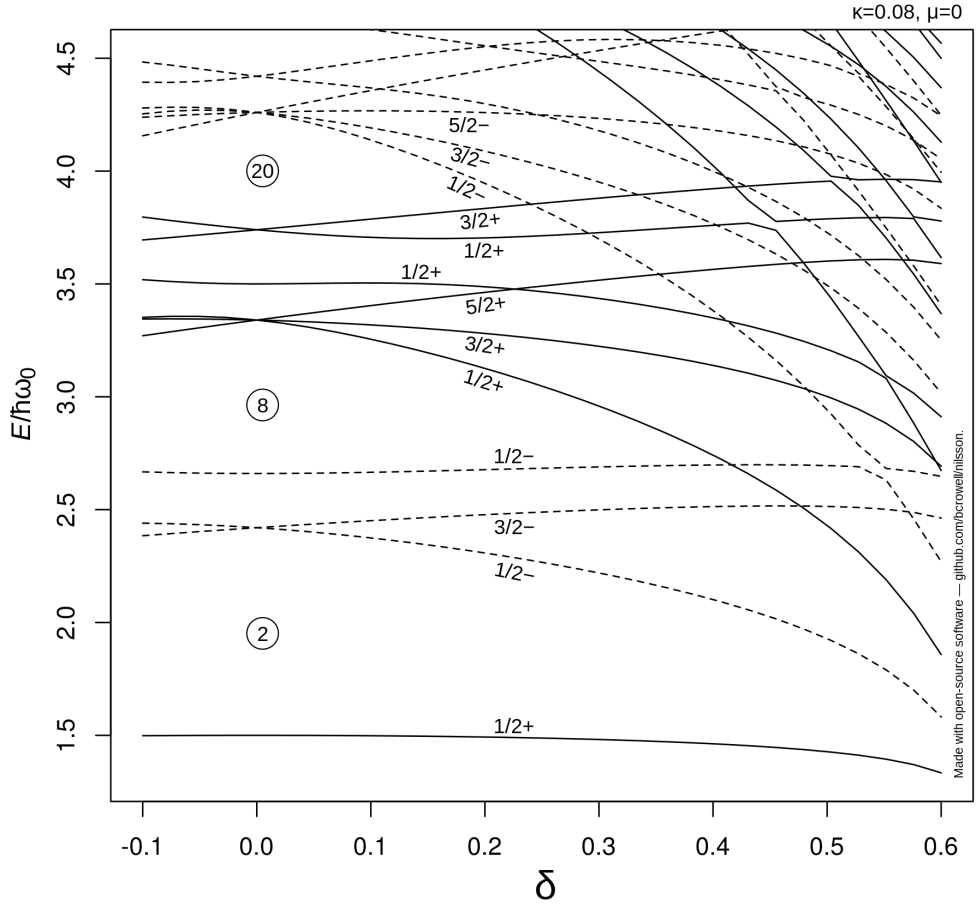

prolate

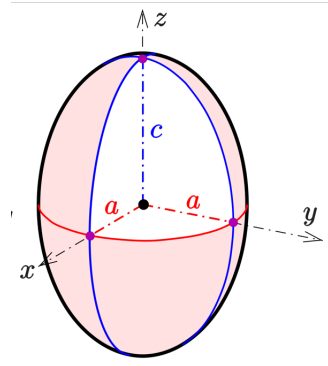

Energy scale of surface deformation of ellipsoid

Can the loss of surface energy in deformation be compensated by Jahn-Teller energy?
Under the density saturation, **the energy scale of deforming surface is about a few MeV**,
comparable to the shell evolution.

Ellipsoid surface area under constant volume (density saturation)

$$S_{\text{oblate}} = 2\pi a^2 \left(1 + \frac{c^2}{ea^2}\,\text{artanh}\, e\right),$$

$$e^2 = 1 - \frac{c^2}{a^2} \text{ and } (c < a),$$

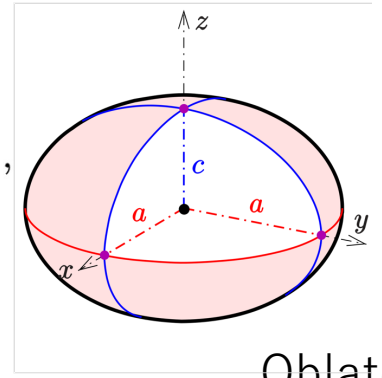

$$V = \frac{4}{3}\pi abc = const.$$

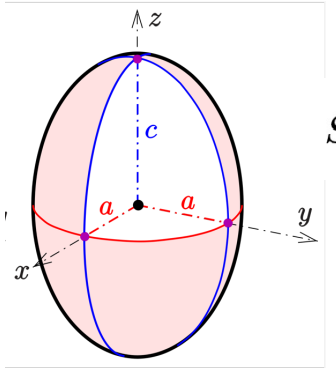

$$S_{\text{prolate}} = 2\pi a^2 \left(1 + \frac{c}{ae}\arcsin e\right)$$

$$e^2 = 1 - \frac{a^2}{c^2} \text{ and } (c > a),$$

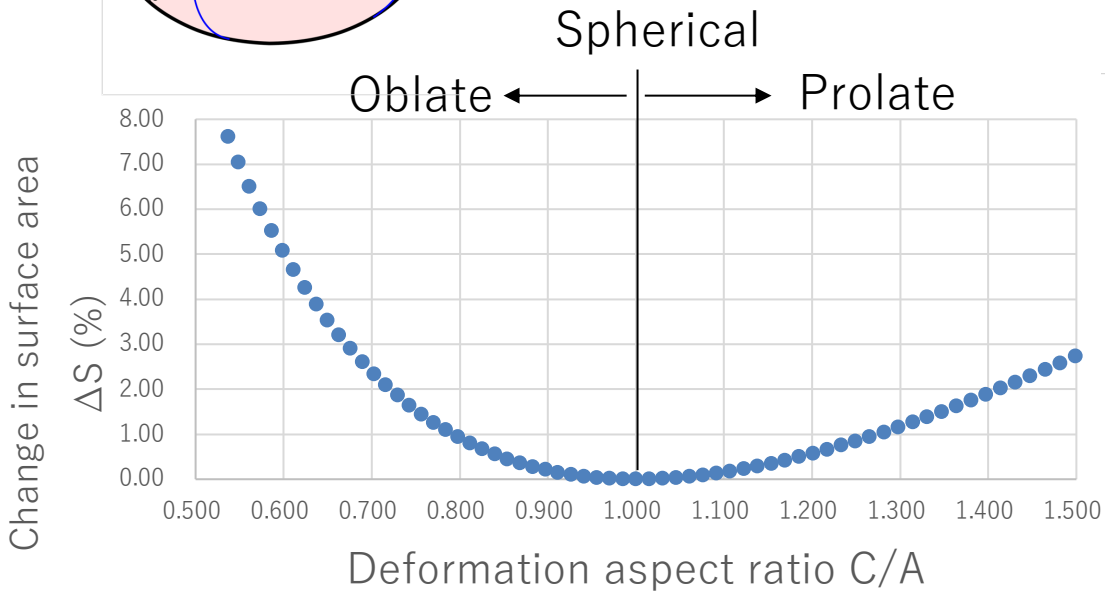

Surface energy loss ~ **1%**

^{24}Mg:
Surface energy 158 MeV
→ loss of **1.6 MeV**

Jahn-Teller effect

Whether JTE gets effective or not depends on the energy balance between energy gain of JTE and energy loss associated with the symmetry breaking.

Spherical symmetry

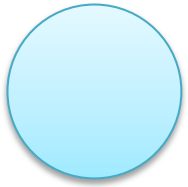

Surface energy

Jahn-Teller energy

Density saturation

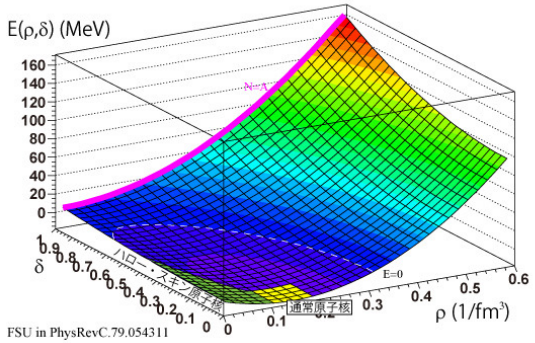

Flat-bottom potential

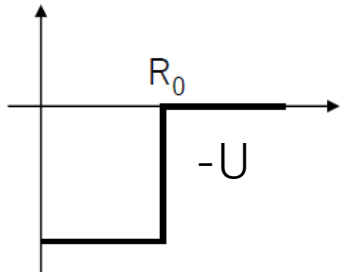

Spin-orbit
Tensor force
Three-body force

Shape deformation

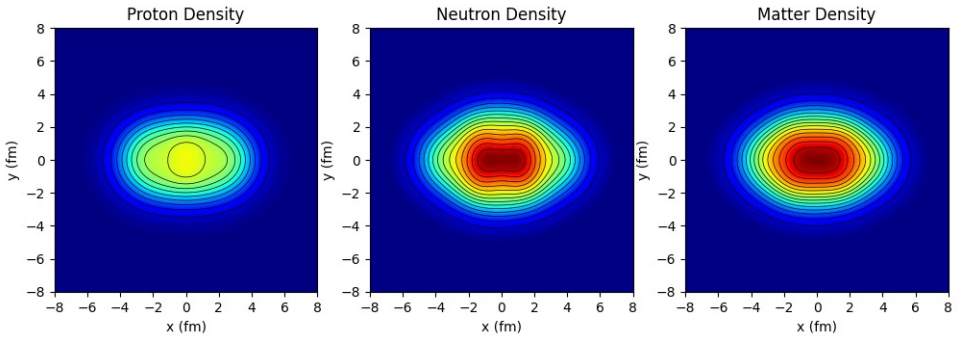

JTE

Energy scale

Shell evolution

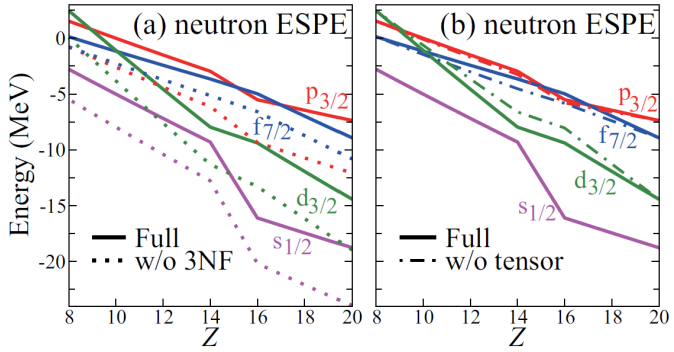

What Jahn-Teller effect brings to nuclei

Emergence of various shapes

Shape coexistence

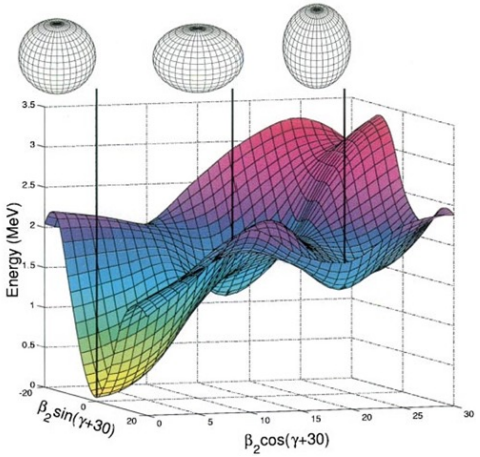

Exotic shape

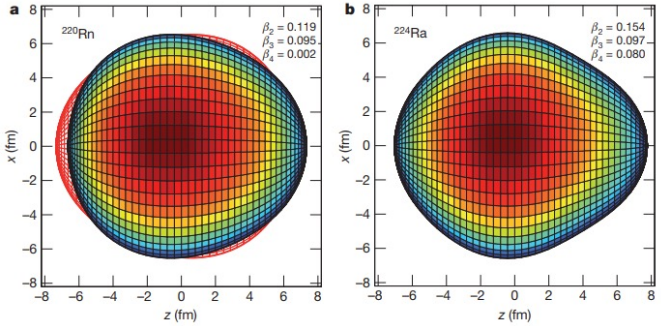

Coherence in evolutions

JTE serves as an interface for different symmetries to interact in organizing structure.

Single-particle motion

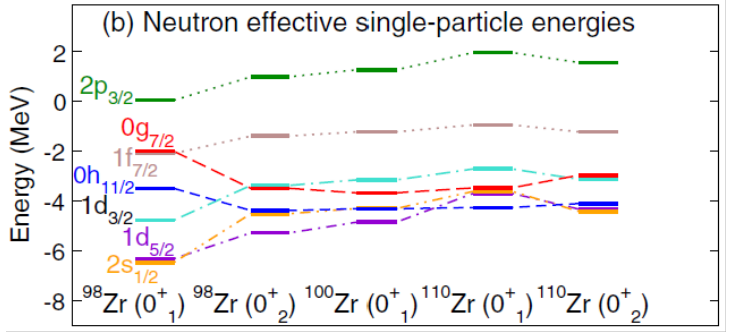

Collective motion

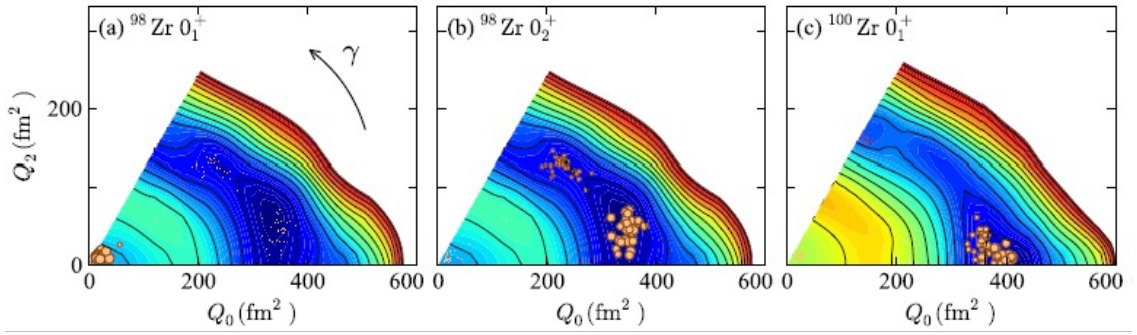

How about atom?

A mean field study was made to see whether an atom has deformation or not.
It is found that single particle deformation can occur, but **no collective deformation.**

'On deformability of atoms—comparative study between atoms and atomic nuclei'
T. Naito, S. Endo, K. Hagino, Y. Tanimura, J. Phys. B: At. Mol. Opt. Phys. 54, 165201 (2021)

$$Q_{ij} = \int \left(3r_i r_j - \delta_{ij} r^2\right) \rho\left(\boldsymbol{r}\right) d\boldsymbol{r}$$

$$\beta_k = \sqrt{\frac{\pi}{5}} \frac{Q_k}{N_{\mathrm{tot}} \left\langle r^2 \right\rangle}$$

unrestricted Hartree-Fock method

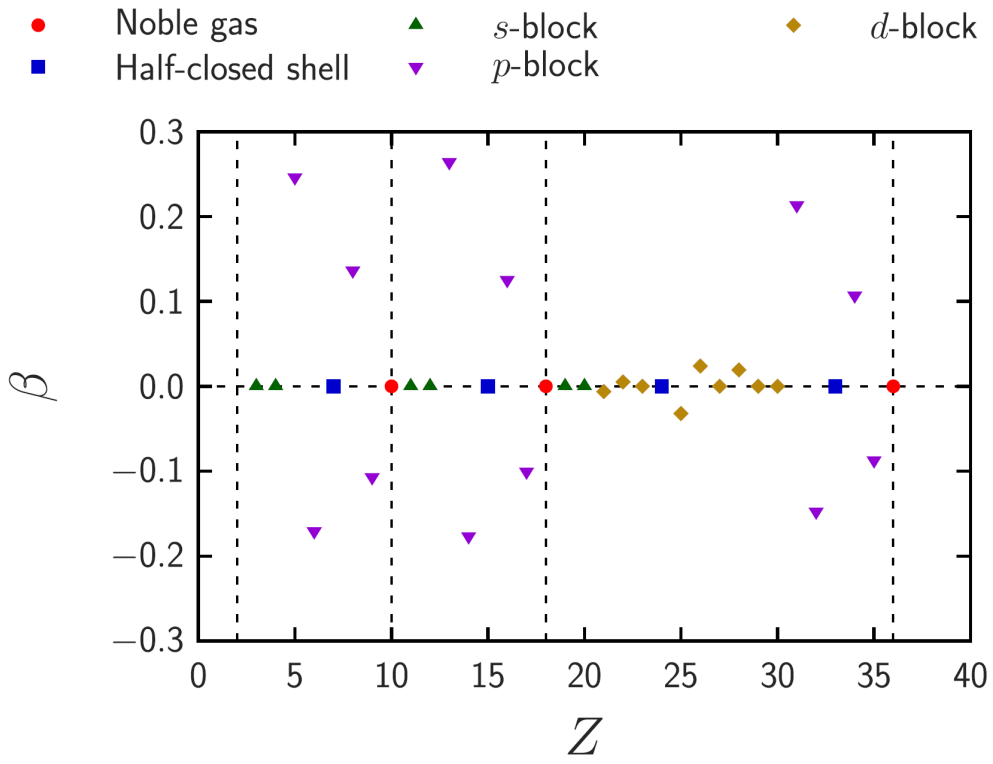

Nuclear physics School for Young Scientists
(NUSYS-2024)

Oxygen puzzle

Single-particle and collective motions near the dripline

Beijing Normal University (Zhuhai, Guangdong)
July 27 to August 2, 2024

- Spectroscopy of ^{24}O and ^{28}O
- How does the weaky-binding nature drive single-particle and collective motions?

Oxygen dripline anomaly

The heaviest bound O isotope is ^{24}O with N = 16. The dripline significantly extends for F.

Tsunoda+ Nature 2020

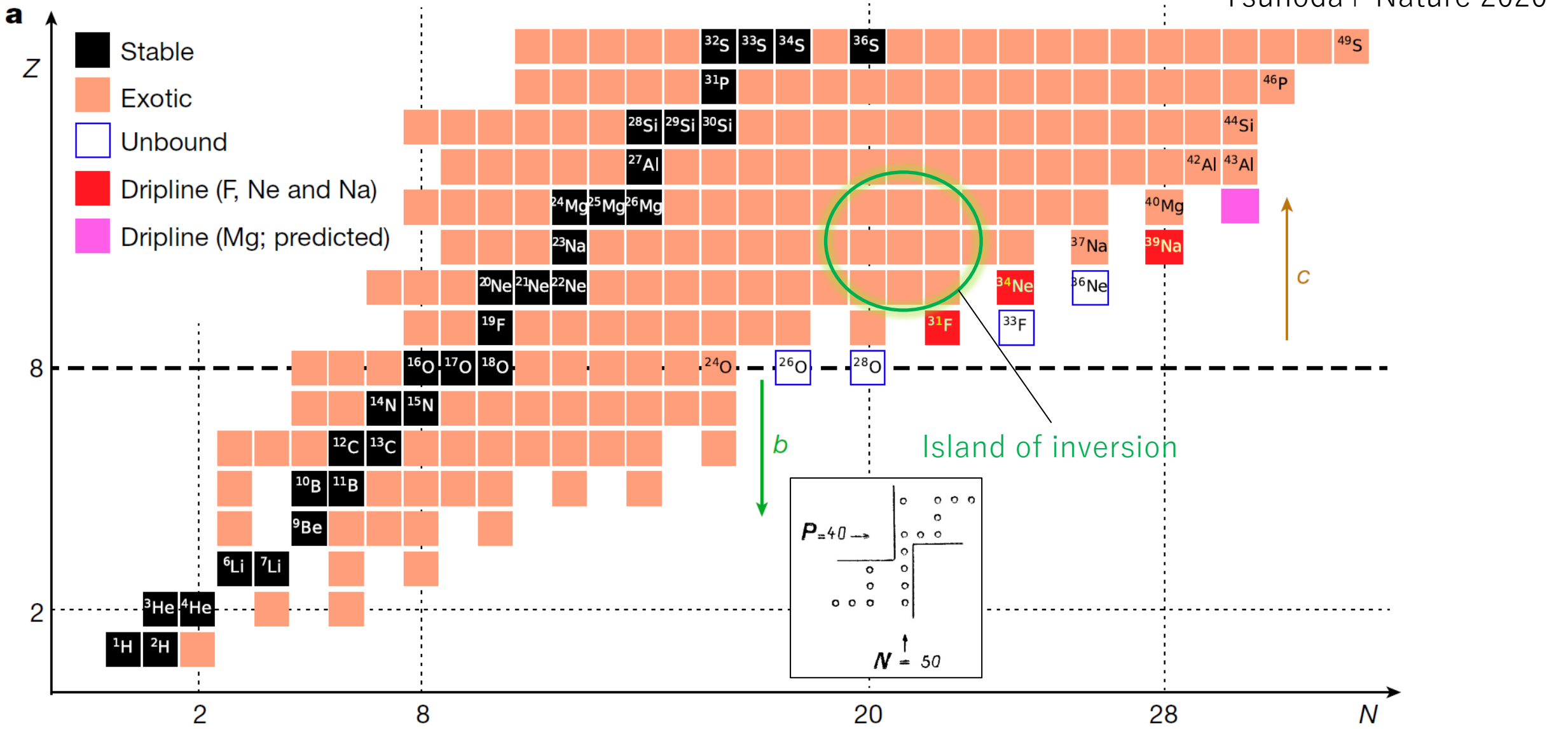

New magic number N = 16

N = 16 becomes magic as approaching the dripline. It was first suggested from the systematics of one-neutron separation energies S_n and later confirmed by spectroscopy of oxygen isotopes.
Magicity at N = 16 makes **the dripline isotope ^{24}O to be doubly magic**.

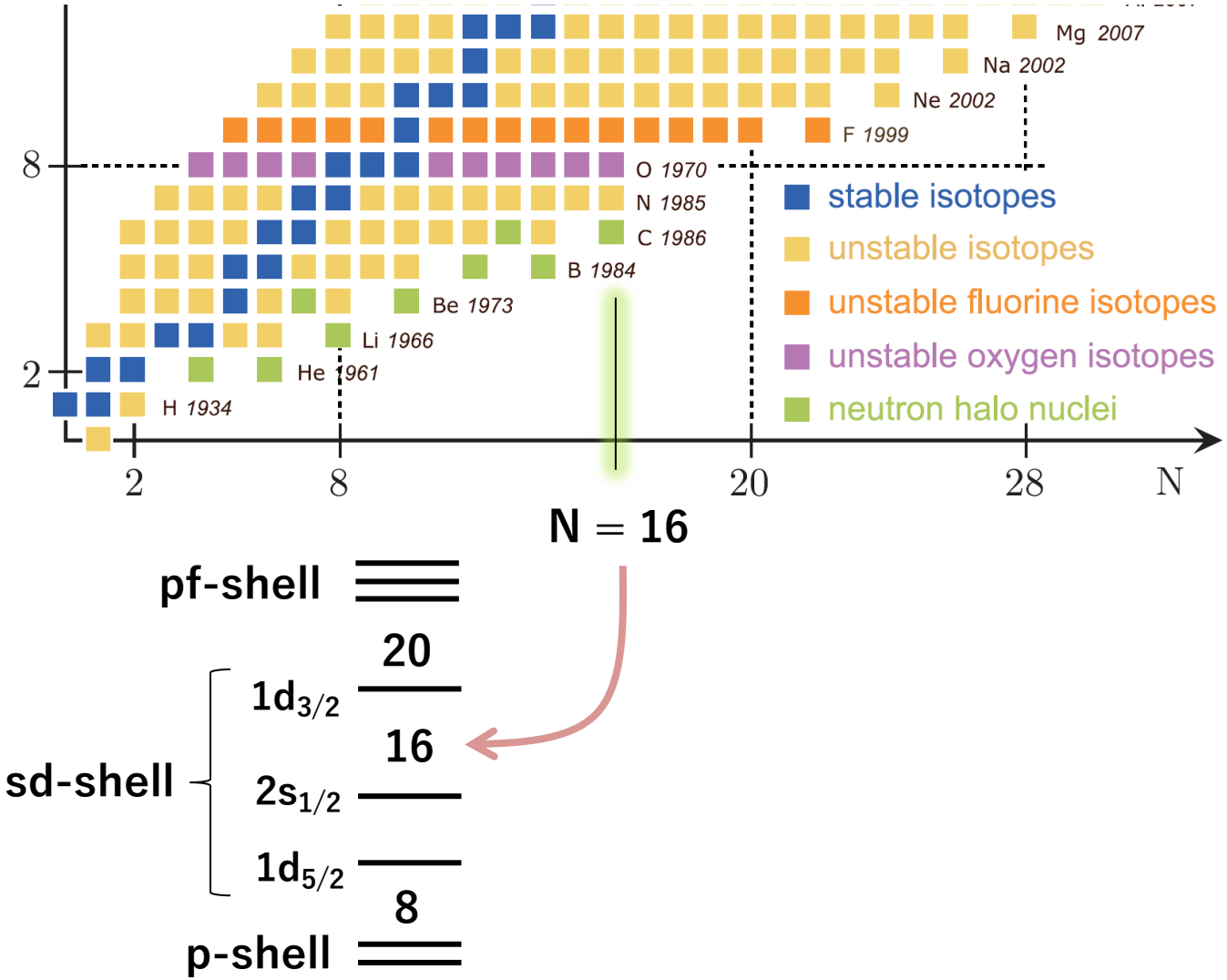

A. Ozawa+ PRL 2000

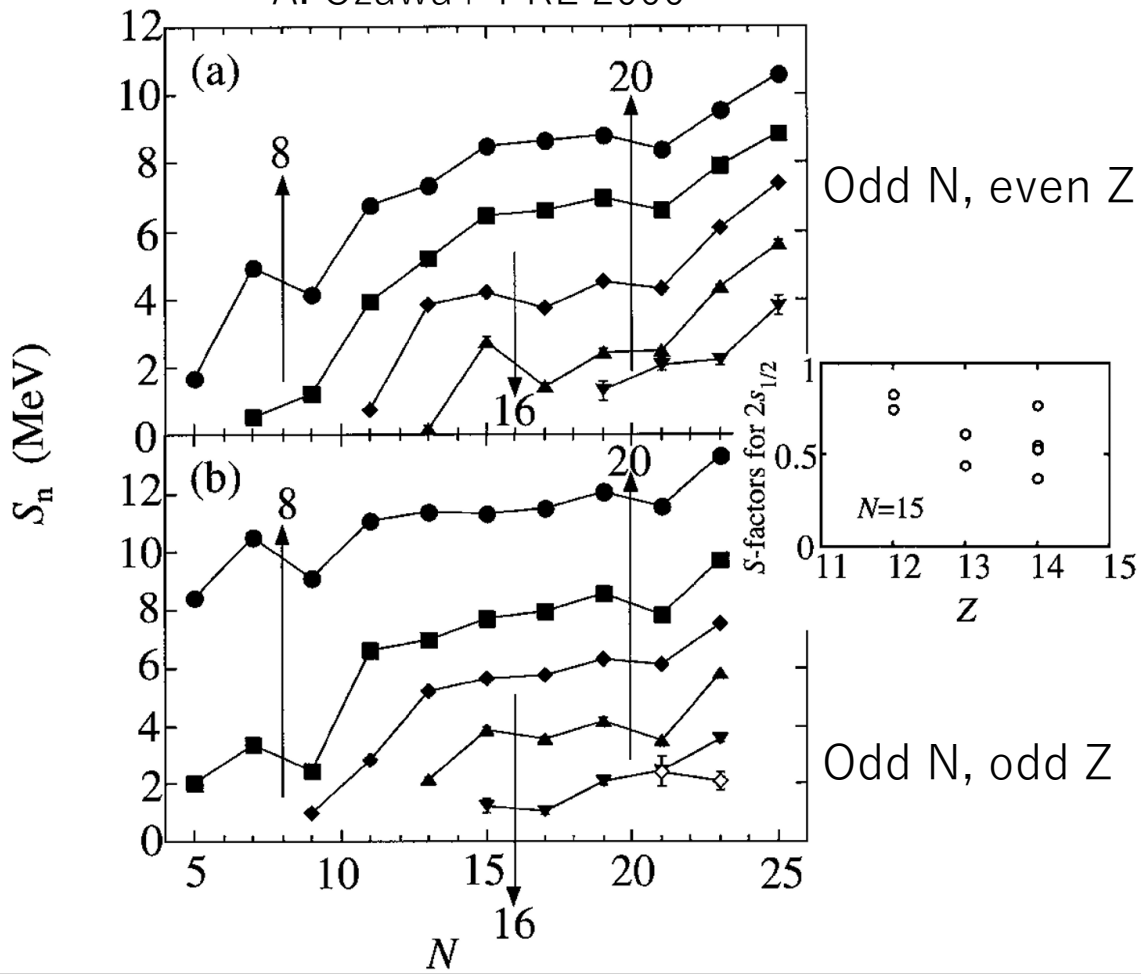

New magic number N = 16

The ^{24}O ground state was studied by one-neutron knockout reaction at GSI. The **parallel momentum distribution shows the $2s_{1/2}$ component is predominant**, thus indicating shell closure at N = 16.

R. Kanungo+ PRL 2009

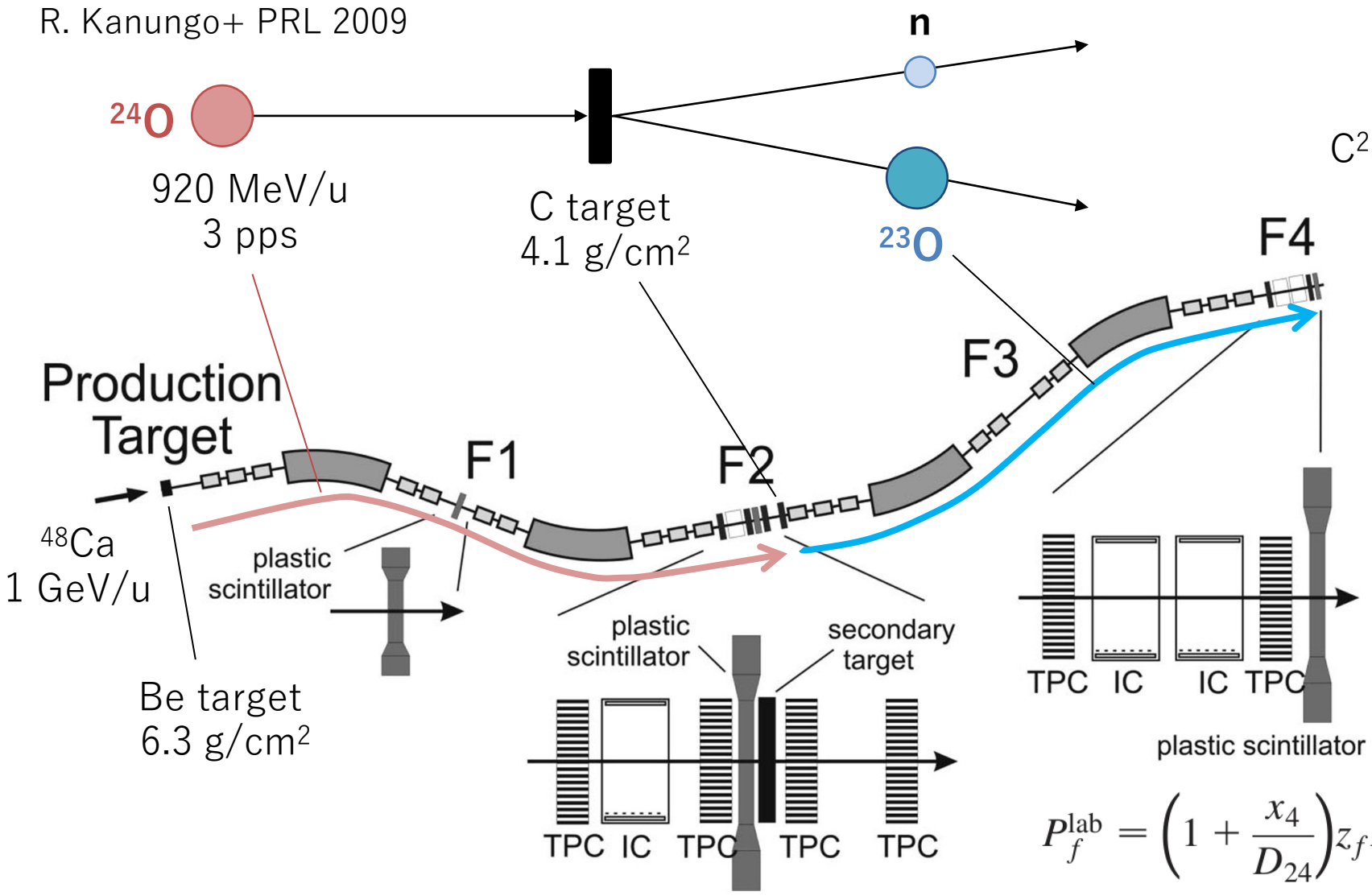

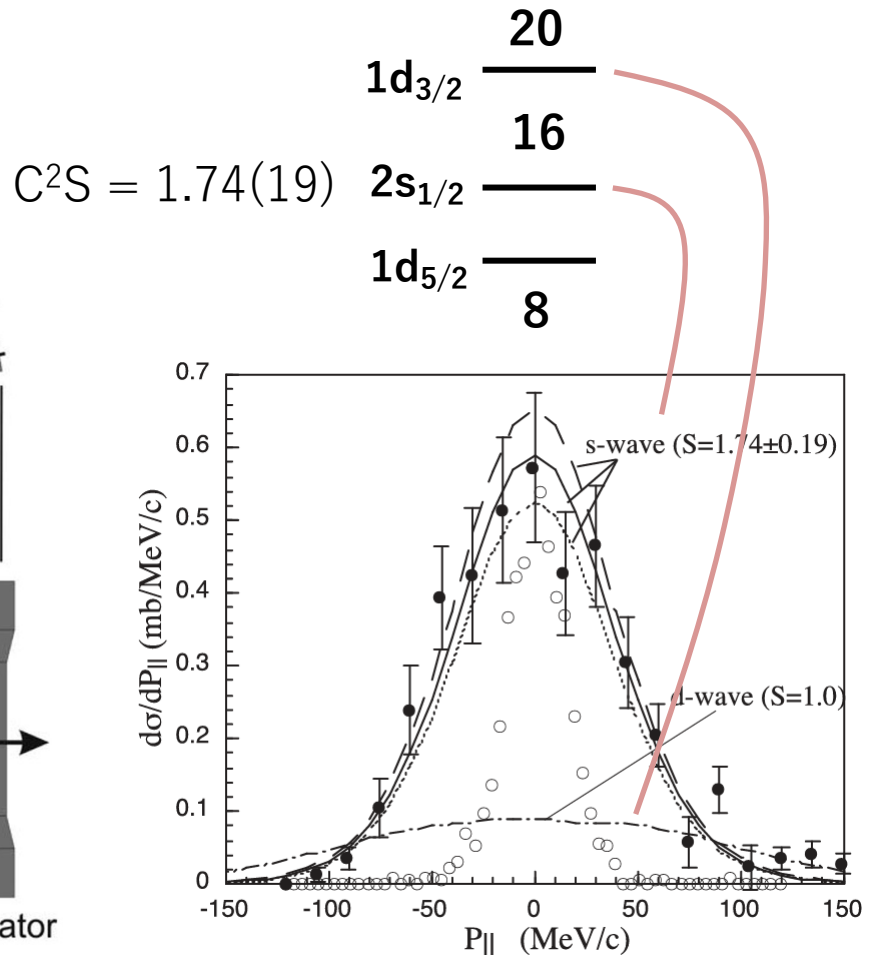

$$P_f^{\mathrm{lab}} = \left(1 + \frac{x_4}{D_{24}}\right) z_f B\rho, \longrightarrow P_{||} = \gamma_b (P_f^{\mathrm{lab}} - \beta_b E_f^{\mathrm{lab}}).$$

Lorentz boost

New magic number N = 16

The 2^+ state of ^{24}O was discovered by the invariant method using one-proton knockout reaction of ^{25}F at NSCL.
The systematics show **high excitation energy at N = 16**, indicating double-magicity of ^{24}O.

C.F. Hoffman+ PLB 2009

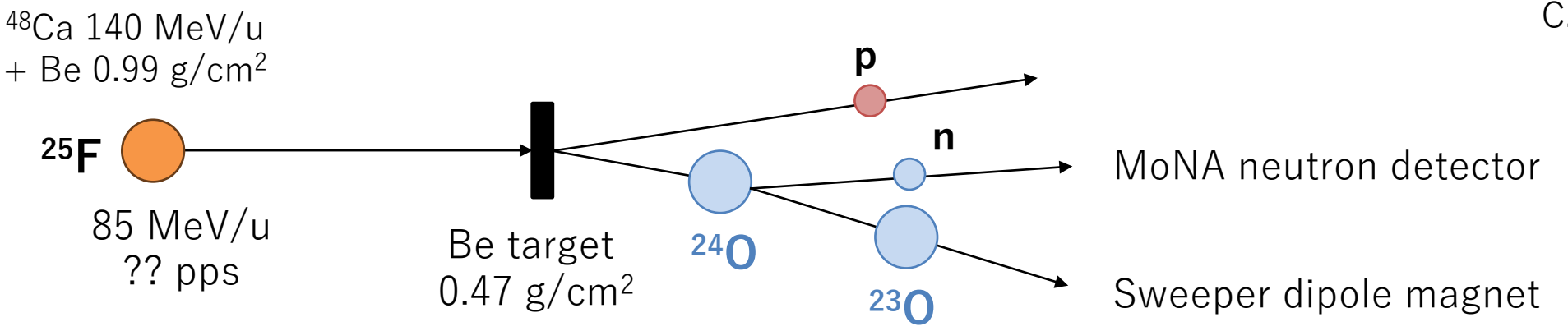

Invariant mass spectrum of ^{24}O

Energy-dependent Breit-Wigner line shape

Asymmetric shape with high energy tail

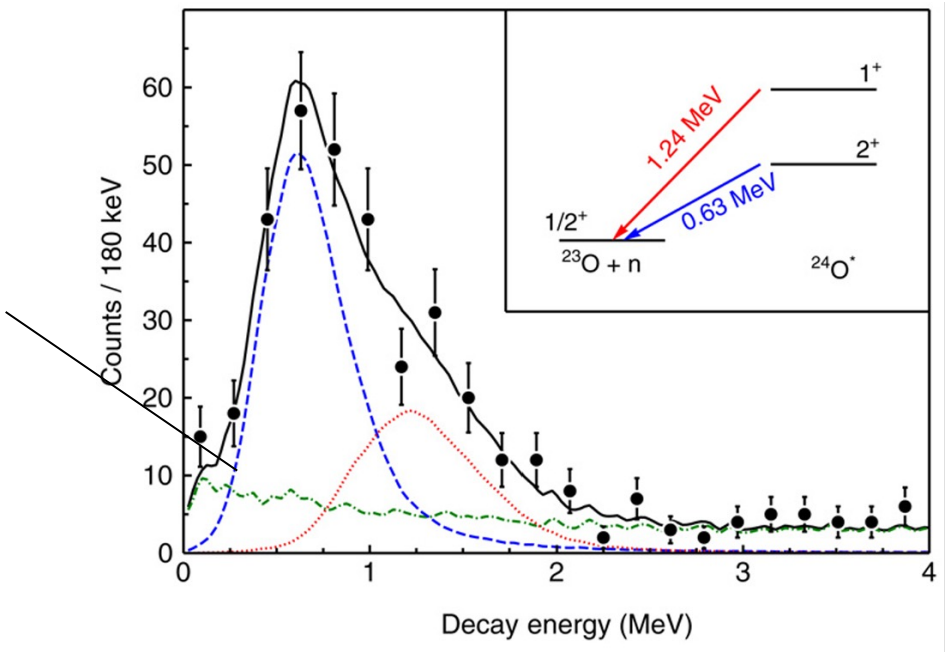

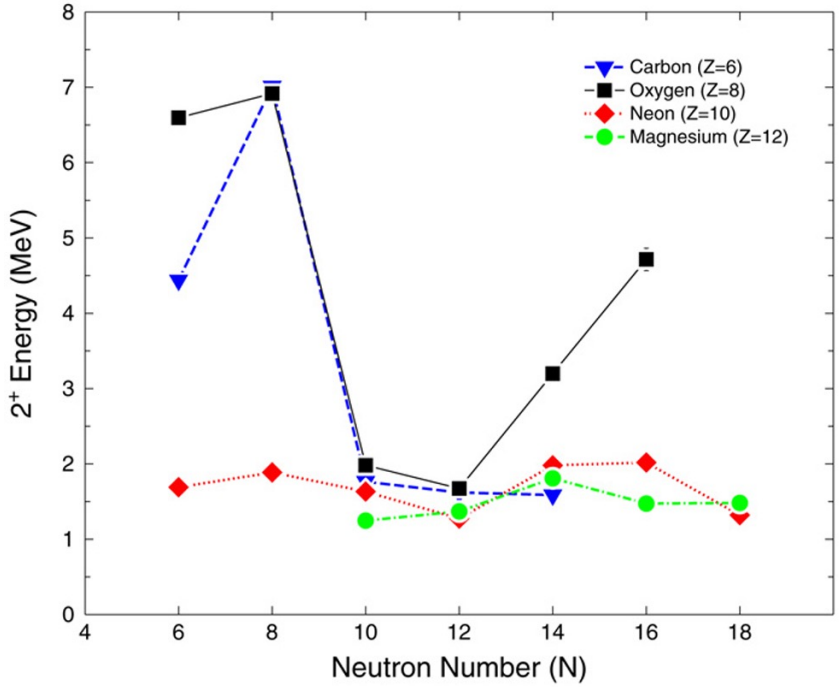

What happens with doubly-magic ^{28}O (Z = 8, N = 20)?

^{28}O is unbound (Sakurai+ 1999).
The ground state resonance has been elusive over two decades until 2023.
Spectroscopy of unbound ^{28}O has been a real challenge, as it decays by 4n emission.

H. Sakurai+ PLB 1999

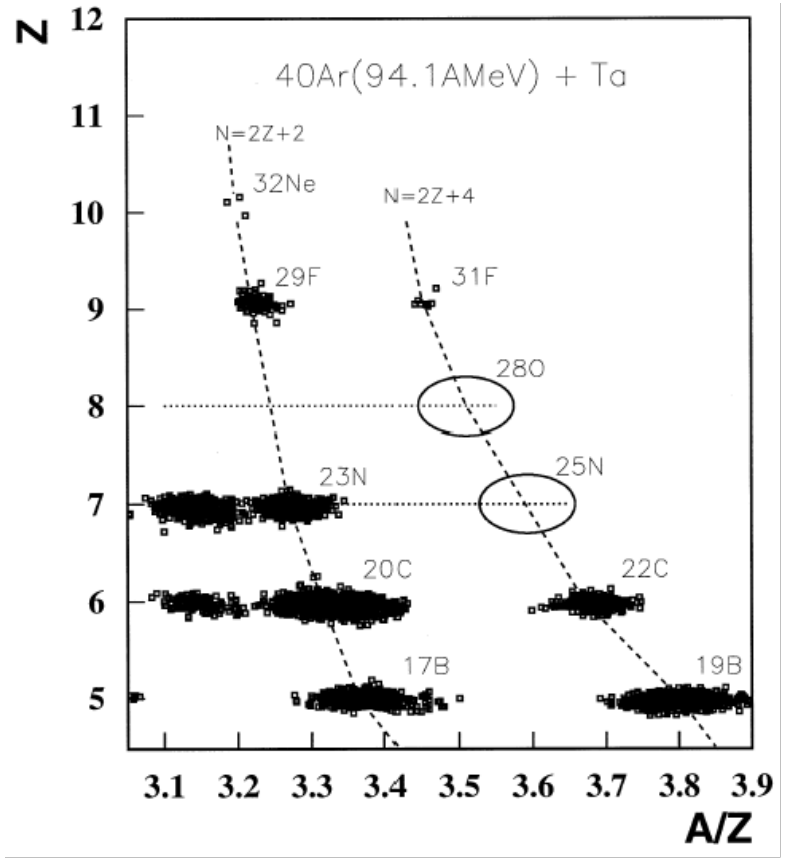

Invariant spectroscopy of ^{27,28}O

After two decades, direct spectroscopy of ^{28}O was finally successful at RIBF.
^{28}O was produced by knockout reaction of ^{29}F. The invariant method requires **simultaneous detection of 4 neutrons**, which is a great challenge in this experiment.

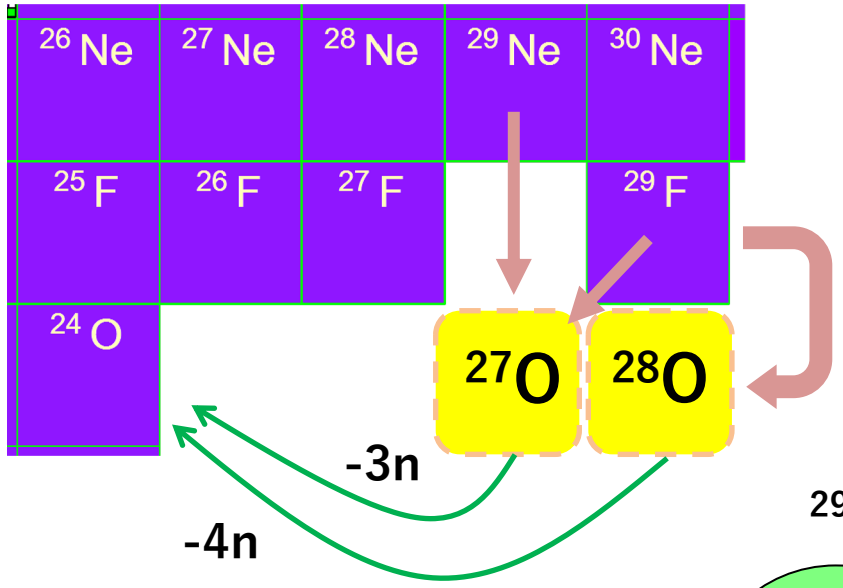

Y. Kondo+ Nature 2023

Invariant mass

$$M = \sqrt{\left(\sum E_i\right)^2 - \left(\sum \mathbf{p}_i\right)^2}$$

→ 4 neutrons coincidence is needed

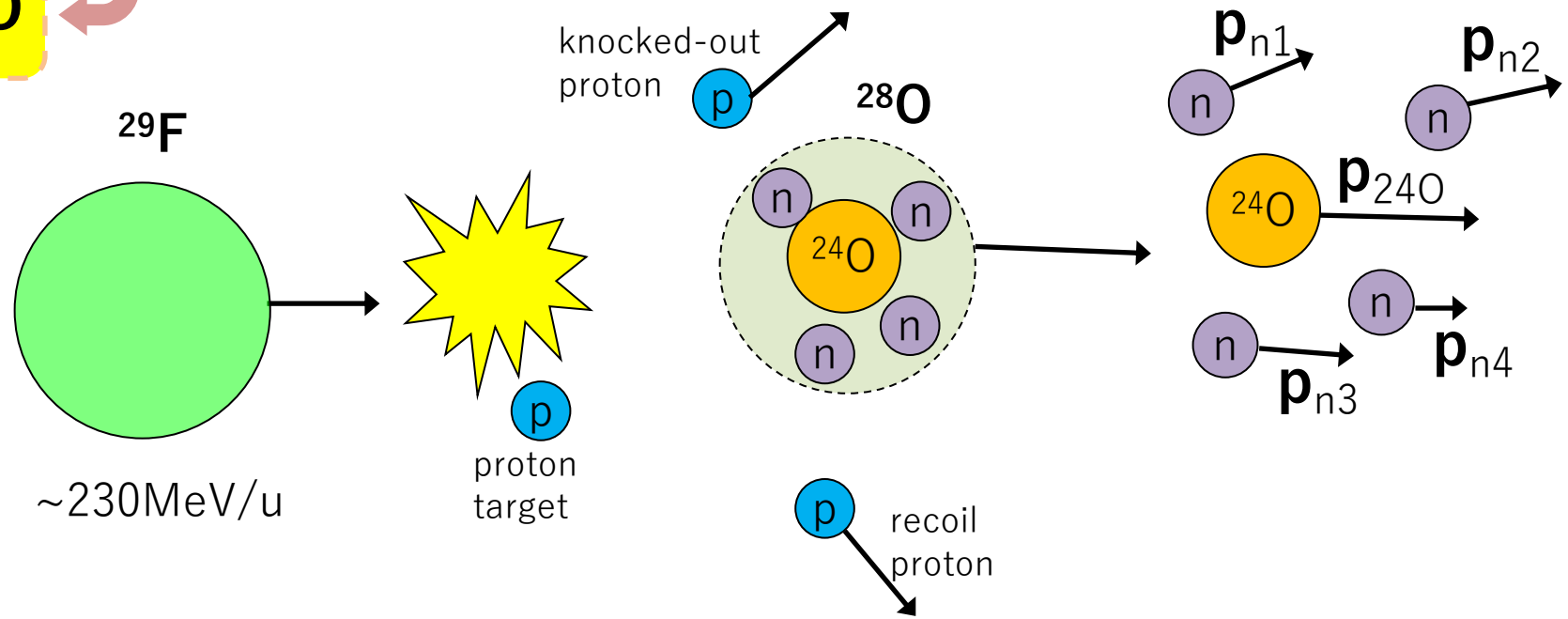

Experimental setup at SAMURAI spectrometer

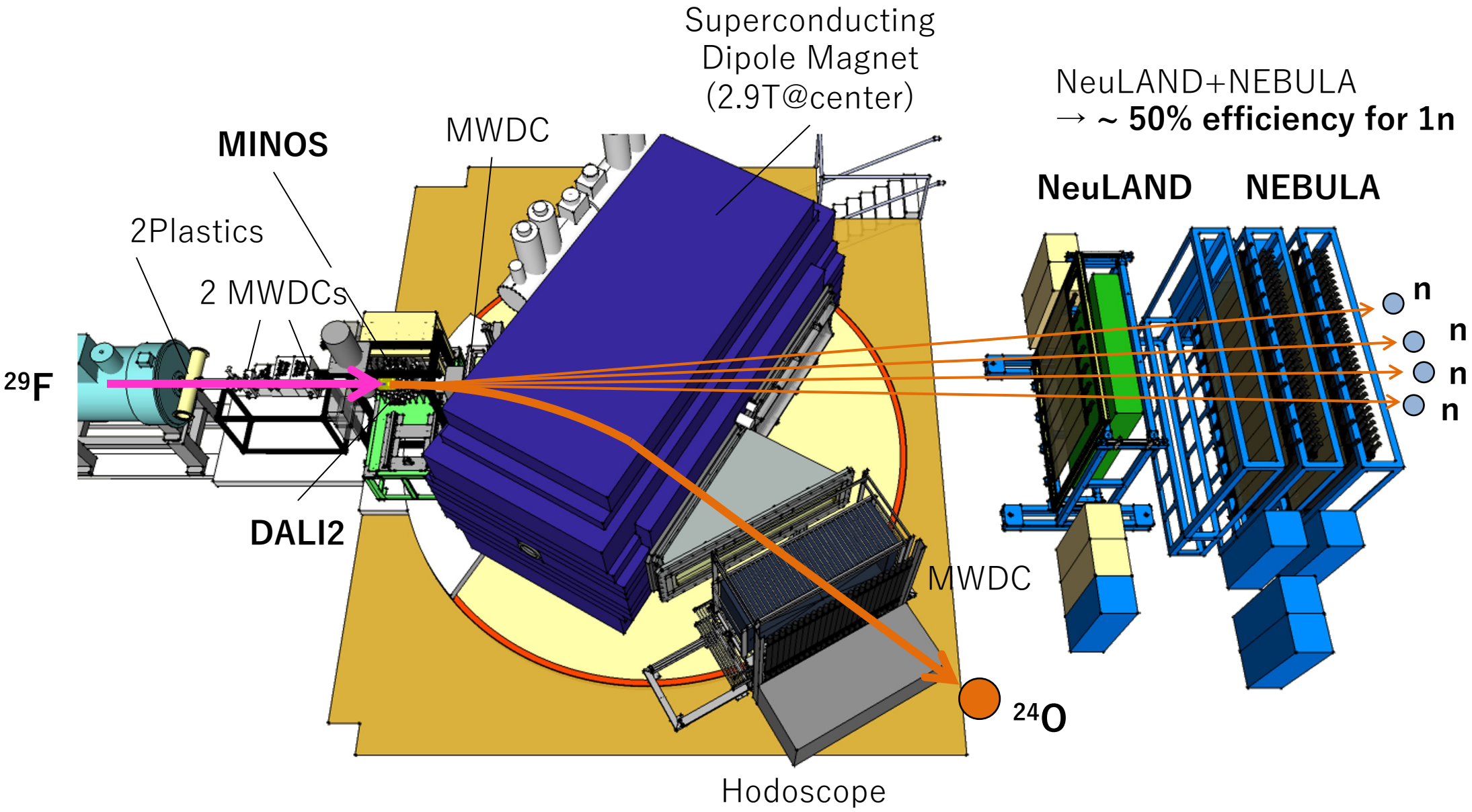

Neutron detectors

Neutrons are detected by an array of plastic scintillators.
Scattering with protons in plastic generates scintillation photons, that are read out by photomultipliers.
Since neutrons do not always transfer all energies to protons, the kinetic energy is deduced from **time-of-flight**.

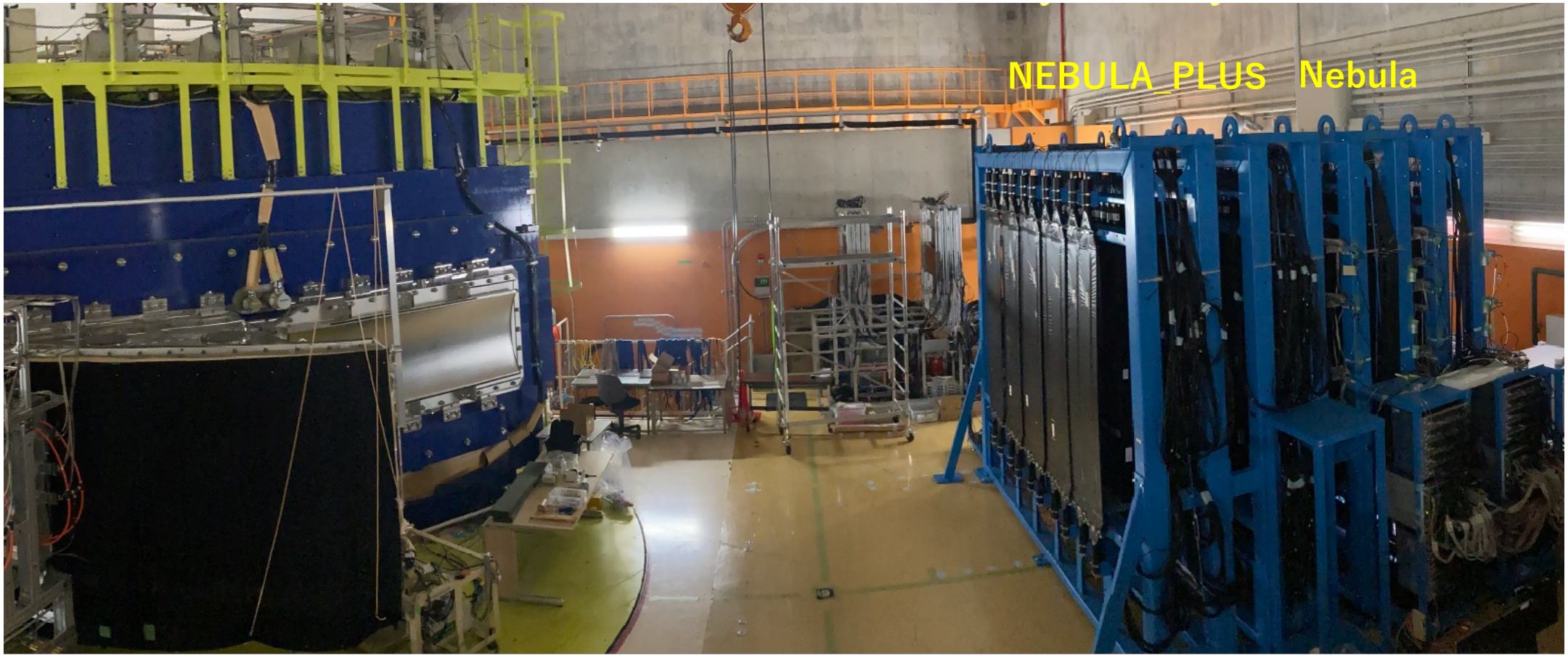

Why plastic (hydrocarbon)?

Protons can efficiently take energies from neutrons with almost the same mass.

Chadwick's setup for neutron discovery

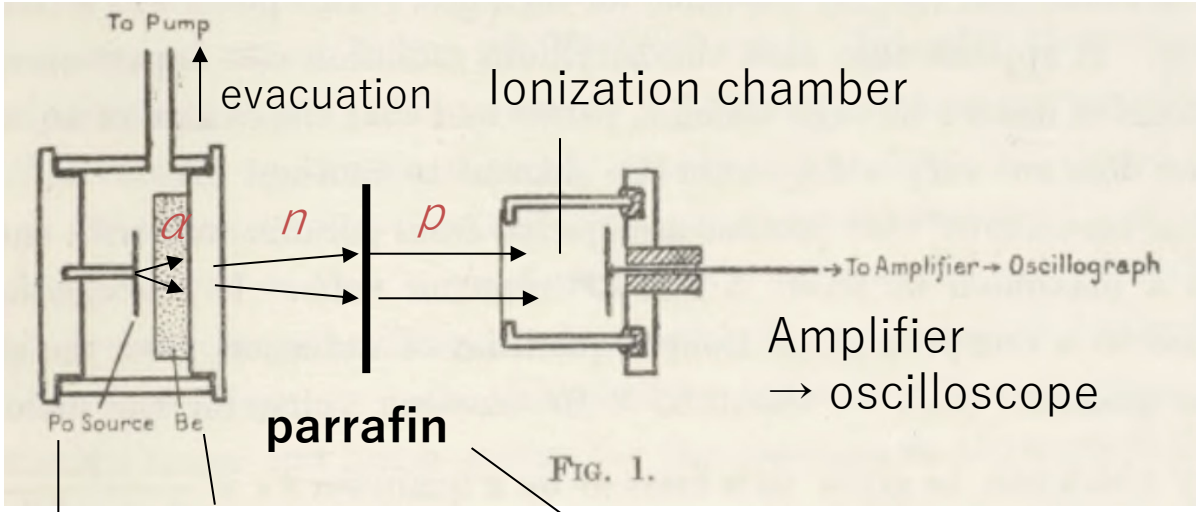

Berylium target

$^{4}He + {}^{9}Be \rightarrow {}^{12}C + n$

Polonium source
(alpha source)

Neutron source

Newton's cradle

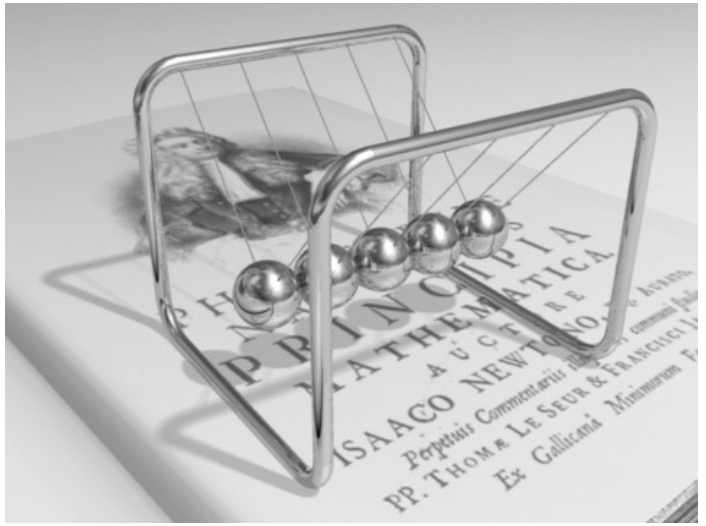

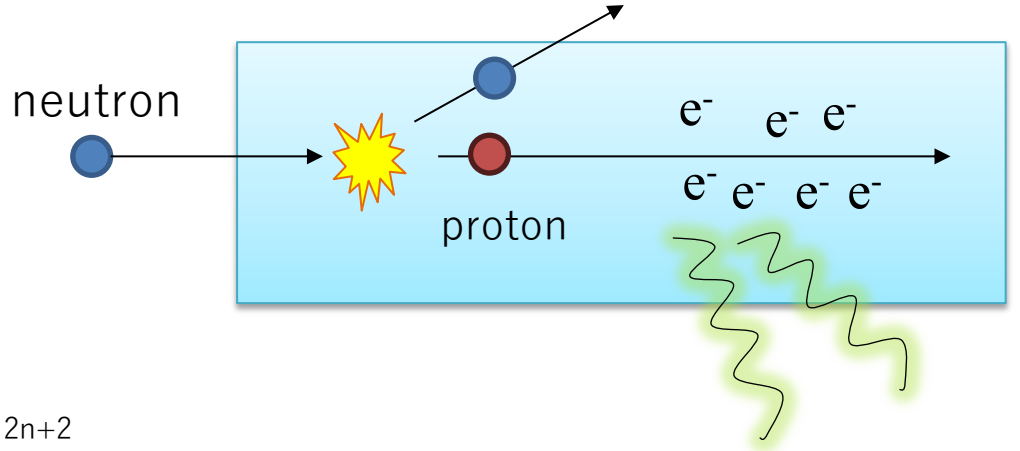

hydrocarbons with the general formula C_nH_{2n+2}

Neutron crosstalk

Multiple hits caused by single neutron make backgrounds for true hits of multiple neutrons and should thus be eliminated.

T. Nakamura et al., Nucl. Instrum. Methods B376,156 (2016)
Y. Kondo et al., Nucl. Instrum. Methods B463, 173 (2020)

Same Wall event

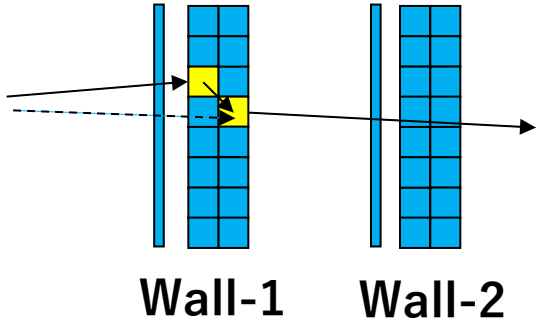

- Position & timing & pulse height information is used.
- Event is regarded as crosstalk if positions & timing are close
- Lose efficiency for small E_{rel}

Different Wall event

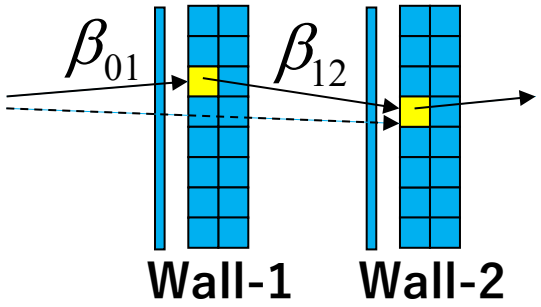

- Velocity & pulse height information
- Event is regarded as crosstalk if $\beta_{01} > \beta_{12}$ because crosstalk neutron must be slower
- Can measure down to E_{rel}~0

hit detector

Decay energy spectrum (^{24}O+4n coincidence)

A resonance corresponding to the ground state was observed.
This marks the first observation of ^{28}O.

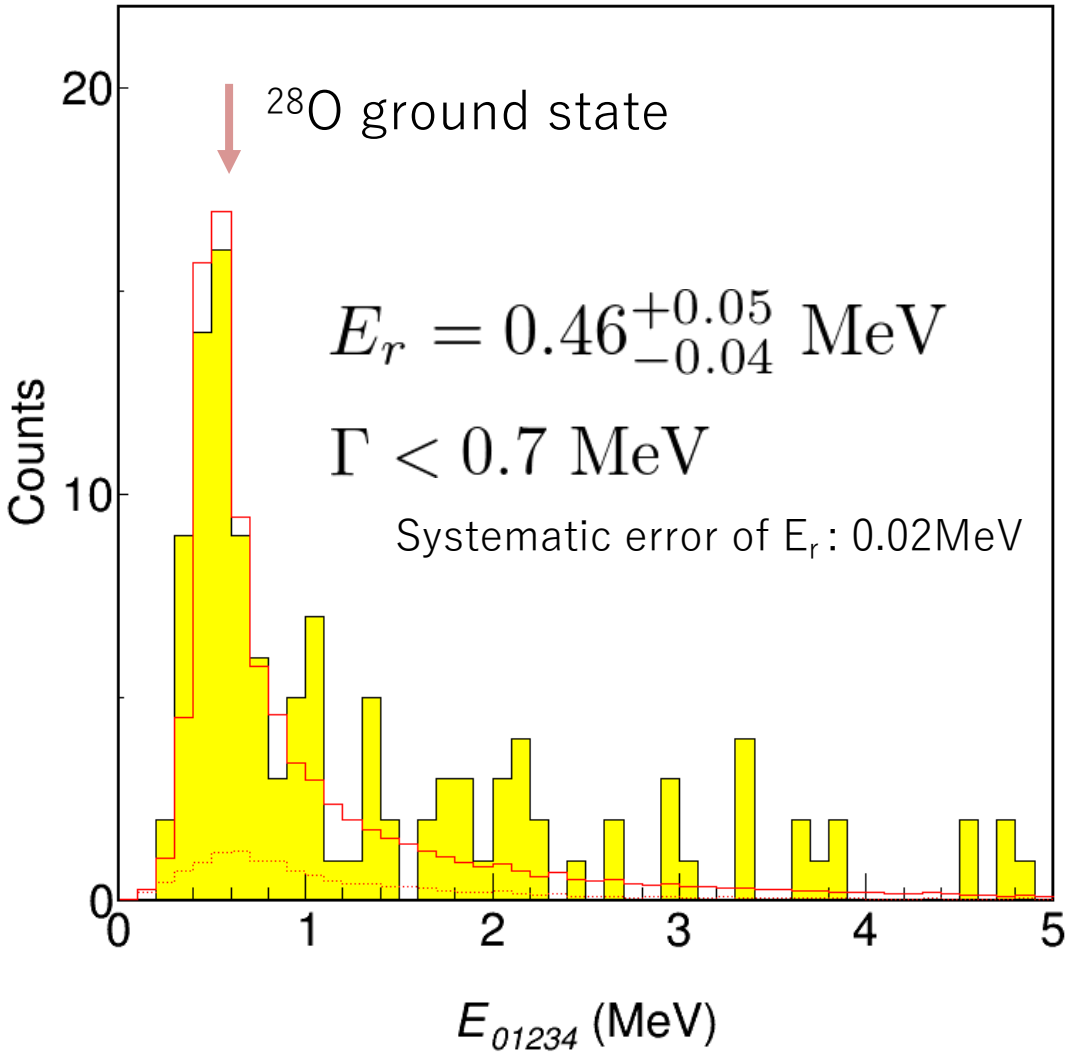

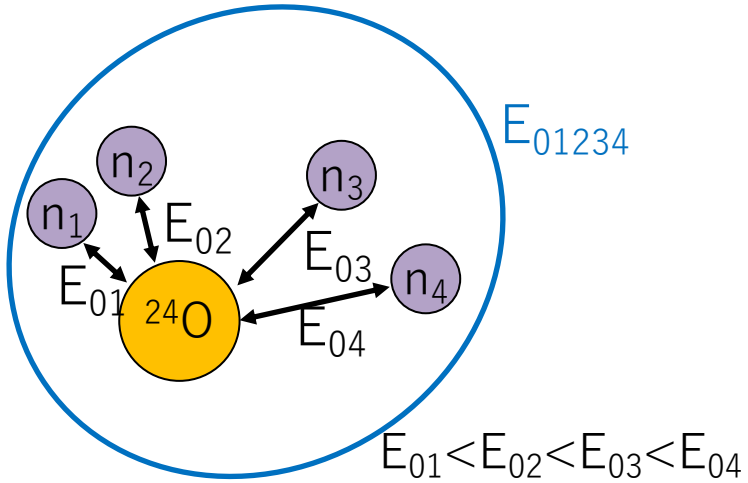

Comparison to theories

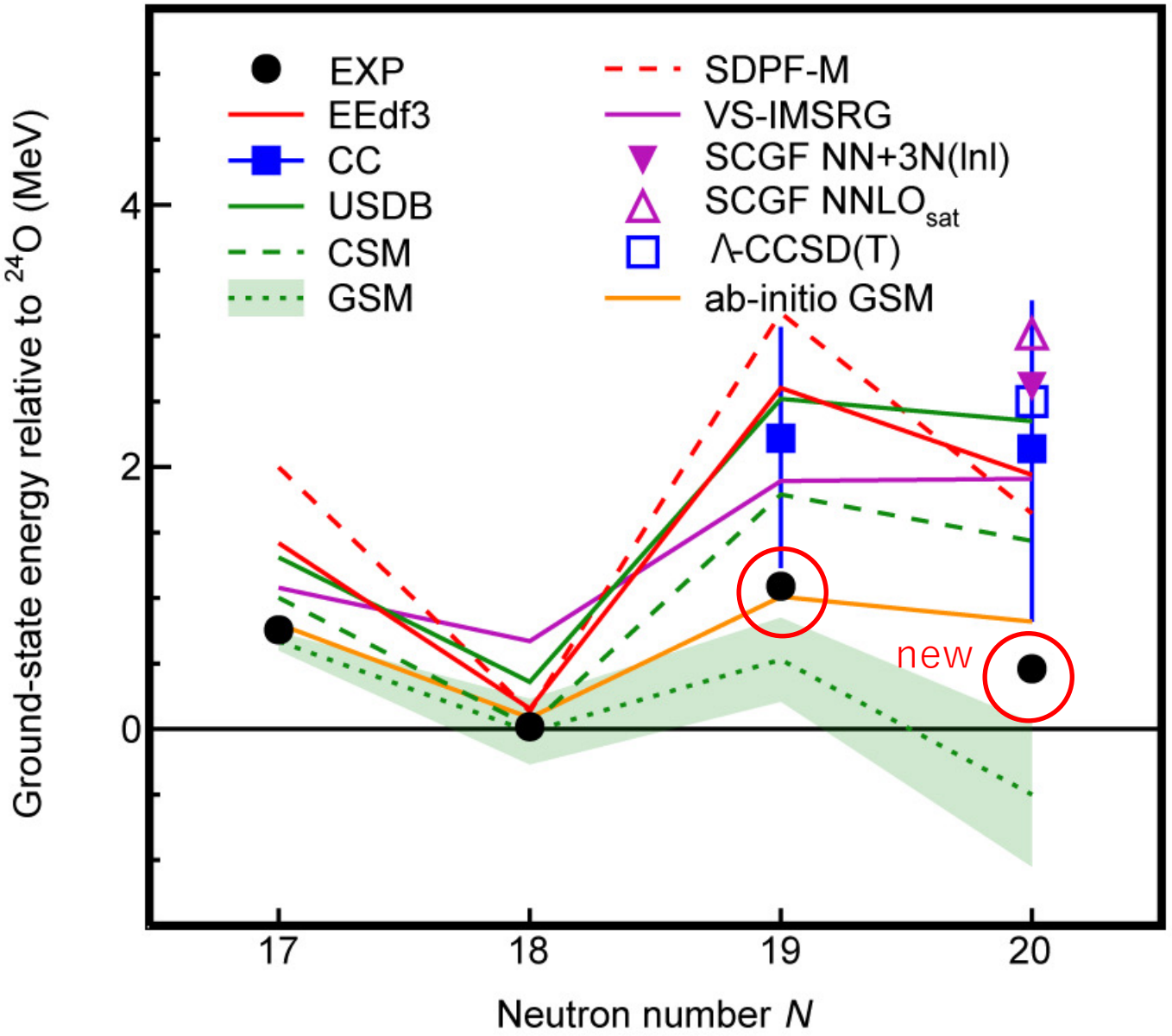

- The total binding energies of the valence neutrons stay less than 1 MeV from ^{25}O to ^{28}O. Almost no increase.
- Most of the theoretical calculations predict ^{27}O and ^{28}O to be more unstable.

AME2020 for ^{25,26}O: M. Wang+ 2021
EEdf3: N. Tsunoda+ PRC 2017
CC: Couple-cluster calculations
USDB: B. A. Brown+ PRC 2006
CSM: A. Volya+ PRC 2006
GSM: K. Fossez+ PRC 2017.
SDPF-M: Y. Utsuno+ PRC 1999
VS-IMSRG: S. R. Stroberg+ PRL 2021
SCGF: V. Soma+ PRC 2020
L-CCSD(T): G. Hagen+ 2016
ab-initio GSM: S.Zhang+ PLB 2020

Comparison to theories of 1990

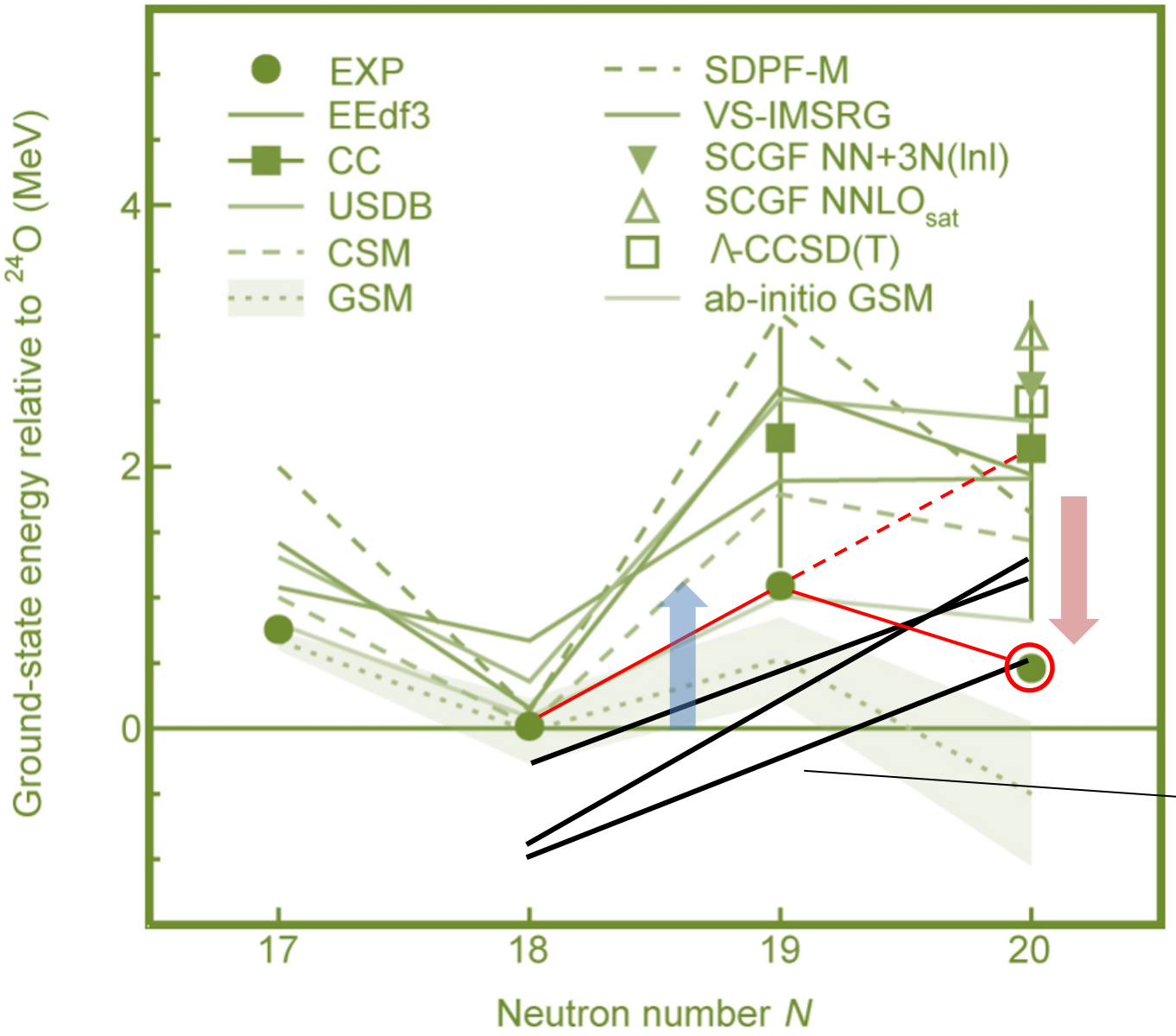

Agreement is not too bad.
The theories predict less binding for ^{28}O with respect to ^{26}O than experimental data.
This is mostly the case for recent calculations too.

What is the mechanism of stabilization?

Nuclide	MN S_{2n}	CKZ S_{2n}	SN S_{2n}	T S_{2n}	JM S_{2n}
^{23}O	7.15	9.22	8.0	7.45	9.19
^{24}O	4.91	6.16	6.78	4.20	5.96
^{26}O	0.67	0.87	5.32	1.26	0.96
^{28}O	0.7	−2.08		−0.13	−1.61

D. Guillemaud-Mueller+ 1990

Binding energies of oxygen from shell model

NN theories give too attractive $1d_{3/2}$-$1d_{5/2}$ interaction.

The **three-body force** of two valence neutrons and a neutron in the core is **repulsive due to the Pauli blocking**.

T. Otsuka+ PRL 2010

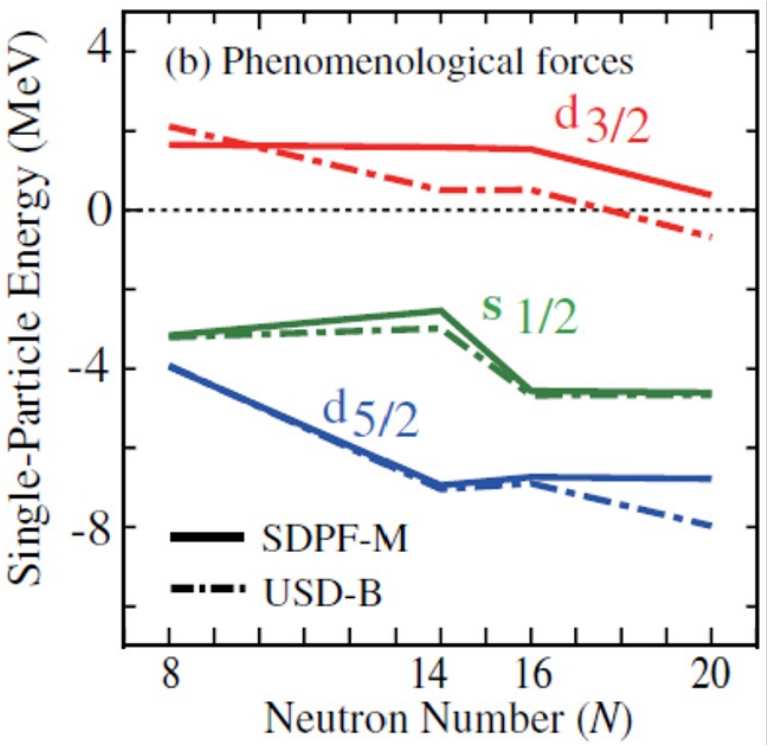

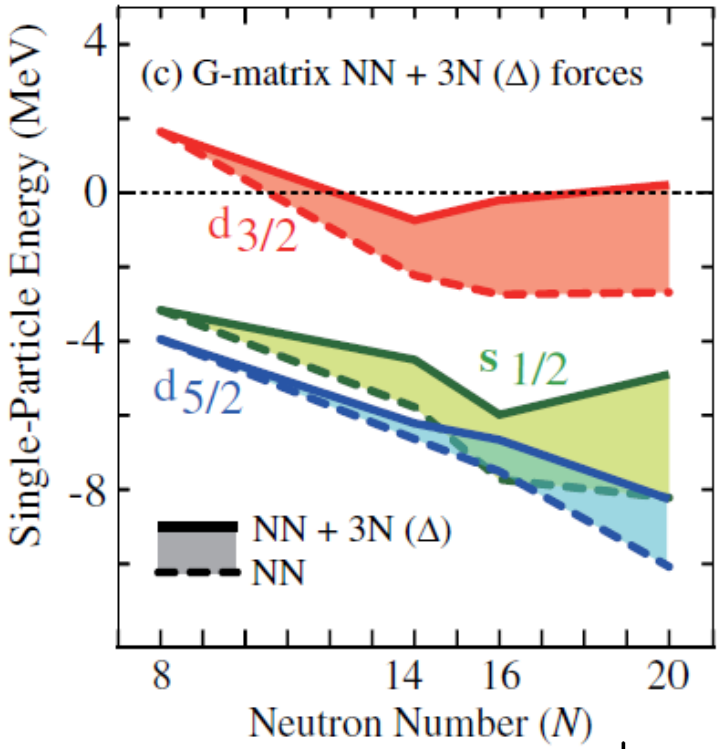

(d) Schematic picture of two-valence-neutron interaction induced from 3N force

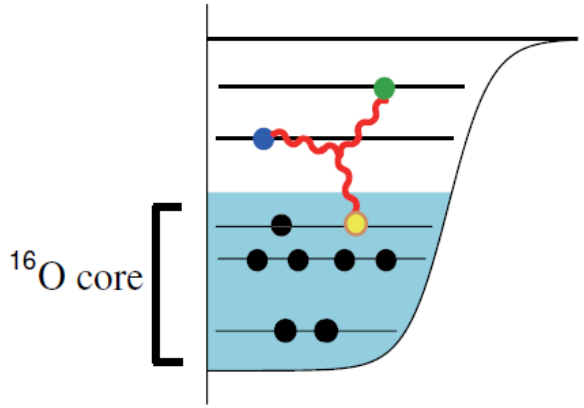

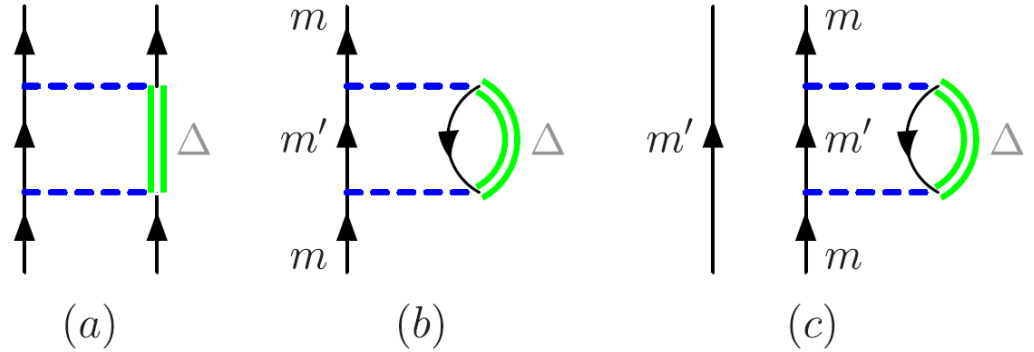

Binding energies of oxygen from shell model

Repulsive nature of three nucleon forces develops as the number of valence neutron increases.
This leads to the unstability of oxygen isotopes beyond doubly-magic ^{24}O.

T. Otsuka+ PRL 2010

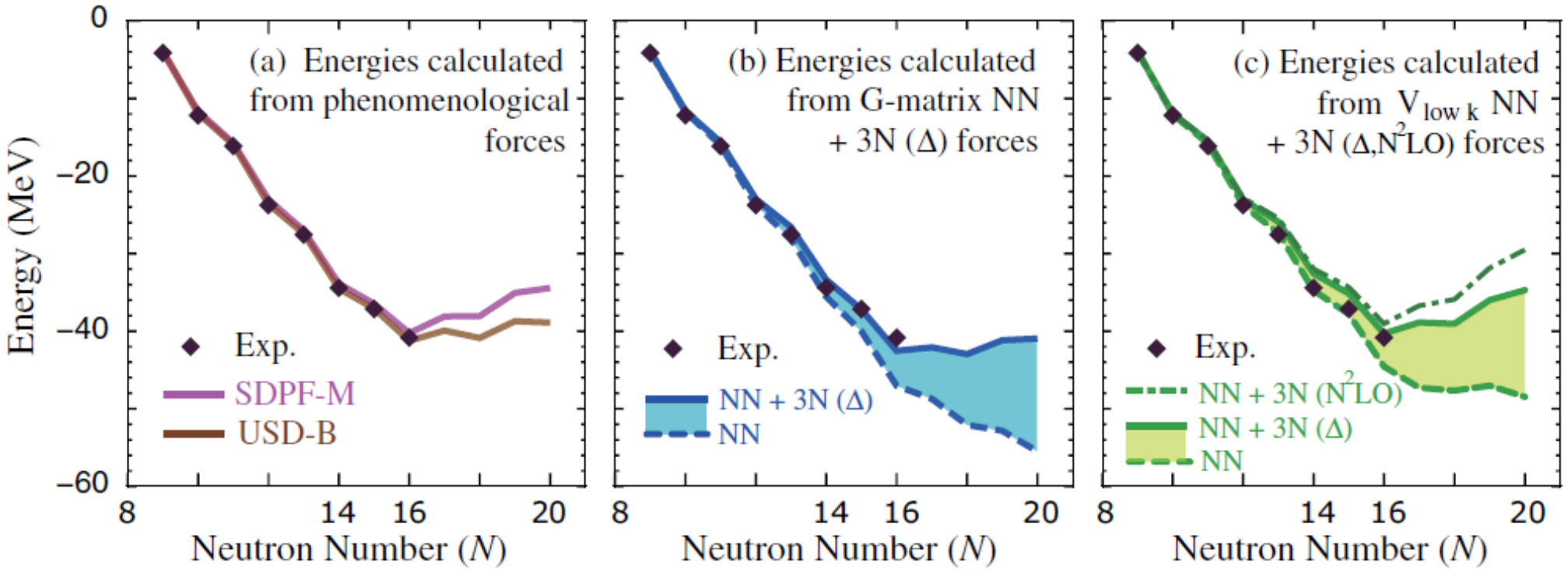

Why does the dripline extend in F and beyond?

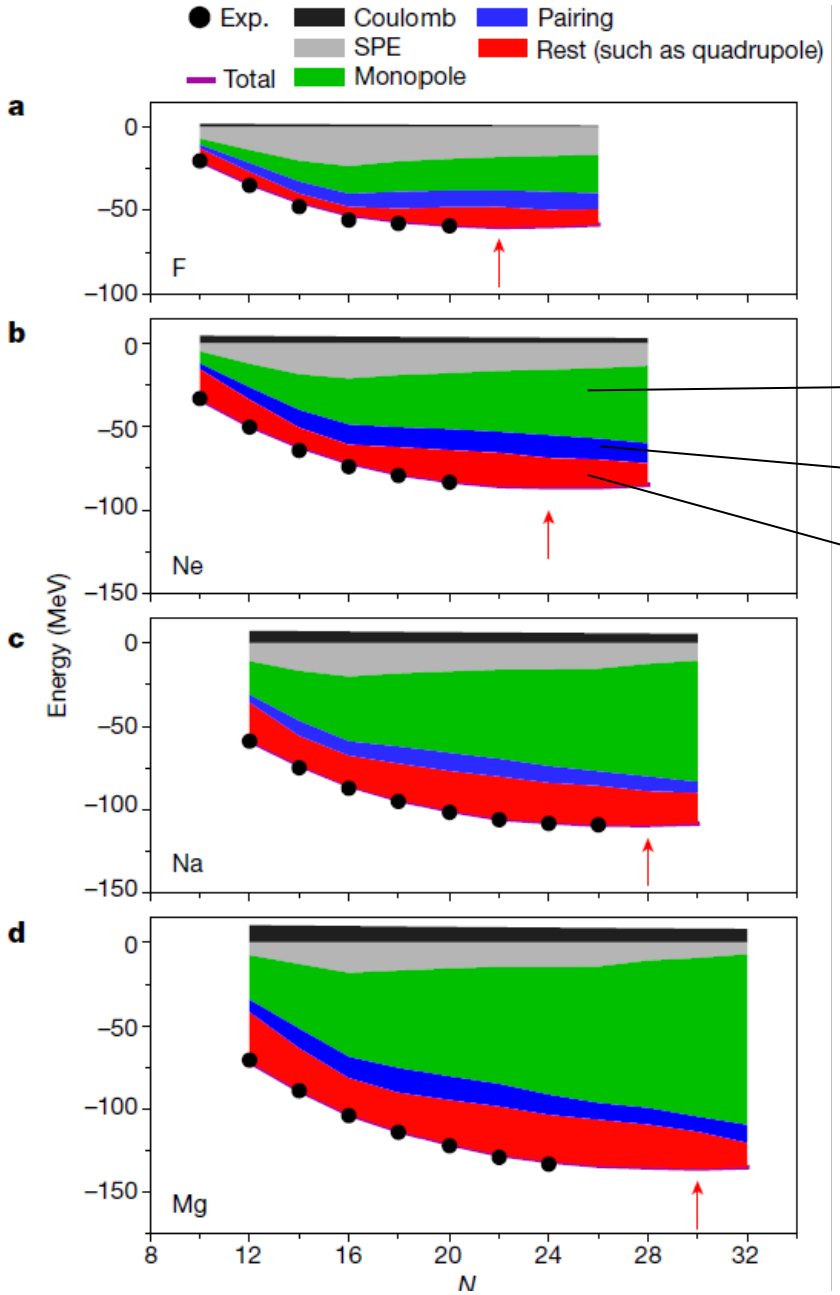

Quadrupole deformation increase binding energies. Oxygen with Z = 8 has a robust spherical shape and cannot benefit from this mechanism.

Tsunoda+ Nature 2020

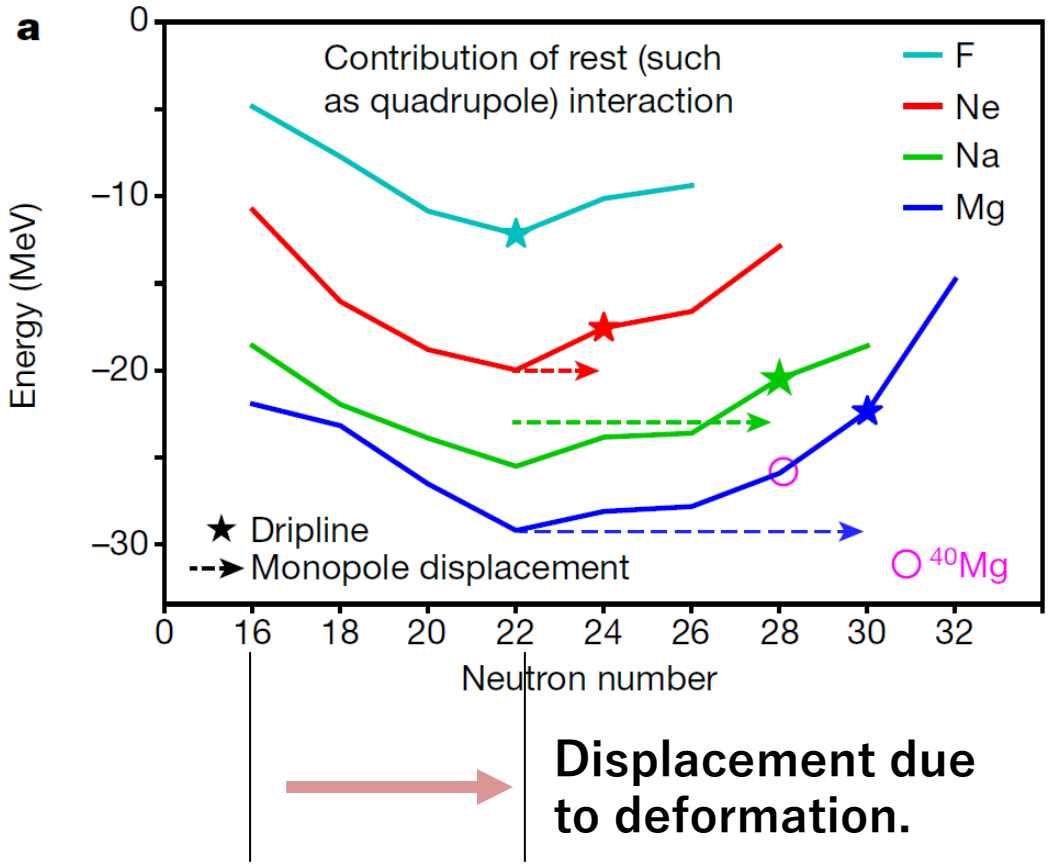

Displacement due to deformation.

Oxygen dripline

^{29}F at the south of Island of inversion

Reaction cross sections of ^{29}F suggest halo structure of **$2p_{3/2}$ configurations**.

S. Bagchi+ PRL 2020

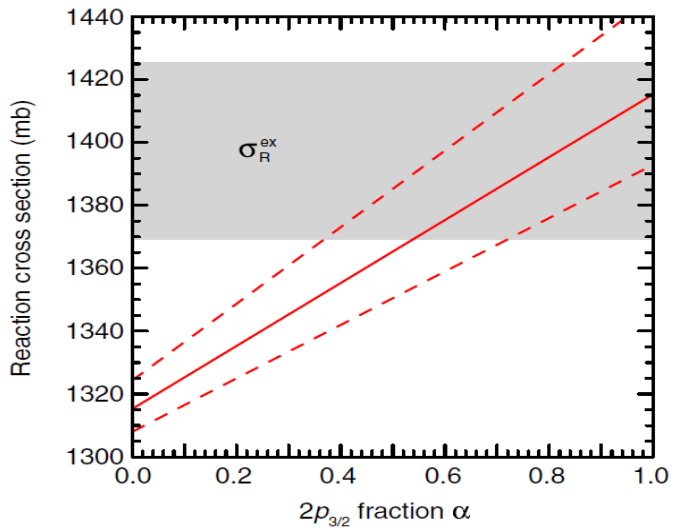

Halo structure of ^{29}F
Importance of $2p_{3/2}$contributions

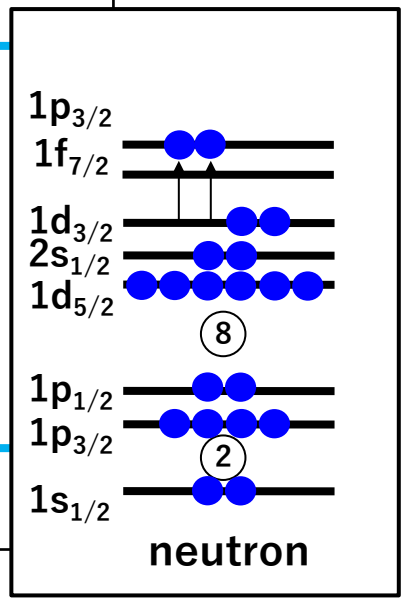

Is ^{28}O doubly magic?

The ground state of ^{29}F is dominated by neutron intruder configurations.

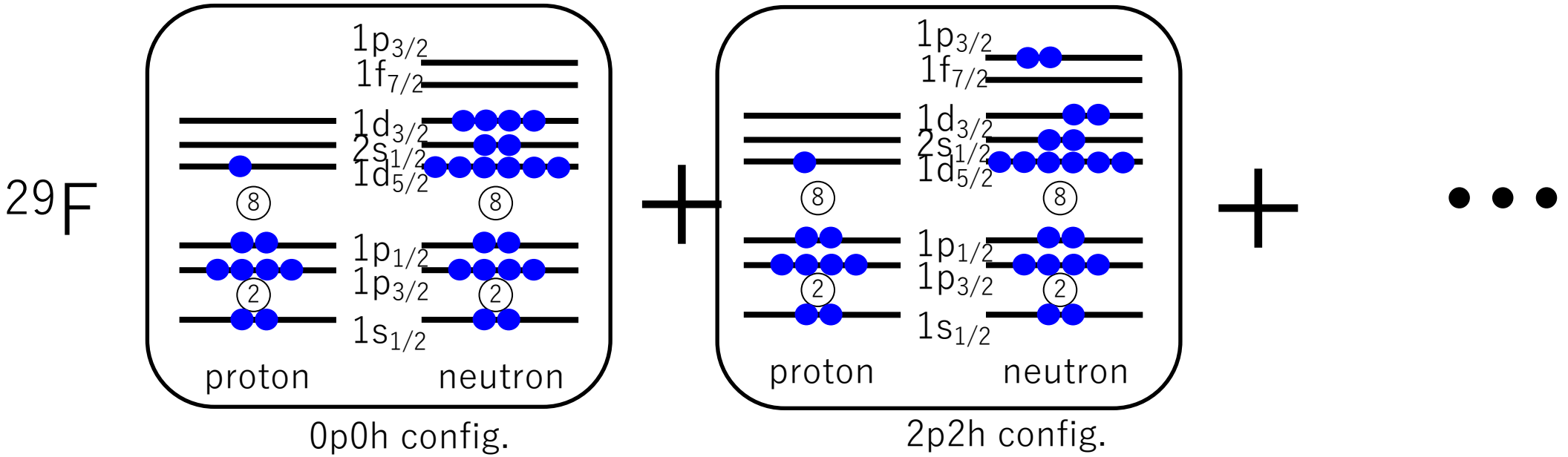

neutron occupation numbers in ^{29}F

	$d_{3/2}$	$f_{7/2}$	$p_{3/2}$	
SDPF-MU	2.68	0.90	0.56	underestimate σ_R
EEdf1	0.84	2.19	1.26	consistent with exp

S. Bagchi+ PRL 2020

Spectroscopic factor for $d_{5/2}$ proton removal from ^{29}F

The spectroscopic factor of ^{28}O with the ground state of ^{29}F can be deduced from the proton removal cross section. **The sizable C^2S indicates the intruder configurations to dominate ^{28}O** due the disappearance of N = 20 magicity.

$$\sigma_{-1p} = 1.36^{+0.16}_{-0.14}\ \mathrm{mb} \quad \rightarrow \quad C^2S = 0.48^{+0.05}_{-0.06} \pm 0.05$$

systematic error 0.13 mb (10%)

Shell model calculation using EEdf3 interaction (mod ver. of EEdf1)
occupation num: 2.5 (pf-shells), 2.0 ($d_{3/2}$) for ^{28}O
→ **C^2S=0.68**
consistent with exp.
(30% reduction known in (p,2p) and (e,e'p))

If ^{28}O has good magicity
→ **C^2S = 0.13**

JTE triggers halo formation

Prolate deformation lowers $\Omega = 1/2^-$ or [330 1/2] orbit

- Magicity gets lost and **mixing of $2p_{3/2}$** occurs.
- **Halo effect of weakly-bound *p*-wave neutrons** further stabilize the orbital.

I. Hamamoto PLB 2021

Neutron one-particle energies in the potential produced by ^{29}F as a fucntion of β.

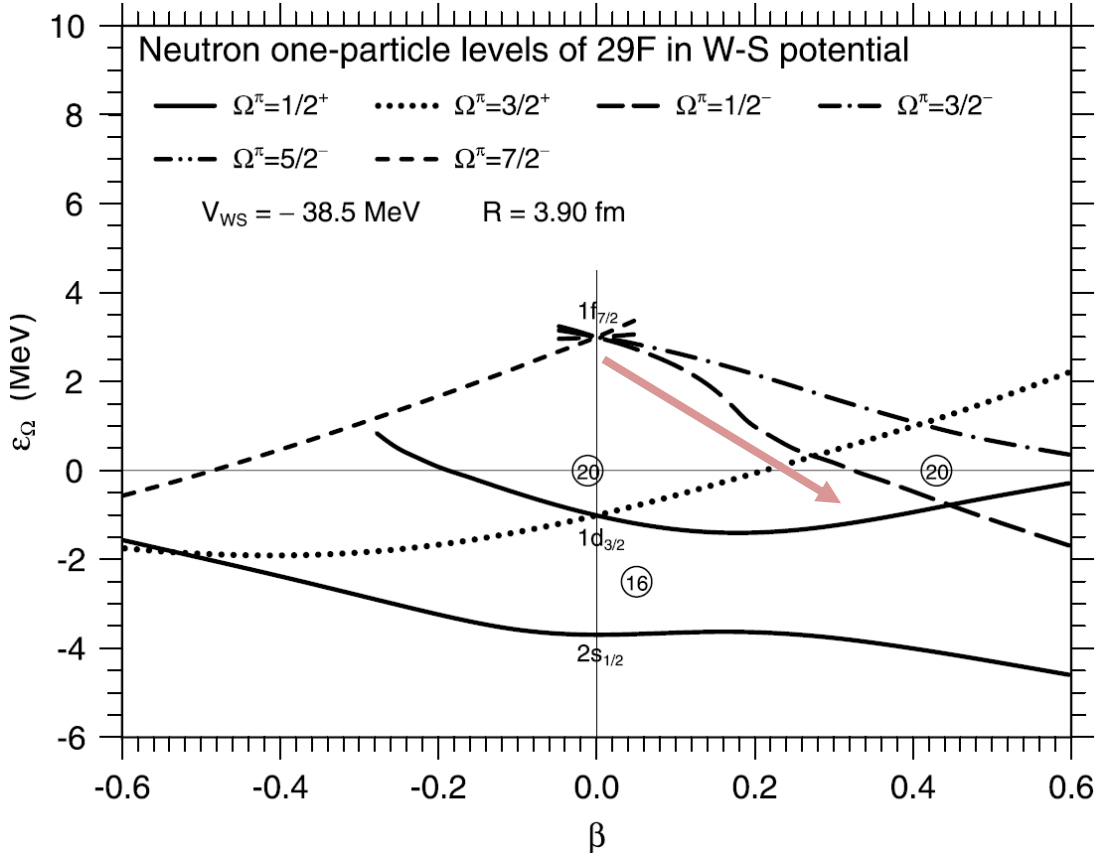

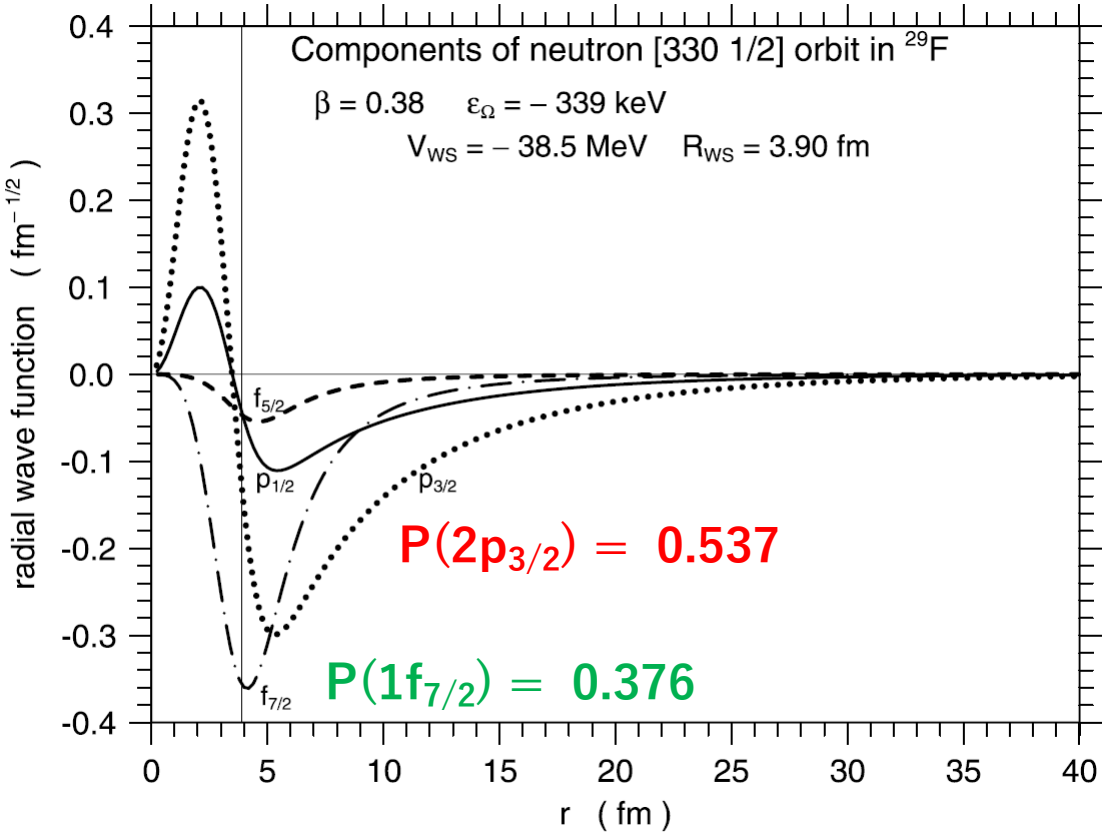

Halo effect

Neutron halo is a phenomenon found in very weakly-bound nuclei, such as ^{11}Li or ^{19}C.
Weakly-bound s-wave neutrons are spatially broad beyond the normal size of nucleus.

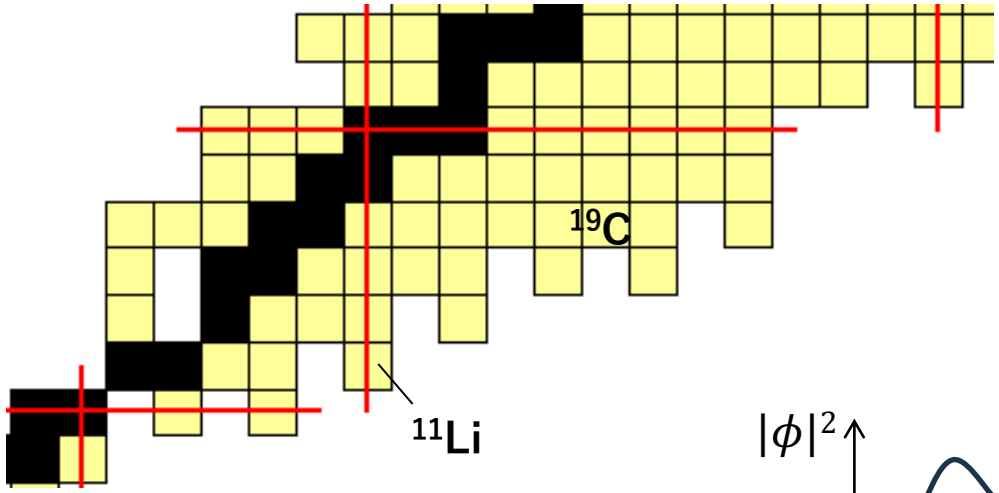

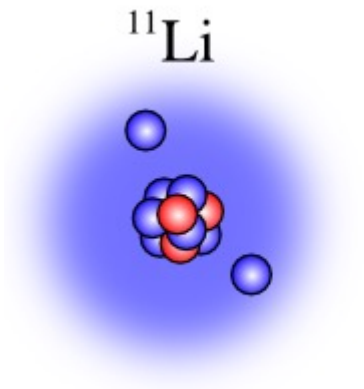

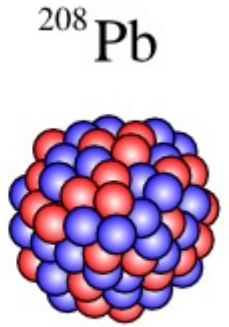

Figure from TRIUMF website

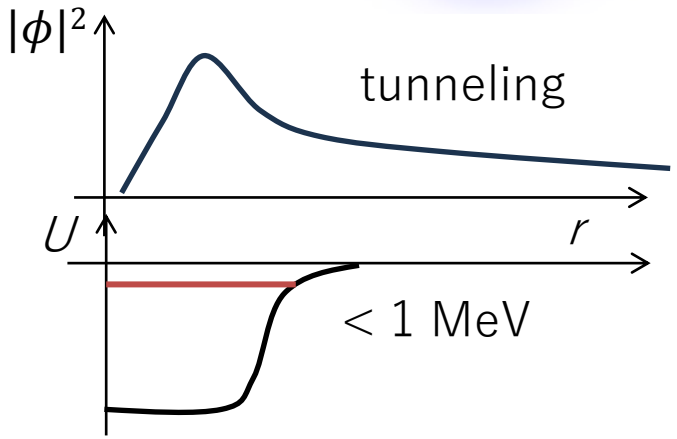

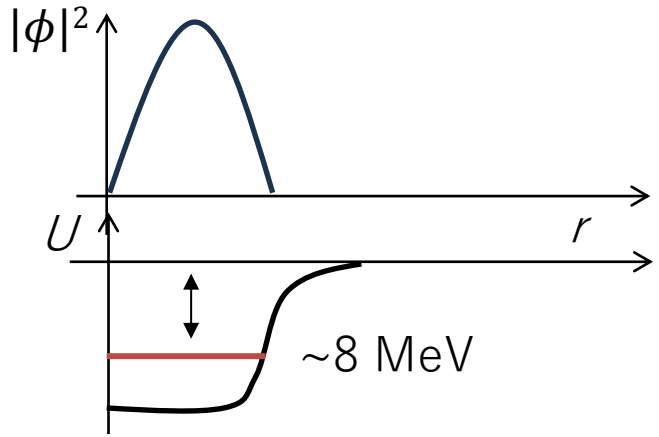

Weakly-binding and single particle energies

The binding energies decreases as approaching the dripline.
Single particles energies are modified by the potential surface.

Hamamoto PRC 2007

Woods-Saxon potential solution
as a function of potential depth.

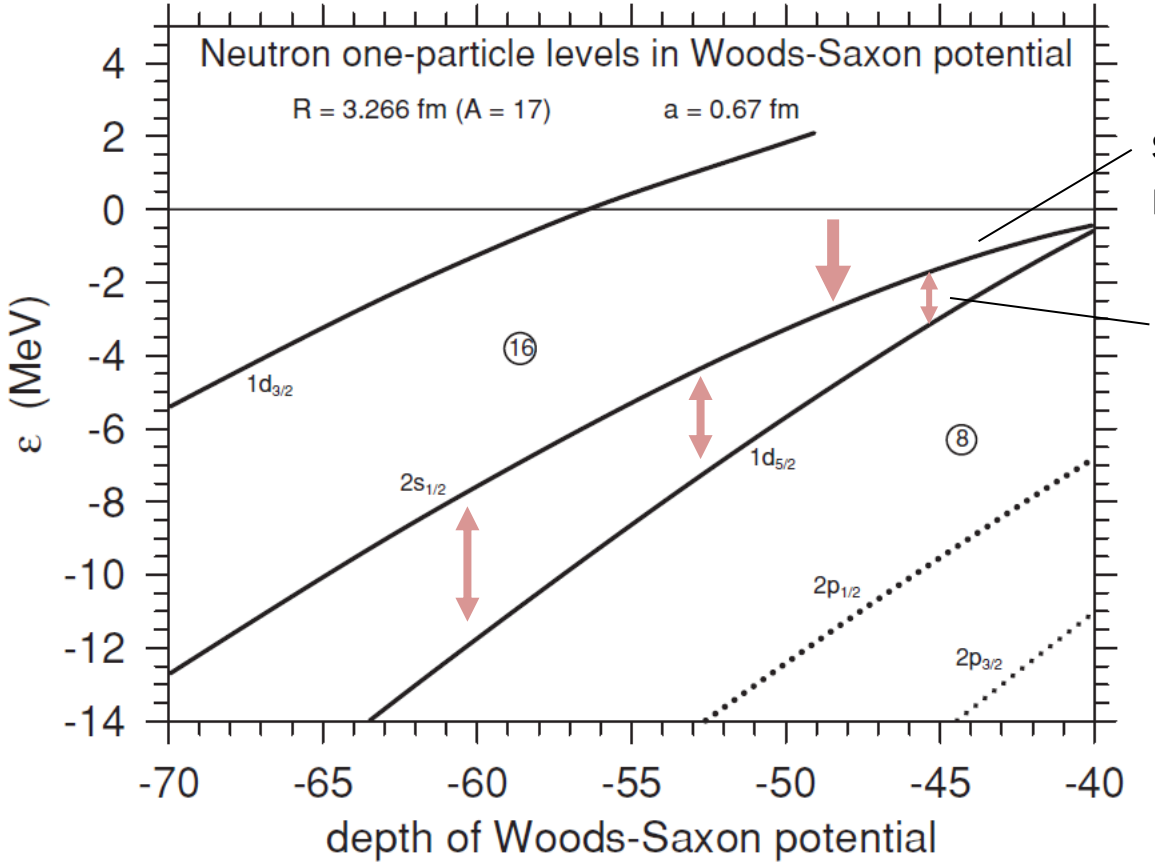

s-orbital with L = 0 is more attractive with respect to d-orbital.

As a result, the energy gap between $2s_{1/2}$ and $1d_{5/2}$ becomes narrower.

Weakly-binding and single particle energies

Neutron halo involves less kinetic energy than deeply bound states.
The saving of the kinetic energy is translated into the binding energy.

Hamamoto PRC 2007

Woods-Saxon potential solution
as a function of potential depth.

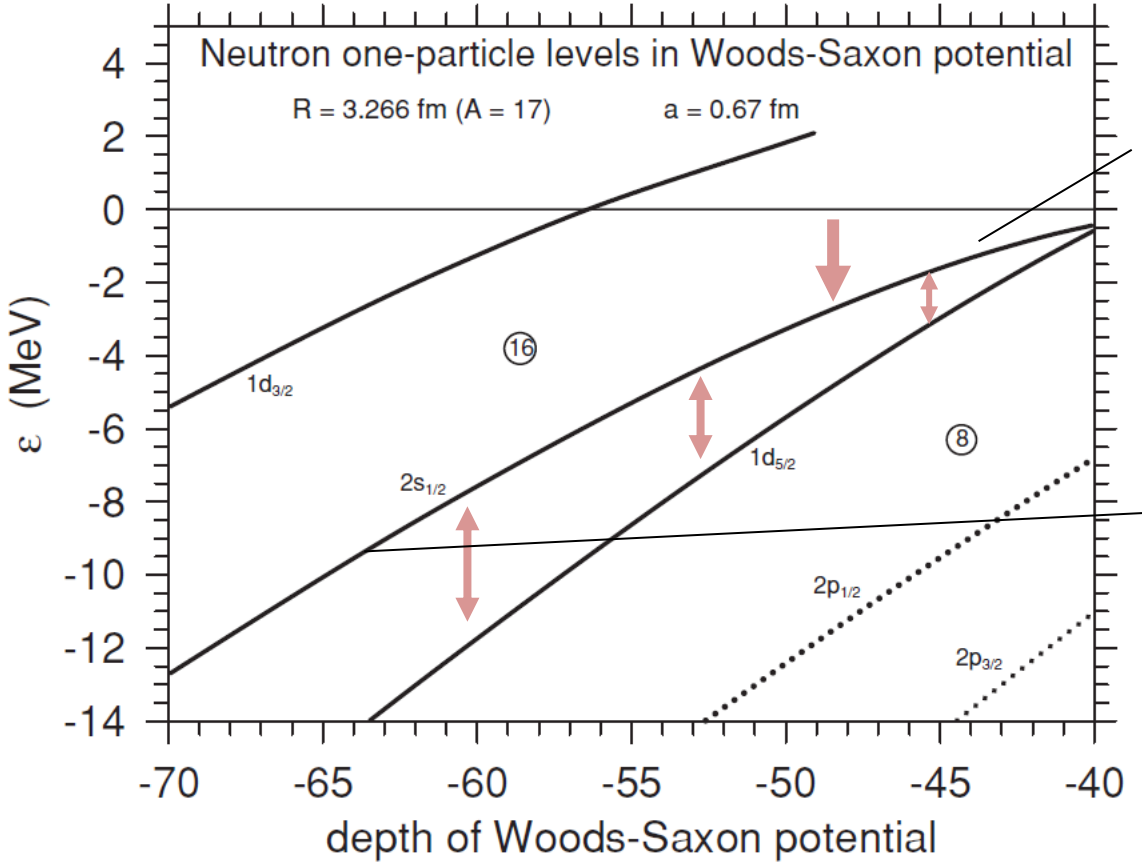

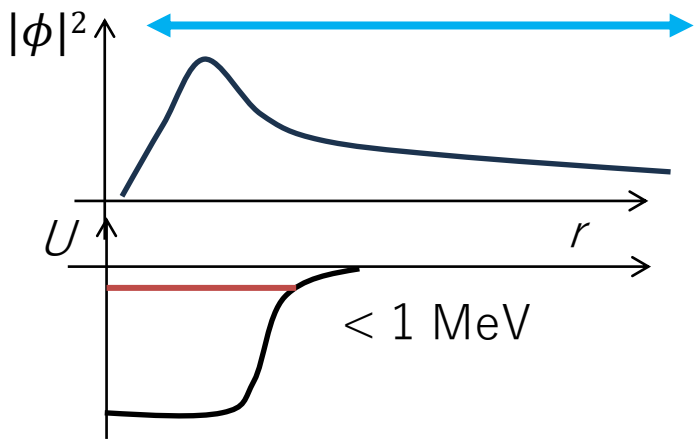

Spatially broad
→ **Slow motion**

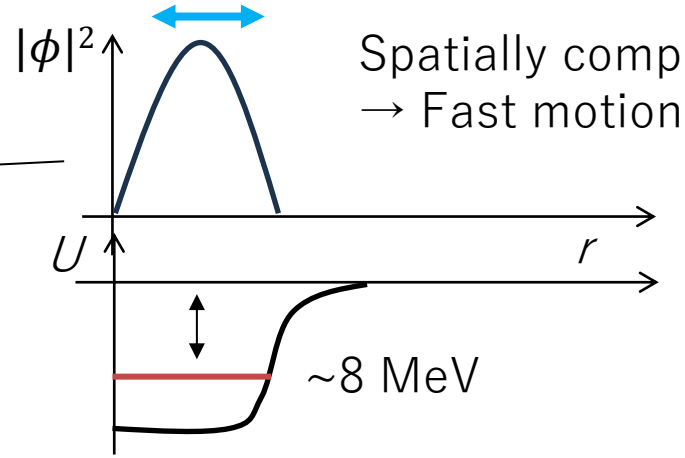

Spatially compact
→ Fast motion

Breaking of symmetry and density saturation

Halo dynamics occurs not only in spherical potentials, but also **in deformed potentials**.

Nilsson diagram

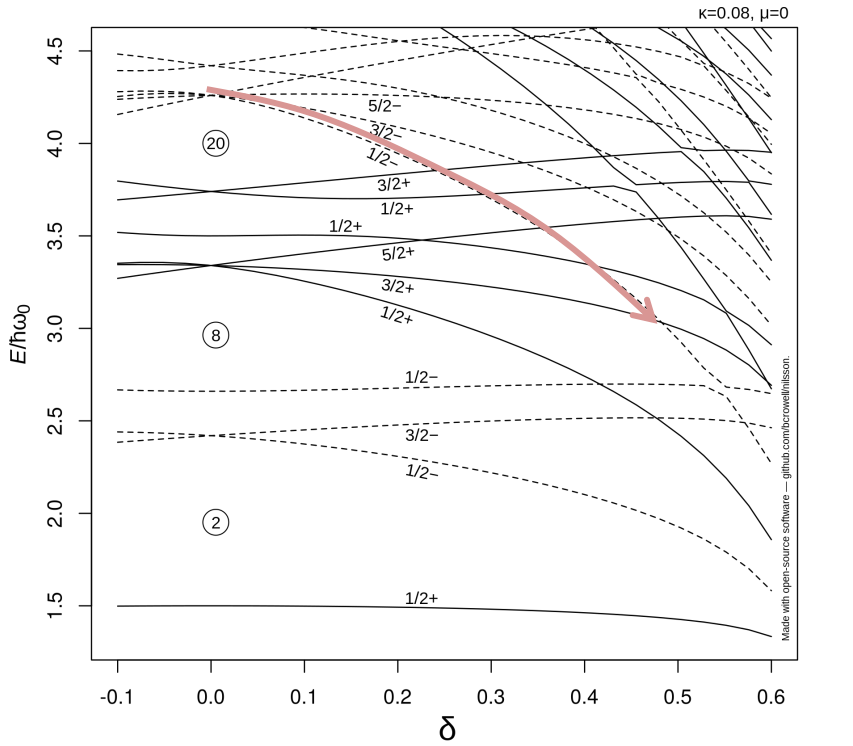

I. Hamamoto, PRC 2004

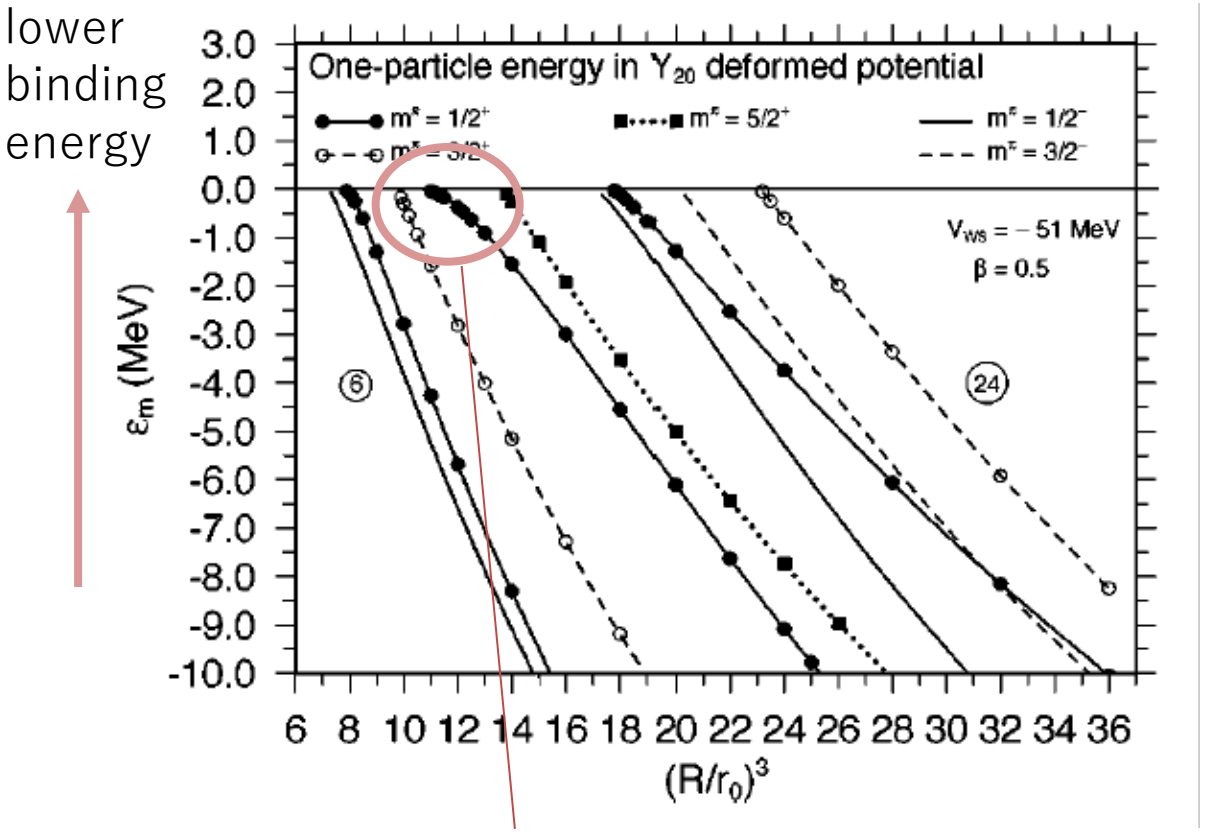

Low density spatial extension

Halo dynamics
to convert kinetic energies to binding potential energies.

Constant density

Breaking of symmetry and density saturation

Halo neutron decouples from the core to help stabilize the whole nucleus.

As approaching the neutron emission threshold, $J = 1/2^+$ state is
increasingly dominated by s-wave neutron with spherical distribution.

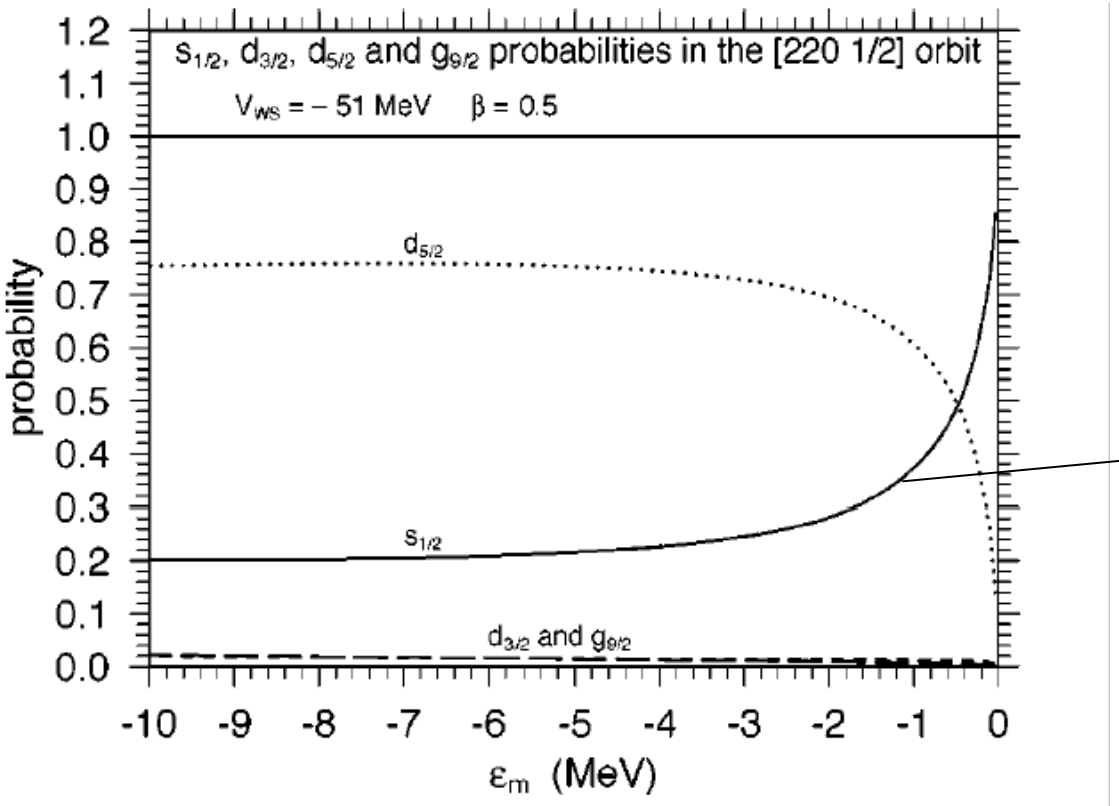

FIG. 2. Calculated probabilities of $s_{1/2}$, $d_{3/2}$, $d_{5/2}$, and $g_{9/2}$ components in the [220 1/2] level as a function of energy eigenvalue ε_m.

I. Hamamoto, PRC 2004

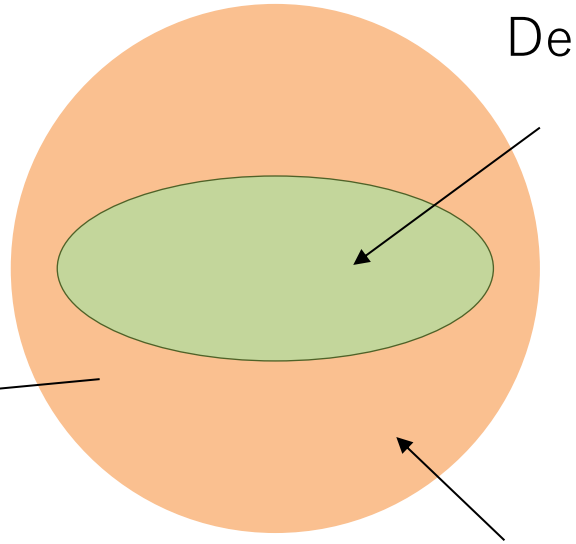

Deformed and saturated core

Stabilized by Jahn-Teller effect

Neutron halo

Stabilized by halo effect

Oxygen dripline anomaly

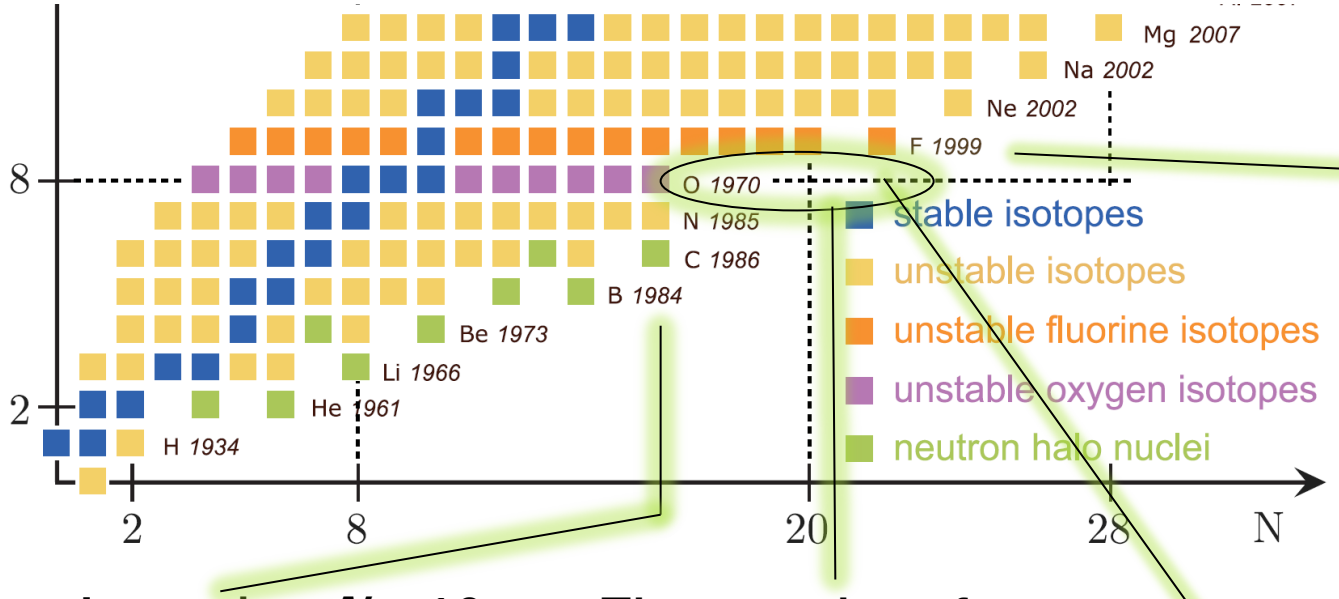

Deformation

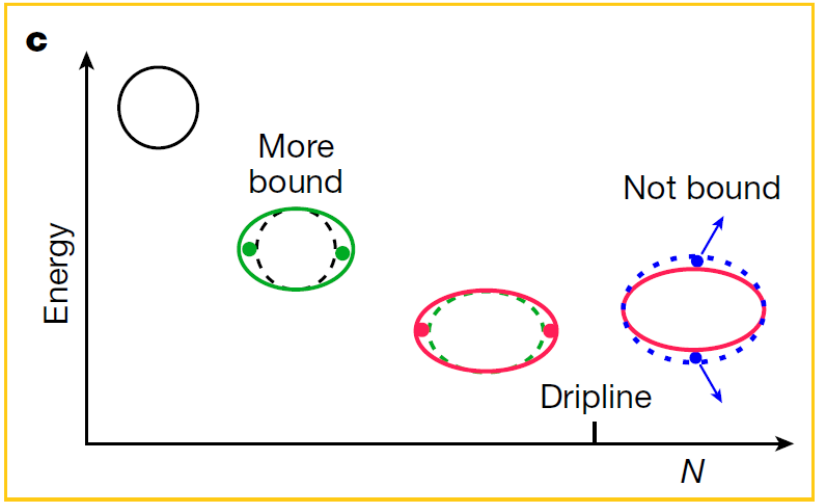

‘New’ magic number $N = 16$

Ozawa+ PRL 2000
Kanungo+ PRL 2009
Hoffman+ PLB 2009

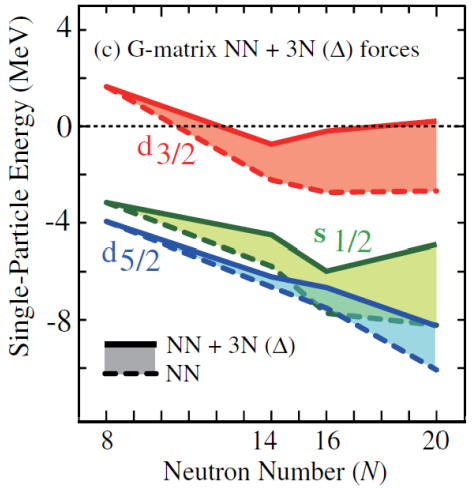

Three nucleon force

Otsuka+ PRL 2010

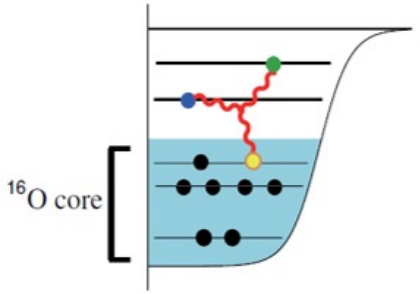

Halo effect

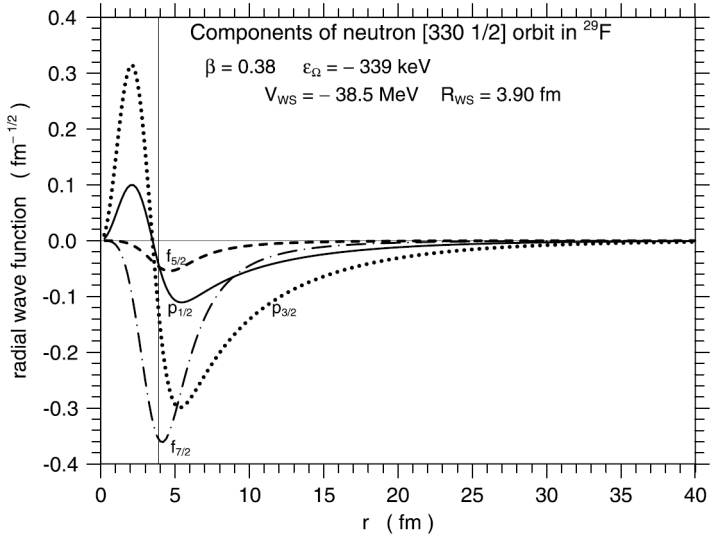

Nuclear structure

Simplicity

- 2 ~ 300 particles
- 2 colors (proton and neutron)
- Nuclear force / Coulomb force
- Quantum states
- Self-organizing object

Complex puzzle

Infinite possibilities of
nucleon many-body states

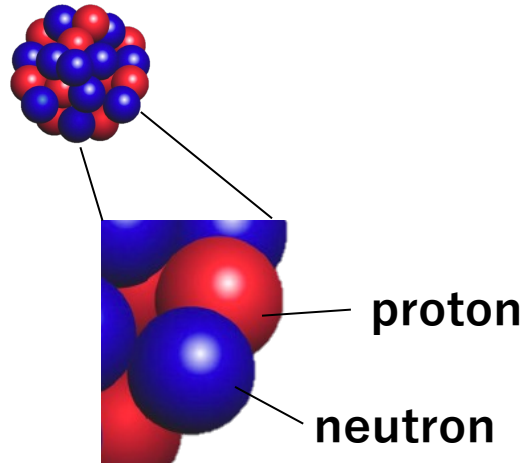

Order

Single-particle motion & collective motion

e.g. magicity, deformation,
tensor/three body force, halo effect

Single-particle and collective motions from nuclear many-body correlation (PCM2025)

Mar 4 – 7, 2025
University of Aizu
Asia/Tokyo timezone

Enter your search term

The year 2025 marks the 50-year anniversary of the Nobel Prize in Physics in 1975 for Bohr, Mottelson and Rainwater to honor the discovery of the connection between single-particle motion and collective motion in atomic nuclei. How such simple and ordered dynamics can emerge in quantum systems that involve complex many-body correlations stays as one of the fundamental questions of nuclear physics. Today investigations of a wide spectrum of structures, responses to external fields or symmetries of nuclei are advancing at far edges of stability or at extreme conditions, which are made possible both with nuclear spectroscopy at various high-performance accelerator-based facilities of stable or radioactive isotopes and with theoretical efforts in understanding of nuclear forces and many-body problems aided by developments of large-scale computational techniques. The symposium aims to broadly bring experimental and theoretical experts to revisit the emergence of single-particle and collective motions in today's context of nuclear structure studies and discuss future perspectives toward deeper insight into the essence of nuclear structures.

This symposium honors the late Professor Ikuko Hamamoto (1936 - 2023), a preeminent theorist in the field of nuclear structures. This event is inspired by her distinguished research achievements and contributions.

The symposium will take place at the University of Aizu, the same location that hosted the international symposium on frontiers of collective motions (CM2002) in 2002, convened upon her retirement.

Nuclear physics School for Young Scientists
(NUSYS-2024)

Q & A

Beijing Normal University (Zhuhai, Guangdong)
July 27 to August 2, 2024

Are you good at Rubik cube?

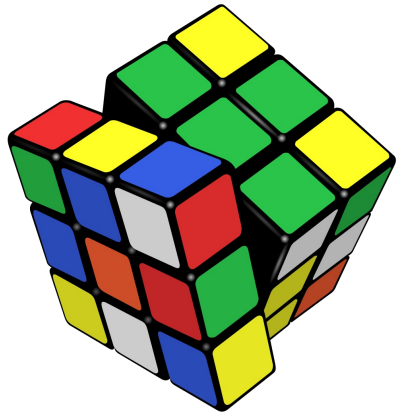

Why neutron-rich side only?

- Why are the magicity loss region distributed on the right side of the nuclear chart.
- Why magic number loss in neutron-rich side. Why not in the proton rich side.
  - Mirror symmetry holds for magicity loss between N = 8 (^{12}Be) and Z = 8 (^{12}O).
  - ^{56}Ni with Z = N = 28. Very magic
  - ^{100}Sn with Z = N = 50 is forefront case. For now, no sign of magicity loss. Search for the 2^+ state was conducted this spring at RIBF.

Status of magicity

Magicity loss / emergence is found universally over the nuclear chart.

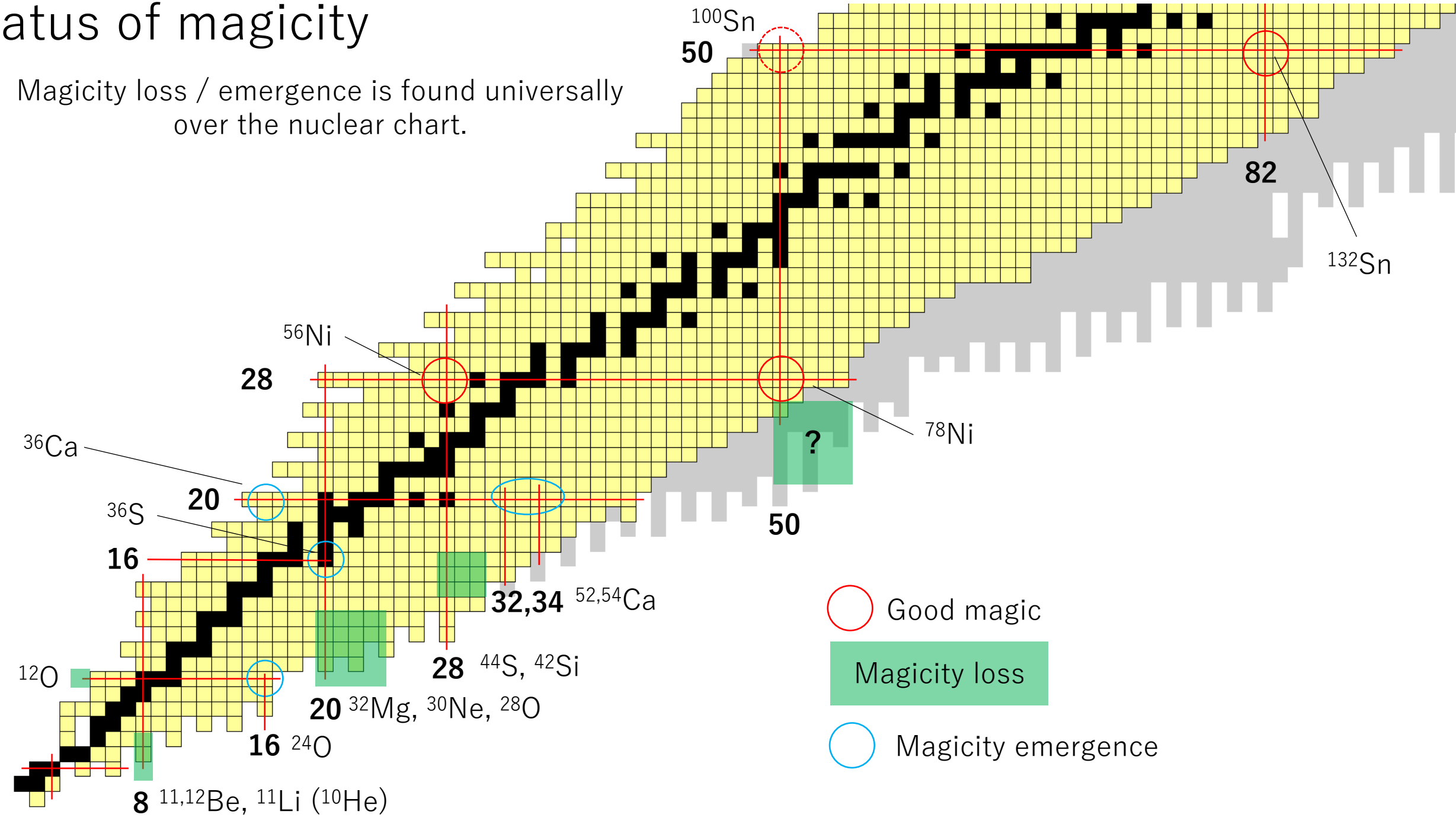

How to confirm magic or non-magic?

- Why did the researchers choose the EM transition in ^{32}Mg to study the N = 20 magicity?

  Clarity of EM operator. Less model dependence. Direct comparison to structural calculations
  Quantification of collectivity

- How we confirm N = 32, 34 are magic? From 2^+ level energies and masses
- How can new magic number be found?
- Relation between B(E2) and magicity.
- Is there any experimental evidence that shows loss of the magicity at N = 20?

How does the magicity at N = 32, 34 fade?

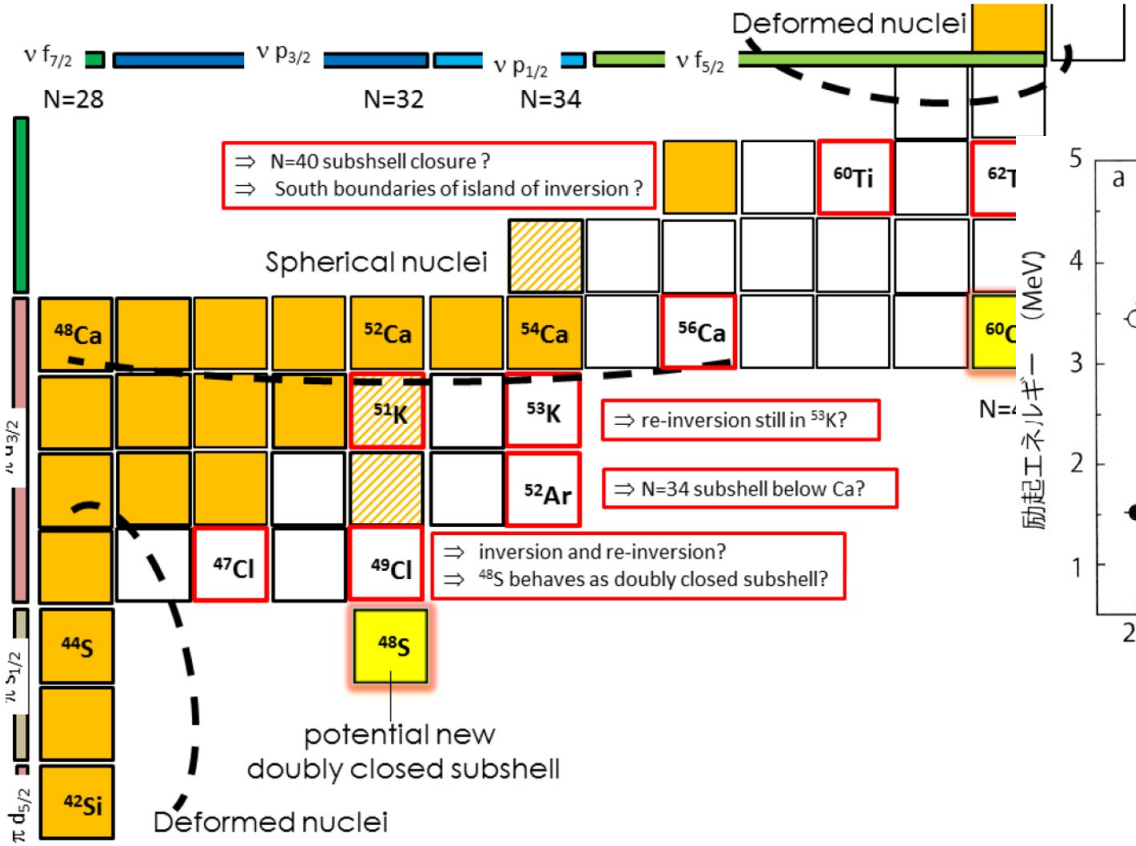

Steppenbeck+ Nature 2013

^{48}Ca

^{52}Ca (ISOLDE, '85)

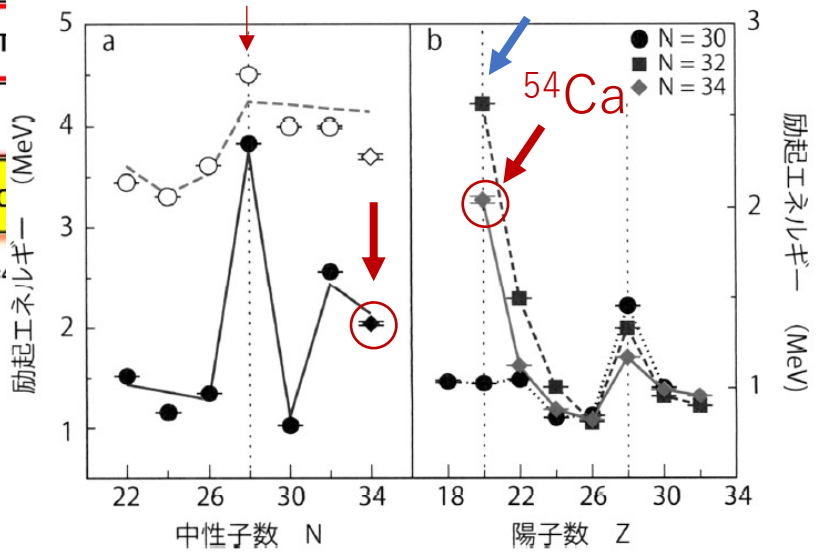

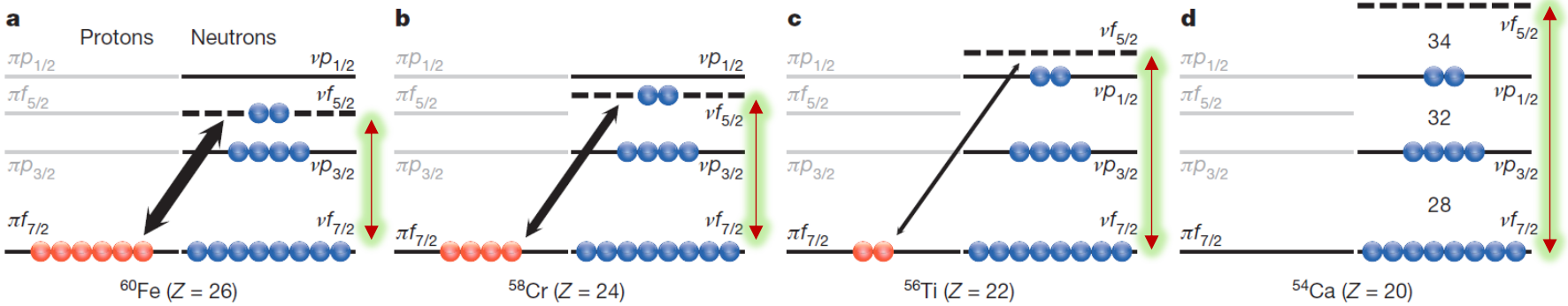

Systematics of two neutron shell gap energies

‘Two neutron shell gap’ defined as

$$\Delta_{2n}(Z,\ N) = S_{2n}(Z,\ N) - S_{2n}(Z,\ N+2)$$

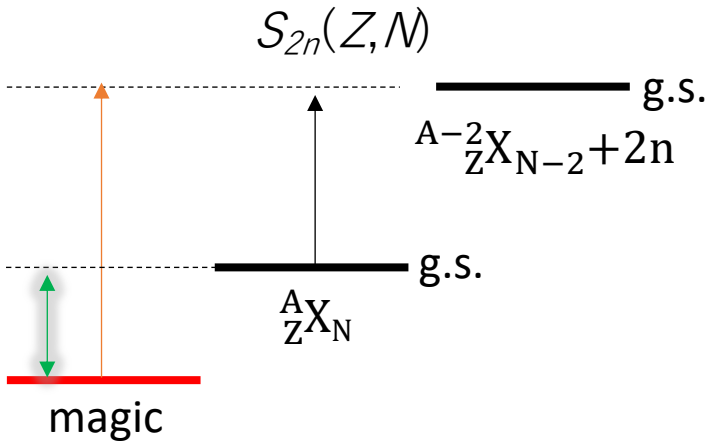

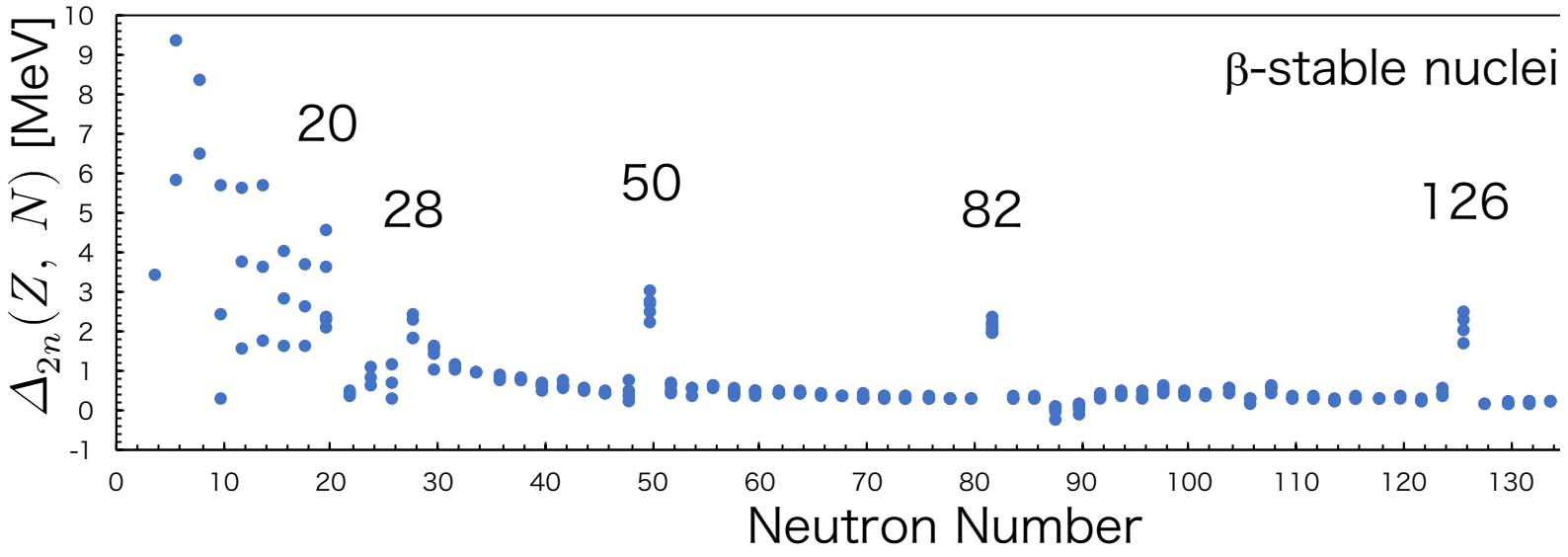

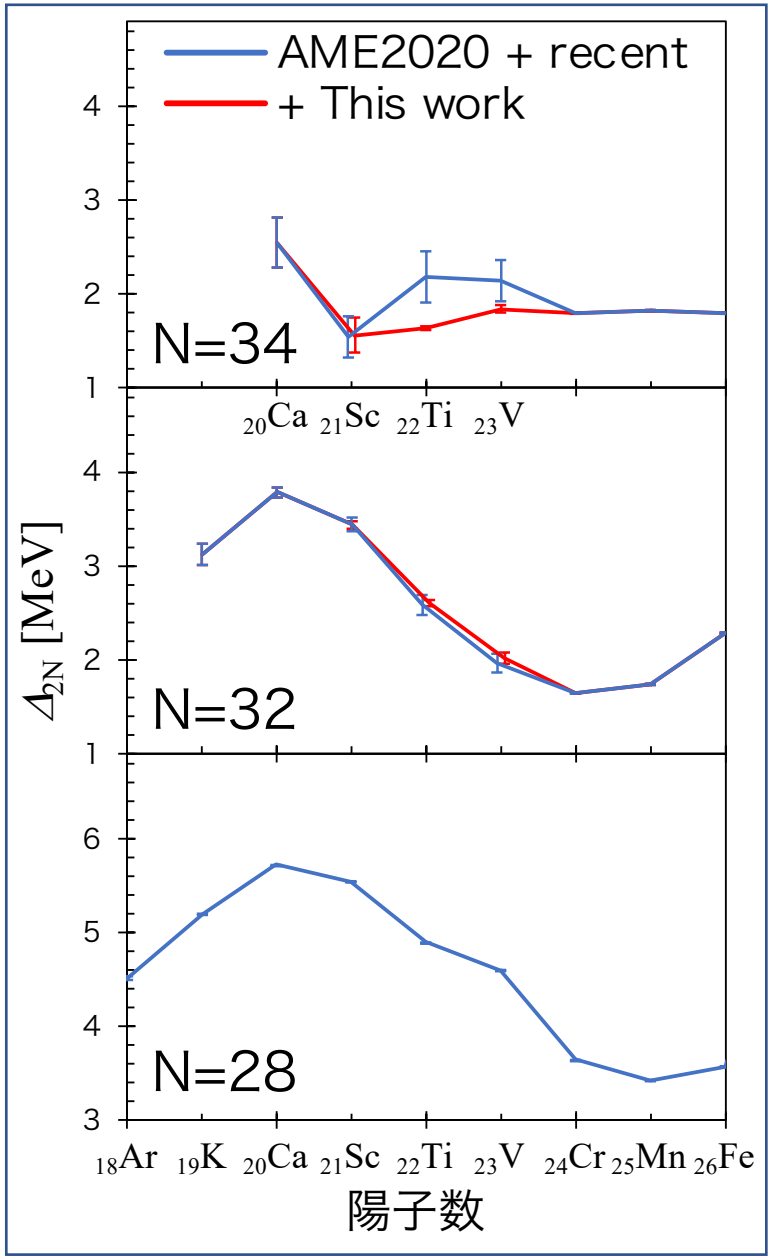

Shun Iimura et al., Phys. Rev. Lett. 130, 012501 (2023)

Where Island of Inversion ends?

- Will the N = 20 Island of Inversion ends at ^{28}O ?

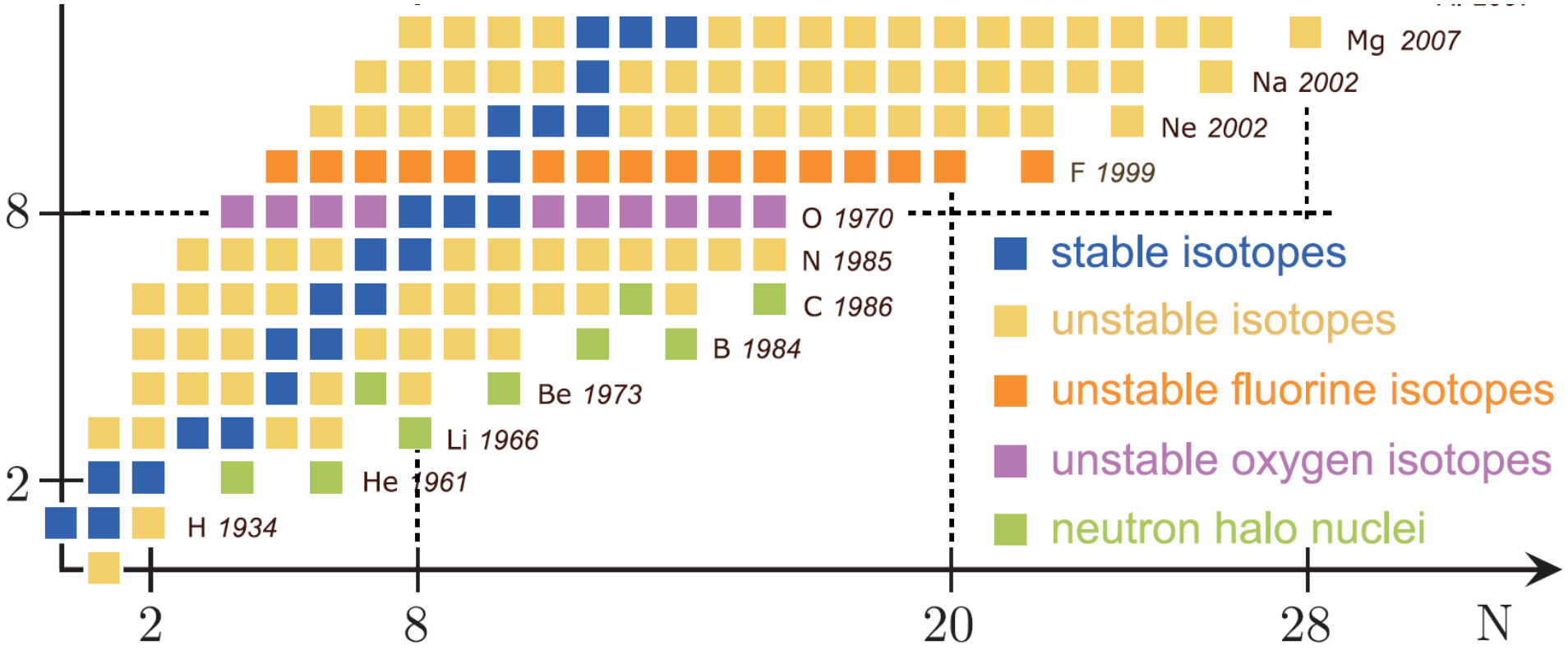

About the origin of magicity loss/emergence

- The reason of magic numbers disappear.
- Does the emergence of new magic number N = 14, 16 have the same origin with the disappearance of N = 20?

- What is the role of tensor forces in evolution of magic numbers?
- What is the origin of the spin-orbit potential?
- What is the connection between particle motion and collective motion?

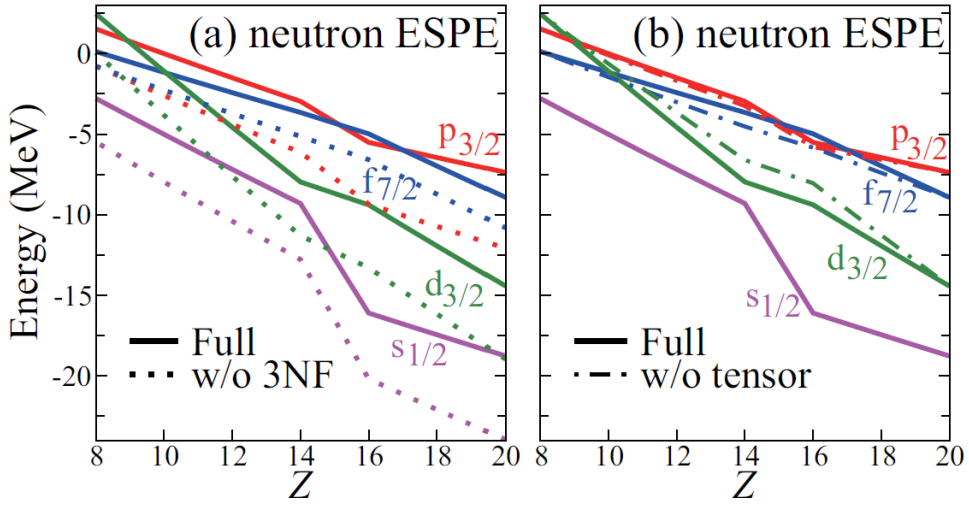

FIG. 5. ESPEs of $N = 20$ isotones for neutrons obtained in the normal filling scheme. (a) The case with and without three-nucleon forces. (b) The case with and without the tensor force.

About experimental technique

- At energies of several hundreds keV, should the energy loss of RI beams in the reaction target be taken into account?

- Can the Coulomb excitation of radioactive beams only do the high-energy Coulomb excitation?
- How the high-energy Coulomb to include nuclear force?

MISC

- What is the AMD?
- In the beta/beta_sp graph, there is also a sudden decline at about Z = 40 for some isotopes. Why not take '40' as a magic number?

  40 is magic in H.O. potential.
  Some Zr isotopes have spherical ground states, and are often used as benchmark in exeriments (e.g. ^{96}Zr).

- How could symmetry term affect the binding energy?

- ^{26}Mg has a peak in E(2^+) systematics. Why?

- Why are the magicity loss region distributed on the right side of the nuclear chart.
- How we confirm N = 32, 34 are magic?
- What is the origin. The single-particle energy or deformation.

- Will the N = 20 Island of Inversion ends at ^{28}O ?
- ^{26}Mg has a peak in E(2^+) systematics. Why?

- The reason of magic number's disappear.
- Why did the researchers chose the EM transition in ^{32}Mg to study the N = 20 magicity?
- Does the emergence of new magic number N = 14, 16 have the same origin with the disappearance of N = 20?

- What is the role of tensor forces in evolution of magic numbers?
- What is the origin of the spin-orbit potential?
- At energies of several hundreds keV, should the energy loss of RI beams in the reaction target be taken into account?

- How can new magic number be found?

- Relation between B(E2) and magicity.
- What is the connection between particle motion and collective motion?
- Is there any experimental evidence that shows loss of the magicity at N = 20?
- Are you good at Rubik cube?

- The mechanism after the introduction of spin-orbit coupling is less clear.

- Why magic number loss in neutron-rich side. Why not in the proton rich side.
- Can the Coulomb excitation of radioactive beams only do the high-energy Coulomb excitation?
- How the high-energy Coulomb to include nuclear force?

- What is the AMD?
- In the beta/beta_sp graph, there is also a sudden decline at about Z = 40 for some isotopes. Why not take ‘40’ as a magic number?

- How could symmetry term affect the binding energy?